SELECTIVE CATALYTIC REDUCTION (SCR) OF NITRIC OXIDE (NO) WITH AMMONIA OVER VANADIA-BASED AND PILLARED INTERLAYER CLAY-BASED CATALYSTS

A Thesis

by

HYUK JIN OH

Submitted to the Office of Graduate Studies of
Texas A&M University
in partial fulfillment of the requirements for the degree of

MASTER OF SCIENCE

May 2004

Major Subject: Mechanical Engineering

SELECTIVE CATALYTIC REDUCTION (SCR) OF NITRIC OXIDE (NO) WITH AMMONIA OVER VANADIA-BASED AND PILLARED INTERLAYER CLAY-BASED CATALYSTS

A Thesis

by

HYUK JIN OH

Submitted to Texas A&M University
in partial fulfillment of the requirements
for the degree of

MASTER OF SCIENCE

Approved as to style and content by:

Jerald A. Caton (Chair of Committee)	Kalyan Annamalai (Member)
Rayford G. Anthony (Member)	Dennis O'Neal (Head of Department)

May 2004

Major Subject: Mechanical Engineering

ABSTRACT

Selective Catalytic Reduction (SCR) of Nitric Oxide (NO) with Ammonia over Vanadia-Based and Pillared Interlayer Clay-Based Catalysts. (May 2004)

Hyuk Jin Oh, B.S., Chonbuk National University

Chair of Advisory Committee: Dr. Jerald A. Caton

The selective catalytic reduction (SCR) of nitric oxide (NO) with ammonia over vanadia-based (V_2O_5-WO_3/TiO_2) and pillared interlayer clay-based (V_2O_5/Ti-PILC) monolithic honeycomb catalysts using a laboratory laminar-flow reactor was investigated. The experiments used a number of gas compositions to simulate different combustion gases. A Fourier transform infrared (FTIR) spectrometer was used to determine the concentrations of the product species. The major products were nitric oxide (NO), ammonia (NH_3), nitrous oxide (N_2O), and nitrogen dioxide (NO_2).

The aim was to delineate the effect of various parameters including reaction temperature, oxygen concentration, NH_3-to-NO ratio, space velocity, heating area, catalyst arrangement, and vanadium coating on the removal of nitric oxide. The investigation showed that the change of the parameters significantly affected the removals of NO and NH_3 species, the residual NH_3 concentration (or NH_3 slip), the temperature of the maximum NO reduction, and the temperature of complete NH_3 conversion.

The reaction temperature was increased from the ambient temperature (25°C) to 450°C. For both catalysts, high NO and NH_3 removals were obtained in the presence of a small amount of oxygen, but no significant influence was observed from 0.1 to 3.0% O_2. An increase in NH_3-to-NO ratio increased NO reduction but decreased NH_3 conversions.

For V_2O_5-WO_3/TiO_2, the decrease of space velocity increased NO and NH_3 removals and broadened the active temperature window (based on NO > 88% and NH_3 > 87%) about 50°C. An increase in heating area decreased the reaction temperature of the maximum NO reduction from 350 to 300°C, and caused the active reaction temperature

window (between 250 and 400°C) to shift toward 50°C lower reaction temperatures (between 200 and 350°C). The change of catalyst arrangements resulted slight improvement for NO and NH_3 removals, therefore, the change might contribute to more gas removals. The catalyst with extra vanadium coating showed higher NO reductions and NH_3 conversions than the catalyst without the extra vanadium coating.

DEDICATION

To my parents and wife

For your patience, understanding and support.

ACKNOWLEDGEMENTS

I would like to give special thanks to my adviser, Dr. Jerald A. Caton, for the opportunity to work on this thesis project. He has generously offered me constant support by his extensive knowledge about the nitric oxide removal processes.

Many thanks also go to Dr. In-Sik Nam (Pohang University of Science and Technology in S. Korea) for providing the necessary catalyst samples.

I would like to thank graduate students, Saurabh Gupta and Young Hun Park, for advising me about the experimental procedures.

Finally, I would like to express my gratitude to my brother, Ungjin Oh, and sister, Rion Oh. Without their support, this work would never have been completed.

This research project was sponsored in part by a grant from the Texas Higher Education Coordinating Board under Grant No. 000512-0012-2001. The contents of this paper, however, do not necessarily reflect the opinions or views of the sponsors.

TABLE OF CONTENTS

Page

Page

LIST OF FIGURES

FIGURE Page

FIGURE Page

FIGURE Page

FIGURE Page

FIGURE Page

FIGURE Page

FIGURE Page

FIGURE Page

FIGURE Page

FIGURE Page

FIGURE Page

FIGURE Page

LIST OF TABLES

TABLE Page

1. INTRODUCTION

Since the 1960s, the number of automobiles and trucks in the world has been growing quickly [1]. The use of fuel combustion in such devices as stationary engines, industrial boilers, power generations, gas turbines and process heaters continues to increase. Due to these phenomena, pollution from mobile sources and the fuel combustion have become an important issue. Several pollutants coming from stationary sources and mobile sources are shown in figure 1 [2]. The use of automobiles and trucks now generates more air pollution than any other single human activity today [1].

Among the many pollutants, nitrogen oxides (NO_x) are emitted from mobile and stationary sources (fuel combustion). A recent study by the EPA (Environmental Protection Agency) reported that 50% of all anthropogenic NO_x emissions come from mobile sources [3]. NO_x in combination with other air pollutants such as SO_2 (sulfur dioxide) or VOC (Volatile Organic Compounds) contributes to acid rain, ground-level ozone and photochemical smog [4].

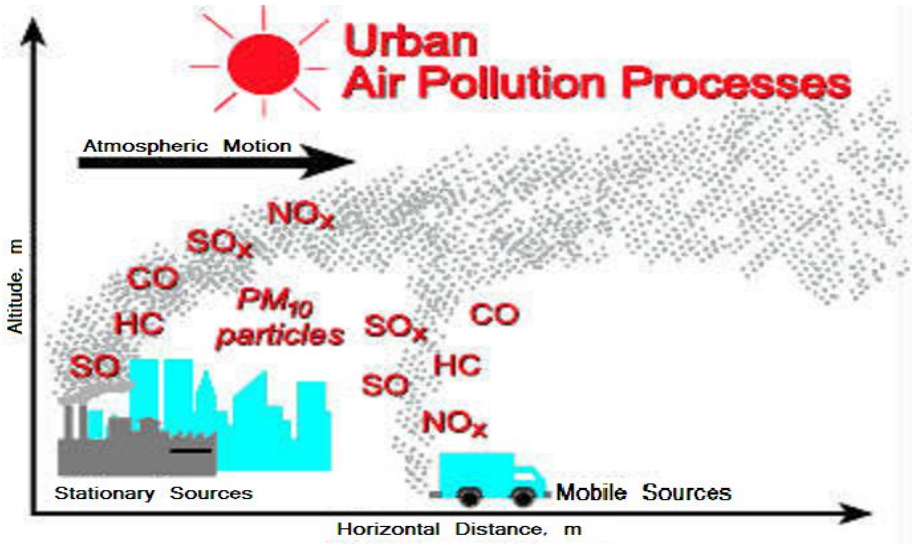

Figure 1. Urban air pollution processes [2].

This thesis follows the format and style of *Combustion and Flame.*

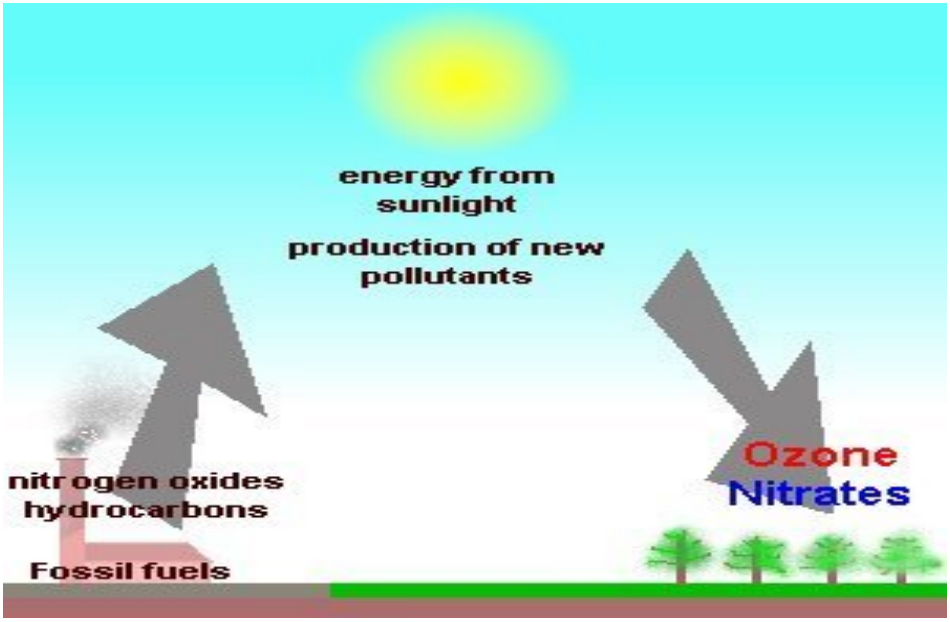

Figure 2. The formation of ozone in the atmosphere [9].

1.1 What is NO_x?

There are seven nitrogen oxides known to occur: NO, NO_2, NO_3, N_2O, N_2O_3, N_2O_4 and N_2O_5 [5, 6]. Nitrogen oxides identified as NO_x are byproducts of fossil fuel combustion and are primarily NO and NO_2. The other nitrogen oxides are known to exist, but they rarely occur in measured quantities in atmosphere [6]. NO_x is formed largely by the reaction of nitrogen and oxygen under extremely high temperature that occurs during the combustion process in internal combustion engines [7]. The concentration of NO_x in the exhaust gas ranges from less than 50 ppm in gas-fired boilers and turbines, to more than 1000 ppm in solid-fueled boilers and incinerators [8].

Figure 2 presents the formation of ozone by the reaction of NO_x with unburned hydrocarbon (HC) or VOC in the presence of sunlight in the lower level of the atmosphere [9]. The concentration of ozone depends on the amount of NO_x and hydrocarbon [7]. Ozone in the upper level of the atmosphere adsorbs the harmful ultraviolet rays from the sun, while the ground level ozone causes human respiratory problems [10].

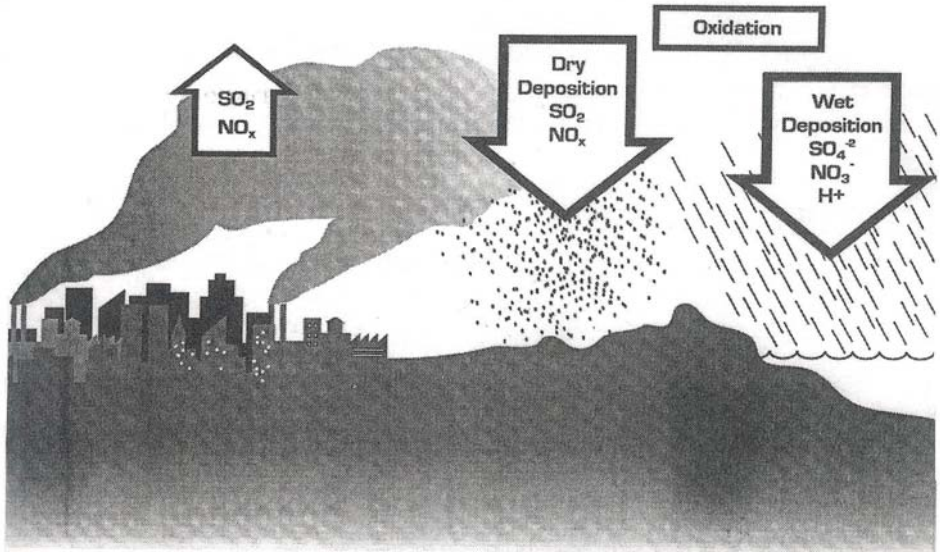

Figure 3. The formation of acid rain [7].

NO_x is a harmful gas and has adverse effects on human health, causing decreased pulmonary function and increased susceptibility to respiratory infection [7]. Many of the nitrogen oxides mentioned above are colorless, yet nitrogen dioxide (NO_2) is toxic, corrosive and reddish-brown gas with a sharp odor [7]. Nitrous oxide (N_2O) causes the greenhouse effect and also is known as a drug [7].

In figure 3, when SO_2 and NO_x from many industrial plants react with gases in the atmosphere, they produce sulfur acid and nitric acid, making the resulting rainfall more acidic [7]. Industrial manufacturing plants, power plants and chemical plants contribute most of the SO_2 and NO_x precursors in the atmosphere [7].

1.2 Formation of NO_x

The formation of NO_x mainly occurs through three reaction mechanisms: the Zeldovich mechanism (Thermal NO_x), the Fenimore mechanism (Prompt NO_x) and Fuel NO_x [11]. The most significant one among them is the Zeldovich mechanism. The reactions occurring at the elevated temperature during combustion processes generate both

nitrogen and oxygen atoms by dissociation of the respective molecules which subsequently lead to the formation of NO [11, 12]. The three main reactions of the Zeldovich mechanism are:

$$O + N_2 = N + NO \quad (1.1)$$

$$N + O_2 = O + NO \quad (1.2)$$

$$N + OH = H + NO \quad (1.3)$$

NO is formed in both the flame front and the postflame gases [12]. The reaction (1.3) takes place mainly in a near stoichiometric and a very rich mixture gas. Although the formation rate of thermal NO_x is slow compared to combustion reactions, thermal NO_x contributes the largest portion to the total NO_x formed [13]. The quantity of NO_x formed depends on residence time, local stoichiometric composition (equivalence ratio), turbulence, and especially, reaction temperature [13].

The prompt NO_x is formed directly at the flame front and provides less than 10% of overall NO_x emission [12, 14]. The hydrocarbon fragments such as C, CH and CH_2 react with the atmosphere nitrogen and their subsequent combination to produce nitrogen species such as CN, HCN, H_2CN and NH [15]. The reaction mechanisms are [15]:

$$CH + N_2 = HCN + N \quad (1.4)$$

$$N + O_2 = NO + O \quad (1.5)$$

$$HCN + OH = CN + N_2O \quad (1.6)$$

$$CN + O_2 = NO + CO \quad (1.7)$$

In the fuel NO_x process, the reaction occurs in the combustion process from chemically/bound nitrogen in fuels [16, 17]. Many fossil fuels such as coke and coal consist of a number of chemicals, which can also contain nitrogen. Once this fuel is burned, the nitrogen in the fuel reacts to form NO_x [17].

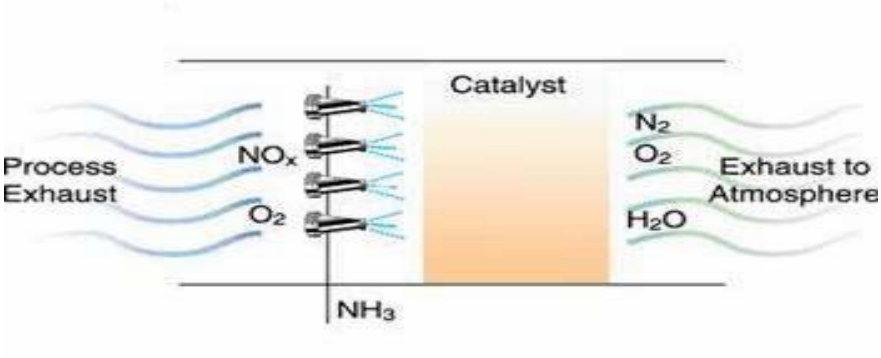

Figure 4. The schematic of SCR of NO_x with ammonia [18].

1.3 The Technologies of NO_x Emission Control

The most common methods of NO_x emission control technologies are categorized as pre-combustion and post-combustion methods [11]. EGR (Exhaust Gas Recirculation), retarding spark timing, modification of the equivalence ratio and change of compression ratio are classified as pre-combustion methods to control NO_x emission [12]. These methods achieve significant amounts of NO_x reduction, but often do not reach the stringent regulation levels required today. To achieve higher NO_x reduction, post-combustion methods known as "after treatment methods" are required. Selective Catalytic Reduction (SCR) and Selective Non-Catalytic Reduction (SNCR) are two of the most prevalent post-combustion methods.

1.4 Selective Catalytic Reduction (SCR) of NO_x

Selective catalytic reduction of nitric oxide with NH_3 described in figure 4 has been known to be the best emission control technology for the removal of NO_x from stationary sources [14]. The SCR process uses a catalyst along with a reducing agent, usually NH_3, to remove NO_x to N_2 in the exhaust gas of combustion engines. Since NO is the primary component of NO_x emitted from combustion sources, the reactions (1.8) and (1.9) are the overall main reactions which occur during the SCR process with NH_3 [19]. Over Pt-supported catalysts in excess oxygen, the main reactions of producing N_2 are the reactions (1.9) and (1.10) [19]. NH_3 can react selectively with NO_x [19, 20].

$$4NH_3 + 6NO \rightarrow 5N_2 + 6H_2O \quad (1.8)$$

$$4NH_3 + 4NO + O_2 \rightarrow 4N_2 + 6H_2O \quad (1.9)$$

$$4NH_3 + 2NO_2 + O_2 \rightarrow 3N_2 + 6H_2O \quad (1.10)$$

The side reactions occur along with the above main reactions. N_2O is undesirably produced at high temperature as shown (1.11) [20]. Some injected ammonia can be wasted to produce N_2 or completely oxidized to NO in nonselective reaction as shown by (1.12) and (1.13) [20].

$$2NH_3 + 2O_2 \rightarrow N_2O + 3H_2O \quad (1.11)$$

$$4NH_3 + 3O_2 \rightarrow N_2 + 6H_2O \quad (1.12)$$

$$4NH_3 + 5O_2 \rightarrow 4NO + 6H_2O \quad (1.13)$$

The most undesired side reaction is the oxidation reaction of NH_3. Below the temperature 200ºC, the ammonia can react with NO_2 to produce explosive gas, NH_4NO_3 as observed in (1.14) [20].

$$2NH_3 + 2NO_2 + H_2O \rightarrow NH_4NO_3 + NH_4NO_2 \quad (1.14)$$

Minimizing the formation of NH_4NO_3 requires NH_3 to react stiochiometrically with NO_x (1:1 mole basis) or less than 1 [20]. In the case that NH_3/NO_x ratio is higher than 1, NH_3 slip which reduces NO_x conversion appears [20]. These major reactions involved in SCR of NO_x are simply depicted schematically in figure 5 [21].

Platinum (Pt) type, V_2O_5/TiO_2 and zeolite catalysts are the most prevalent catalysts of the selective catalytic reduction process [21]. Reduction is accomplished with Pt-supported catalysts below the temperature 250ºC [21]. Due to their poor selectivity, Pt-supported catalysts were not applicable above 250ºC [21]. Thus, the use of Pt-supported catalysts is decreasing. Vanadium-supported catalysts are preferred between 250ºC and

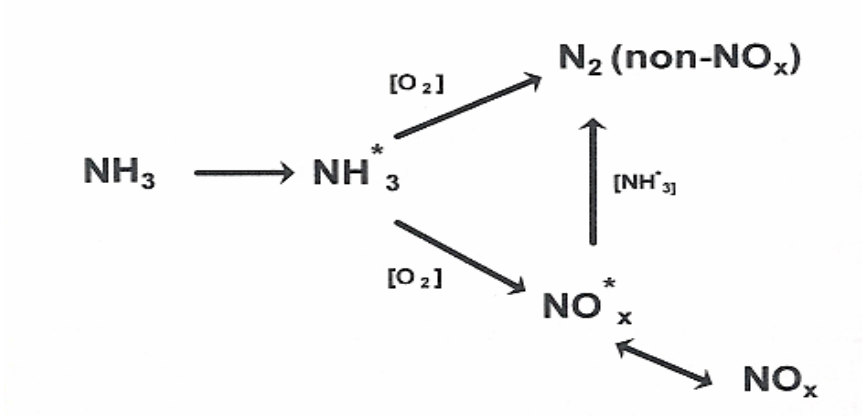

Figure 5. Reaction networks: catalytic reaction scheme of NH_3, NO_x and O_2 [21].

450ºC [21]. Vanadium-supported catalysts will be described in detail in the next section. Two undesirable reactions (1.12) and (1.13) cause low catalytic activity of Pt type and V_2O_5 catalysts, respectively [19, 20]. Above the temperature 450ºC, a metal ion exchanged zeolite catalyst is required [21]. The zeolite-based catalysts are also sulfur-insensitive [19]. Copper and cobalt, which are exchanged ions of zeolite, have been widespread.

The selective non-catalytic reduction (SNCR) process uses only a reducing agent without catalysts. The comparisons of the two techniques are described in table 1 [22].

Table 1. Comparison of SCR and SNCR emission control techniques [22].

Features	SCR	SNCR
Operating temperature (°C)	200 - 500	800 – 1100
Operating cost	Moderate	Moderate
Capital cost	High	Low
NH_3 slip (ppm)	< 5	5 – 20
NH_3/NO molar ratio	0.4 – 1.0	0.8 – 2.5
NO_x removal efficiency (%)	70 - 90	30 – 80

The SNCR process has lower NO_x removal efficiency at relatively higher operating temperatures [22]. The operation cost is almost the same for both processes. The capital cost of the SNCR process, however, is lower than the SCR process. NH_3 slip reducing the effective of NO removal occurs more in SNCR.

1.5 Vanadia (V_2O_5)-Based Catalysts

Selective catalytic reduction of NO_x with ammonia (NH_3) has been used for over 20 years for NO_x abatement from the industrial boiler flue gas and power plants. The most common catalysts in commercial material today are vanadia-based catalysts [19]. The supports including alumina, silica, zirconia, and titania were commonly used for vanadia-based catalysts. Alumina has a higher specific surface area, superior mechanical strength, and is highly resistant to sintering, compared to titania [19]. However, for the SCR of NO_x with NH_3 using alumina support (Al_2O_3), SO_2 in the flue gas reacts with ammonia and then deactivates the catalytic activity [19]. It indicates that Al_2O_3 is weakly poisoned by sulfur components

Among many metal oxide supports, TiO_2 support exhibits the best effective for the selective catalytic reduction of NO_x with NH_3 because of its durability to sulfur compounds [23]. The sulfation of the TiO_2 supported catalyst even enhances the level of NO removal [23]. Therefore, due to its high activity and durability to sulfur compounds, V_2O_5 supported on TiO_2 is well known to be the most effective and widely used commercial catalyst for the SCR processes [23].

A ternary catalyst, V_2O_5-WO_3/TiO_2, was also recently introduced. Promoters such as WO_3, SiO_2 and MoO_3 are usually added to V_2O_5/TiO_2 catalyst [24, 25]. The promoters create acid sites on the catalyst surface, and the catalysts exhibit a higher catalytic activity than that of a single TiO_2 supported vanadium catalyst [24]. The addition of WO_3 provides some poison resistance and improves NH_3 oxidation. There are still many studies to promote the activity of vanadia-based catalysts, but V_2O_5-WO_3/TiO_2 indicates more reliable results for removal of NO_x.

1.6 Pillared Interlayer Clay (PILC)-Based Catalysts

The developments of a new catalyst support were tried to overcome the disadvantages of titania such as limited surface area, a low sintering resistance, a high cost, and poor mechanical strength [19]. Studies on the pillared interlayer clays (PILCs) with titania as a pillar (Ti-PILC) has been extensively investigated recently because of its peculiar characteristics which may overcome the limits of titania [24, 25]. The pillared interlayer clays (PILCs) are particularly promising as a catalyst support. PILCs are generally called a unique two-dimensional zeolite-like material [25]. Both Lewis and Brønsted acid sites exist on pillared clays [24]. It has been well known that the number of Brønsted acid sites increases when sulfur exists on the catalyst surface [24]. Ti-PILC catalyst contains large surface area, strong mechanical strength, high resistance to SO_2, hydrothermal stability and multimodal pore size distribution [24, 25]. Vanadia shows good performance for the SCR of NO_x with ammonia, and therefore, V_2O_5/Ti-PILC catalyst has been examined recently [24].

One of the advantages of PILCs support is the variety of physical and structural characteristics with respect to the technique of the catalyst preparation [25]. The modification of pore structure of catalyst indicates important role for catalytic activity and sulfur tolerance for NO reduction with NH_3 [25]. According to the examination of pore structure of Ti-PILC catalysts, micropores may lead to capillary condensation causing catalyst deactivation during the process [25].

The pillaring of titania on the catalyst enhances the surface acidity, and both Lewis and Brønsted acid sites exist on pillared clays [19]. The surface acidity, the most important characteristic of the SCR catalyst, and both Lewis and Brønsted acid sites enhance the catalytic activity [20]. Therefore, Ti-PILC catalysts have high surface acidity and high catalytic activity.

It was reported that the catalytic activity increased in the order Al_2O_3-PILC < ZrO_2-PILC < TiO_2-PILC < Fe_2O_3-PILC < Cr_2O_3-PILC as a SCR catalyst support [24]. Due to the most active catalyst Cr_2O_3-PILC is severely weak by SO_2, TiO_2-PILC and Fe_2O_3-PILC catalysts have been widely used for commercial catalysts.

2. LITERATURE REVIEW

In this section, previous studies on the selective catalytic reduction (SCR) of nitrogen oxides process using ammonia as the reducing agent on the two types of catalysts: vanadia (V_2O_5)-based catalysts and pillared interlayer clay (PILC)-based catalysts will be presented.

2.1 Vanadia (V_2O_5)-Based Catalysts

Among the various catalysts studied for the selective catalytic reduction (SCR) of nitric oxide (NO) with ammonia, vanadia-titania-based catalysts are known to be the most popular for industries [26]. Bosch and Janssen reported a very extensive survey of catalyst formulations found active until 1988 [27]. Pure vanadia and vanadia supported on titania, alumia, silica, and zirconia have been investigated [26]. Among the base oxide catalysts such as V_2O_5, Fe_2O_3, CuO, NiO, etc. tested by them, vanadia oxides (V_2O_5) were found to be the most active and selective catalysts for SCR of NO with ammonia [26].

The characteristic of the support affects the catalytic reaction, and titania-support shows very good activity. Therefore, the wide-spread catalysts for industry have been commercialized based on TiO_2 supported V_2O_5, V_2O_5-WO_3 and V_2O_5-MoO_3 oxides [26]. Comparison of Platinum (Pt) type, V_2O_5/TiO_2 and zeolite catalysts for selective catalytic reduction of NO_x with ammonia is described in figure 6 [21]. Vanadia-supported catalysts are preferred to react at the reaction temperatures between 250ºC and 450ºC. The best operating temperature ranges of vanadia-supported catalysts are between 260ºC and 425ºC [21].

In the beginning of the application of vanadia-supported catalysts, V_2O_5/Al_2O_3 catalysts had been used, but more recently, vanadia-titania (V_2O_5/TiO_2) catalysts have replaced them because Al_2O_3 is weakly poisoned by sulfur components. The stability of sulfates on the surface of titania-supports is weaker than that on any other metal oxide

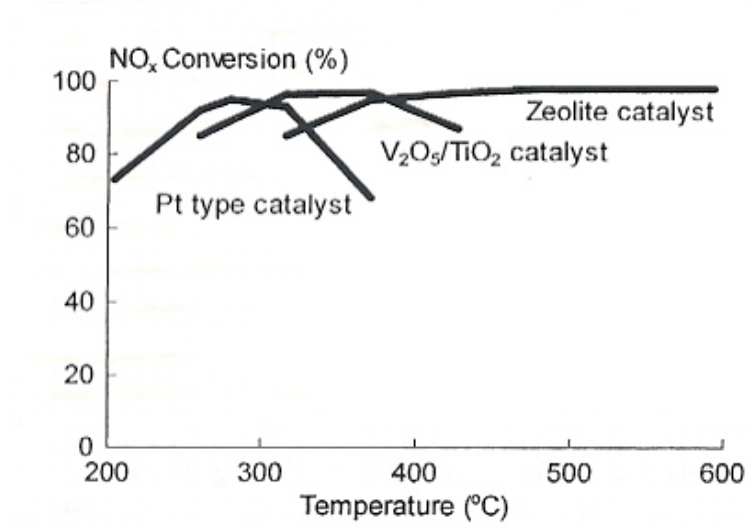

Figure 6. Comparison of three different catalysts for SCR of NO_x with NH_3 [21].

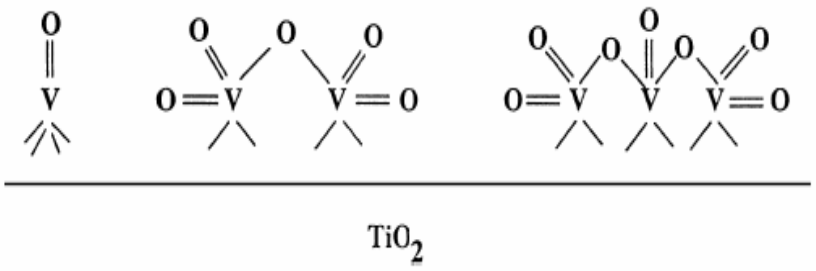

Figure 7. Structural forms of vanadia-supported titania catalysts [28].

supports [19, 20]. Therefore, TiO_2-based catalysts can be partially and reversibly sulfated under the SCR reaction condition containing sulfur dioxide [19]. The sulfation of the catalysts is even more effective to the catalytic activity [19].

The structure of vanadia-supported over TiO_2 catalyst is shown in figure 7 [28]. Mainly monomeric vanadyl species are formed on the anatase surface at low V_2O_5 concentration, and then the monomeric species react to form polymeric vanadates with an increase in vanadium loading [28]. When vanadium loading exceeds on the anatase surface, V_2O_5 crystallites are formed [28].

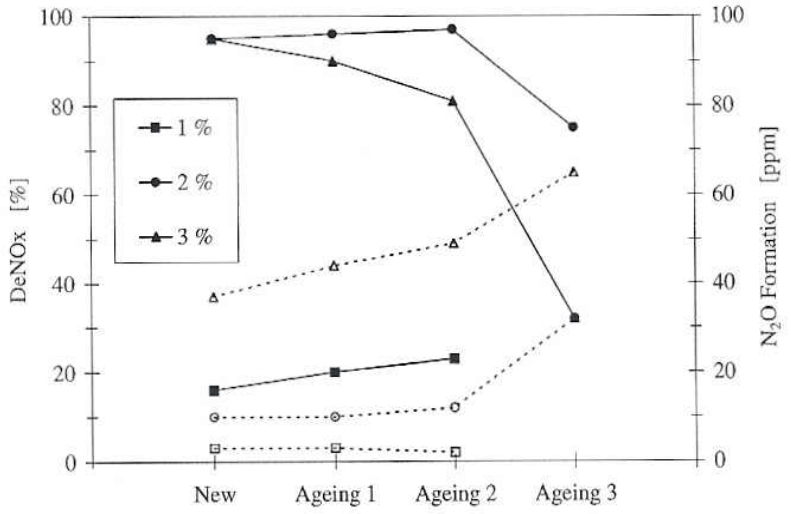

Figure 8. $DeNO_x$ at 10 ppm NH3 slip and N_2O formation for new conditions and after aging procedures 1, 2 and 3 for SCR catalysts with 1%, 2% and 3% V_2O_5. Full symbols: $DeNO_x$, open symbols: N_2O formation. Feed: 1000 ppm NO, NH_3, 5% H_2O, 10% O_2, balance N_2. GHSV = 52000 h^{-1}. Temperatures: 300ºC for $DeNO_x$, 450ºC for N_2O formation [29].

2.1.1 Effect of Vanadium Loading

The vanadium content was found to have a major influence on both the SCR activity and the thermal stability [29, 30]. Figure 8 shows the effect of various vanadium content on NO_x conversion at 10 ppm NH_3 slip at 300ºC for new conditions and after three different aging procedures [29]. The catalytic activity of 1% V_2O_5 catalysts shows very low results for all cases. For 2% V_2O_5 catalysts, high NO conversion is obtained in new condition and slightly improved after aging procedures 1 and 2. Aging procedure 3 causes the NO conversion of 2% V_2O_5 to decline. The catalytic activity for 3% V_2O_5 catalysts is high in the new condition, and decreases slightly after aging treatments 1, 2. Aging treatment 3 cause the catalytic activity for 3% V_2O_5 to decrease rapidly. The catalyst containing 2% V_2O_5 represents an optimal compromise between the SCR activity and thermal stability over the range of aging treatment [29]. 1% V_2O_5 catalysts results in low SCR activity, and 3% V_2O_5 shows a significant low thermal stability [29].

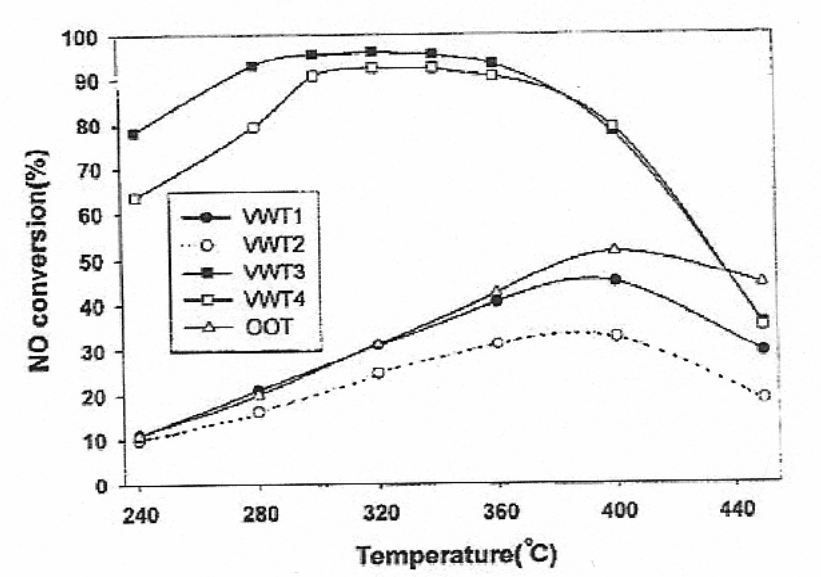

Figure 9. The effect of vanadium loading on NO conversion over V_2O_5-WO_3/TiO_2 catalytic filters for the selective reduction of NO [30].

Figure 9 shows the effect of vanadium loading on NO conversion over V_2O_5-WO_3/TiO_2 catalyst supported on ceramic filters for the selective reduction of NO [30]. The performances occurred for the conditions of 500 ppm NO, 500 ppm NH_3, 2 vol% O_2, N_2 balance, and an actual face velocity of 0.02 m/sec [30]. VWT1 and VWT2 catalysts with the low load of vanadium and tungsten atoms present resulted in very low NO conversion. The loadings of vanadium in VWT1 and VWT2 catalysts are 0.4 and 0.6% w/w, respectively. The NO conversions of VWT1 and VWT2 catalysts are even lower than that of OOT catalyst containing no vanadium and tungsten atoms [30]. When vanadium content increases in the catalysts, the catalytic activity shows better results under the same condition. VWT3 and VWT4 containing 0.46 and 0.47% w/w V_2O_5 loadings exhibit high NO conversion [30].

When vanadium is added to pure TiO_2 catalysts that have only Lewis acid sites (Ti-OH), vanadium generates Brønsted acid sites (V-OH) known as the active sites for NO reduction [30].

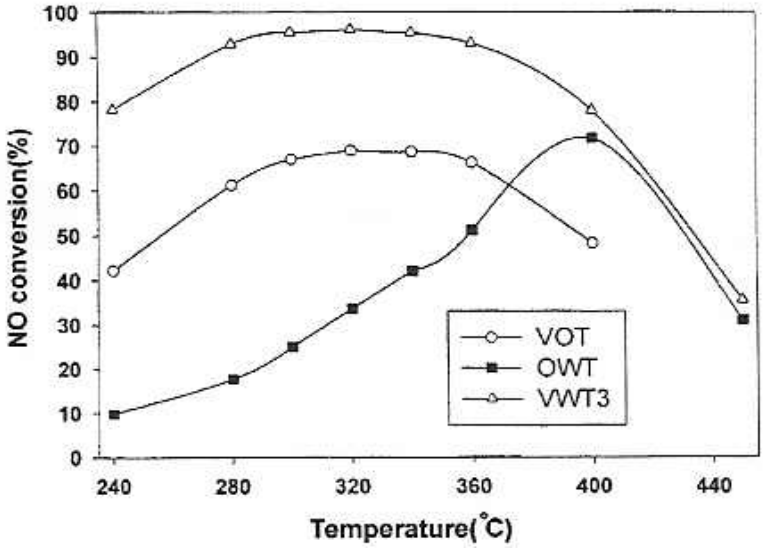

Figure 10. The effect of WO_3 on the catalytic activity for the SCR of NO on V_2O_5-TiO_2/PRD [30].

2.1.2 Effect of Tungsten Species (WO_3) Addition

The promoters such as WO_3, MoO_3 and SiO_2 are commonly added to V_2O_5/TiO_2 catalyst to increase the SCR activity [24, 31]. These promoters preferentially interact with vanadium oxide species on the titania surface to form two-dimensional surface metal oxides, and then create acid sites on the catalyst surface [31]. The strong interaction between vanadia and tungsten species on the TiO_2 support increases the acidity of TiO_2 and exhibits a higher catalytic activity [24]. WO_3 also increases the poison resistance to alkali and reduces ammonia oxidation. Therefore, the role of WO_3 in the V_2O_5/TiO_2 catalytic system is very important [31].

Figure 10 represents the effect of WO_3 on NO reduction activity of SCR catalytic filter [30]. OWT (WO_3-TiO_2/PRD), VOT (V_2O_5-TiO_2/PRD) and VWT3 (V_2O_5-WO_3/TiO_2/PRD) were prepared for the NO conversion over catalytic filters. VWT3 shows the maximum NO conversion of 95%, while VOT and OWT show 68 and 75%, respectively [30]. The results indicate that WO_3 significantly improves the catalytic activity at lower temperature and broadens the temperature window of the maximum NO conversion [30].

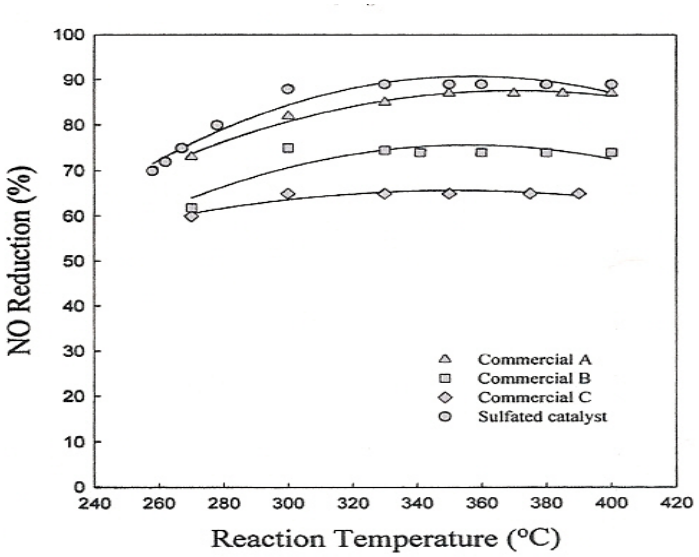

Figure 11. The effect of reaction temperature for SCR of NO by ammonia on sulfated V_2O_5/TiO_2 catalysts and different types of commercial catalysts. (NH_3-to-NO ratio = 1.0, space velocity = 4000 h^{-1}) [32].

Similar trends are observed in the results of Chen and Yang [31] in 1992. They reported that the addition of WO_3 increases the catalytic activity and broadens the reaction temperature window [31]. A wider reaction temperature window allows flexibility in operation of the reaction. The addition of WO_3 also significantly enhances the poison resistance of V_2O_5-based catalyst toward alkali metal oxides that are the strongest SCR poisons [31].

2.1.3 Effect of Reaction Temperature

Figure 11 shows the effect of reaction temperature for SCR of NO by ammonia over sulfated V_2O_5/TiO_2 catalysts at a space velocity of 4000 h^{-1} and NH_3-to-NO mole ratio of 1.0 [32]. NO reductions increase with an increase in reaction temperature 350˚C and reach the maximum values at approximately 350˚C [32]. Then, the catalytic activities decrease at 400˚C. The reaction temperature windows for effective NO reductions exhibit the similar temperature ranges for all catalysts [32].

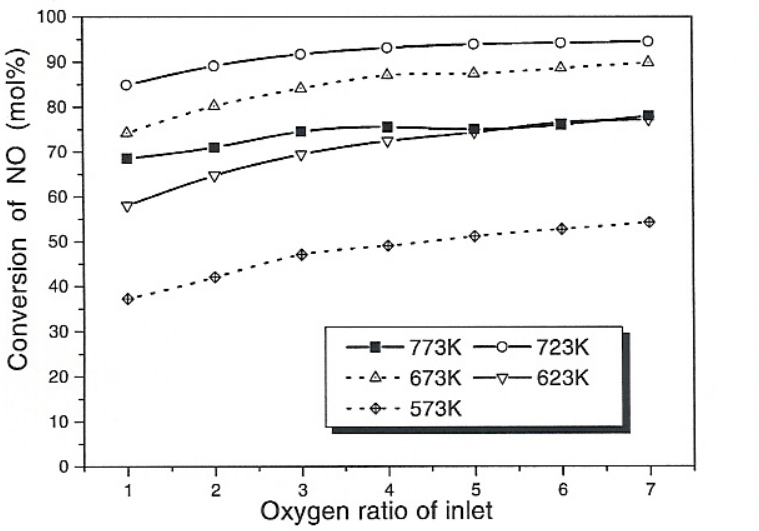

Figure 12. The correlation between the oxygen ratio of inlet and the conversion of NO at various temperatures on V_2O_5-MoO_3-WO_3/TiO_2/Al_2O_3/cordierite-honeycomb. (Reaction conditions: SV = 6000 h^{-1}, NH_3-to-NO = 1.0) [33].

Liuqing et al. [33] reported similar result that a peak of NO conversion could be observed in the temperature range of 673 to 723 K for SCR of NO with ammonia over V_2O_5-MoO_3-WO_3/TiO_2/Al_2O_3/cordierite-honeycomb monolithic catalysts.

2.1.4 Effect of Oxygen Concentration

Figure 12 presents the effect of oxygen concentration of inlet for selective catalytic reduction of NO with ammonia at various reaction temperatures on V_2O_5-MoO_3-WO_3/TiO_2/Al_2O_3/cordierite-honeycomb [33]. The reactions were performed under the conditions of [NO] = [NH_3] = 1000 ppm, 5% O_2, N_2 balance, SV = 6000 h^{-1}, and NH_3-to-NO ratio of 1.0 [33]. After 1% oxygen concentration, NO conversion is slightly increased for all reaction temperatures, and a high NO conversion is obtained in the oxygen concentration range of 5 - 7%. The addition of 1 - 7% oxygen content does not make significant influence to the catalytic reaction [33].

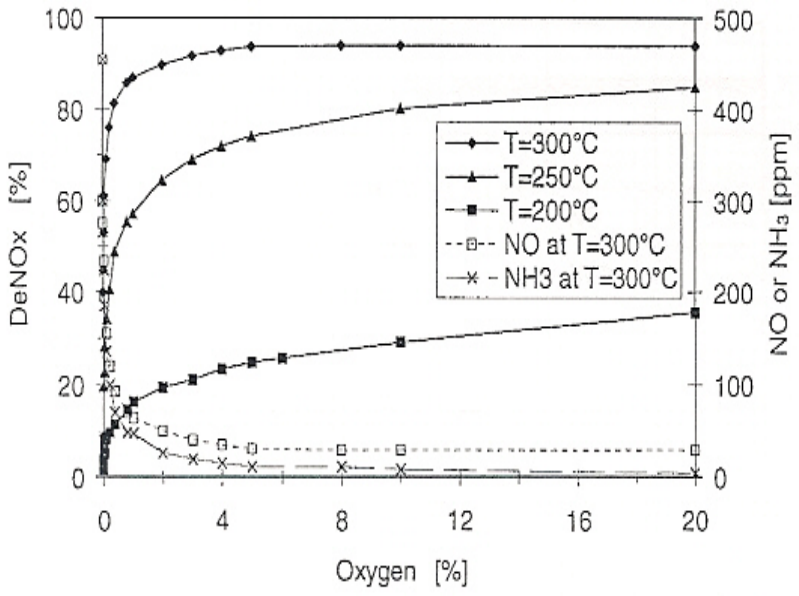

Figure 13. $DeNO_x$ vs. O_2 concentration on TiO_2-WO_3-V_2O_5 catalyst. Feed: 1000 ppm NO, 1000 ppm NH_3, 5% H_2O, O_2 varied, and balance N_2 [34].

In figure 13, the influence of oxygen concentration for SCR of NO with ammonia on TiO_2-WO_3-V_2O_5 catalyst is observed for the conditions of 1000 ppm NO, 1000 ppm NH_3, 5% H_2O, 0 - 20% O_2, and N_2 balance [34]. It is observed that the influence of oxygen concentration is different for the three temperatures [34]. The NO_x conversion ($DeNO_x$) still increases with oxygen concentration up to 20% at 200˚C and 250˚C. The NO_x conversion at 300˚C, however, increases up to approximately 5% oxygen concentration, and then, reaches steady state. For all three cases, the NO_x conversions increase rapidly between 0 - 1% oxygen concentrations.

2.1.5 Effect of Space Velocity

The space velocity, one of the most important factors for a catalytic design, is defined as the volumetric gas flow rate divided by the superficial volume of a sample catalyst [32].

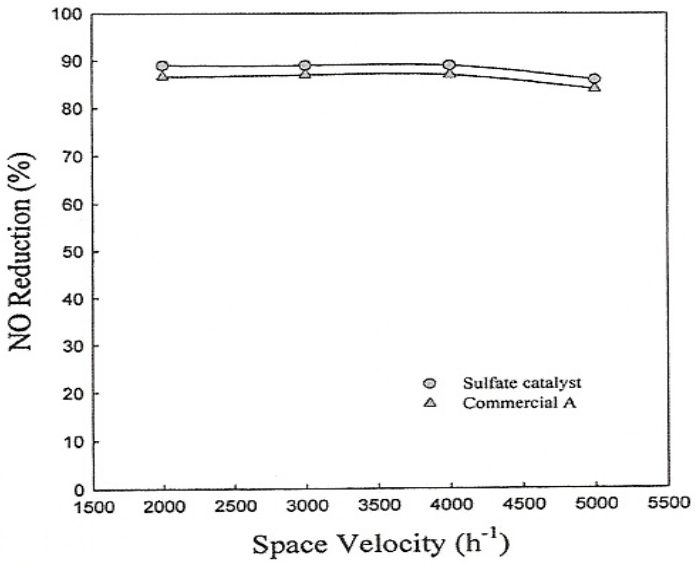

Figure 14. The effect of space velocity on NO reduction for SCR reaction of a sulfated V_2O_5-based catalyst and a commercial A catalyst at 350ºC. (NH_3-to-NO ratio = 1.0) [32].

In figure 14, the effect of space velocity for SCR of NO by ammonia over a sulfate V_2O_5-based catalyst and a commercial A catalyst is exhibited under the conditions of reaction temperature 350ºC and NH_3-to-NO mole ratio of 1.0 [32]. NO reductions for both catalysts are steady at approximately 90% up to a space velocity of 4000 h^{-1}, and then slightly decrease to about 85% with increasing space velocity [32].

Figure 15 presents the predictions of the kinetic model developed over the packed-bed flow reactor for selective catalytic reduction of NO_x with ammonia under the wet condition for V_2O_5/TiO_2 catalyst [35]. NO conversions increase with a decrease in space velocity varied from 100,000 to 400,000 h^{-1} [35]. NO conversions for space velocities of 100,000 and 200,000 h^{-1} increase sharply up to the temperature of 300˚C, and then reach the steady conditions. For the space velocity of 300,000 and 400,000 h^{-1}, NO conversions are increased steeply up to 350˚C and stay in the steady condition. The maximum conversion of NO is dropped approximately 30% when the space velocity increases from 100,000 to 400,000 h^{-1}.

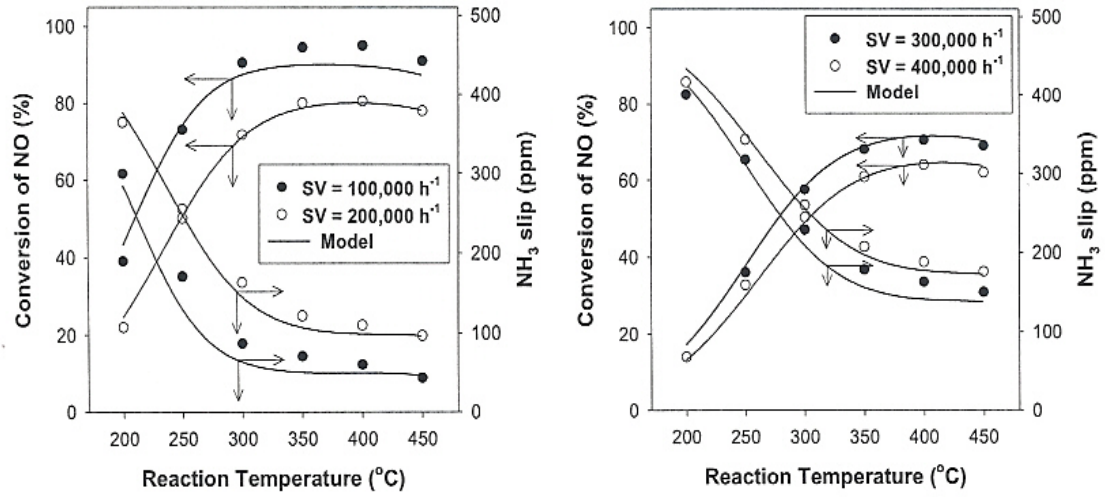

(a) (b)

Figure 15. Prediction of the kinetic model developed over the packed-bed reactor of wet condition of V_2O_5/TiO_2 catalyst with respect to the reactor space velocity for selective catalytic reduction of NO_x with ammonia [35].

Figure 15 (a) and (b) show the effect of space velocity on the NO reduction and the ammonia slip under the same conditions [35]. Lower space velocity leads to lower ammonia slip. Ammonia slips decrease rapidly until the reaction temperature 350˚C and stay steady for all cases.

Figure 16 exhibits the correlation between space velocity and the conversion of NO for SCR reaction with ammonia at various reaction temperatures on V_2O_5-MoO_3-$WO_3/TiO_2/Al_2O_3$/cordierite-honeycomb catalyst [33]. The reactions occurred under the conditions of [NO] = [NH_3] = 1000 ppm, 5% O_2, N_2 balance, and NH_3-to-NO ratio of 1.0 [33]. Unlikely the result of the temperature of 573K, the increase in space velocity results in the decrease of the NO conversion for the temperature above 623 K [33]. In general, the higher NO conversion is more liable to be obtained at lower space velocity [33]. These results are in good agreement with the results in figure 15. It is also reported that the optimal reaction temperature differs with the space velocity [33]. Lower optimal reaction temperature is obtained with lower space velocity [33].

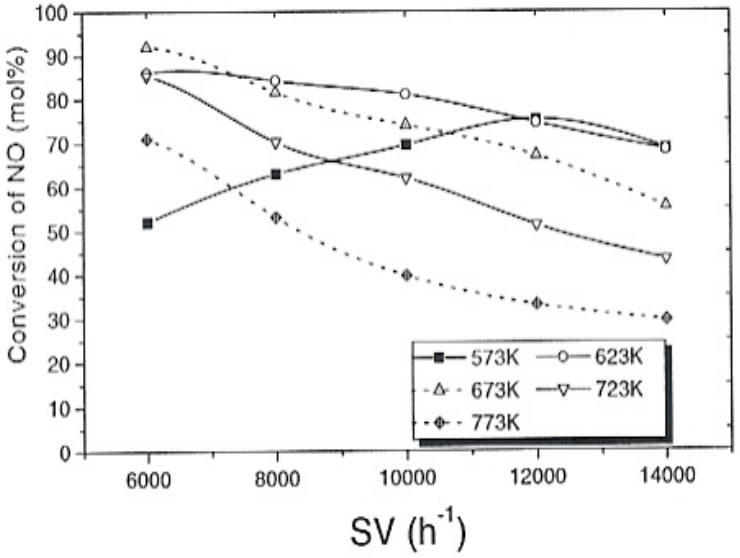

Figure 16. The correlation between space velocity and the conversion of NO at various reaction temperatures on V_2O_5-MoO_3-WO_3/TiO_2/Al_2O_3/cordierite-honeycomb catalyst. (oxygen ratio = 5%, NH_3/NO = 1.0) [33].

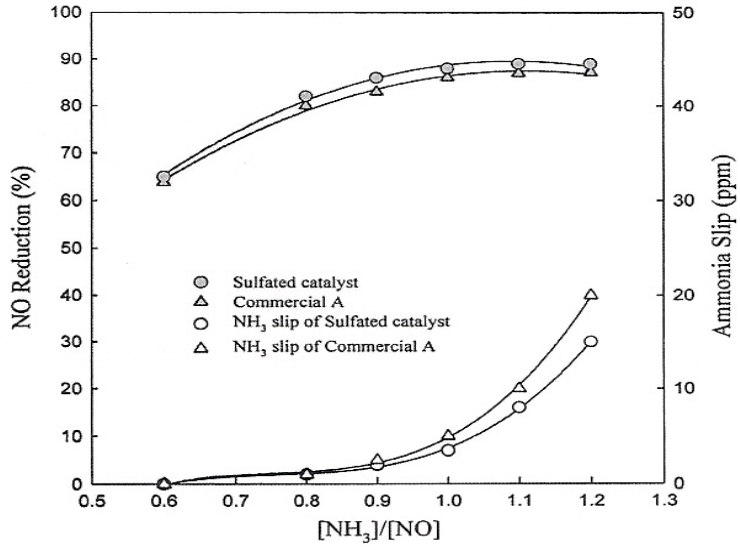

Figure 17. The effect of NH_3-to-NO mole ratio on NO reduction and ammonia slip of V_2O_5-based catalysts at 350ºC. (space velocity = 4000 h^{-1}) [32].

2.1.6 Effect of NH_3-to-NO Mole Ratio

NH_3-to-NO mole ratio is one of the critical values for catalytic reactions because it can affect NO removal and ammonia slip [32]. This ammonia slip leads to secondary impacts such as the formation of ammonia sulfates in the presence of SO_3 [32]. In the catalytic reactions, it is recommended that ammonia slip is kept below 5 ppm to prevent the formation of ammonia sulfates, and NO reduction should be obtained more than 85% [32, 36].

Figure 17 describes the effect of NH_3-to-NO mole ratio on the NO reduction and the ammonia slip of V_2O_5-based catalysts at a reaction temperature of 350ºC and space velocity of 4000 h^{-1} [32]. NO reduction increases with increasing NH_3-to-NO mole ratio, however, the ammonia slip increases as well. The NO reduction and ammonia slip increase rapidly in the ranges of low and high NH_3-to-NO mole ratio, respectively. Therefore, NH_3-to-NO mole ratio should be between 0.9 and 1.0 to satisfy low ammonia slip and high NO reduction [32].

Figure 18 shows the influence of NH_3-to-NO ratio of inlet on the conversion of NO at various reaction temperatures on V_2O_5-MoO_3-WO_3/TiO_2/Al_2O_3/cordierite-honeycomb catalysts with space velocity of 6000 h^{-1} and oxygen ratio of 5% [33]. Higher NO conversion is obtained between NH_3-to-NO ratio of 1.2 - 1.6 for all cases, but no significant .effect is described [33]. NO conversions of NH_3-to-NO ratio of 1.2 have been found to be reasonable for the reactions [33].

2.1.7 N_2O and NO_2 Production

It is well known that the production of nitrous oxide (N_2O) is responsible for a decline of the selectivity of the SCR reaction [29]. N_2O formation is usually observed at temperatures above about 350ºC. The values of N_2O formation at 450ºC are described in figure 8. It can be observed that the formation of N_2O increases with an increase in vanadium content of the catalyst [29]. When the vanadium content increases from 2 to 3%, the large increase of N_2O formation is seen. The large increase of N_2O formation for 3% vanadium content catalyst could explain the decrease of NO conversion [29].

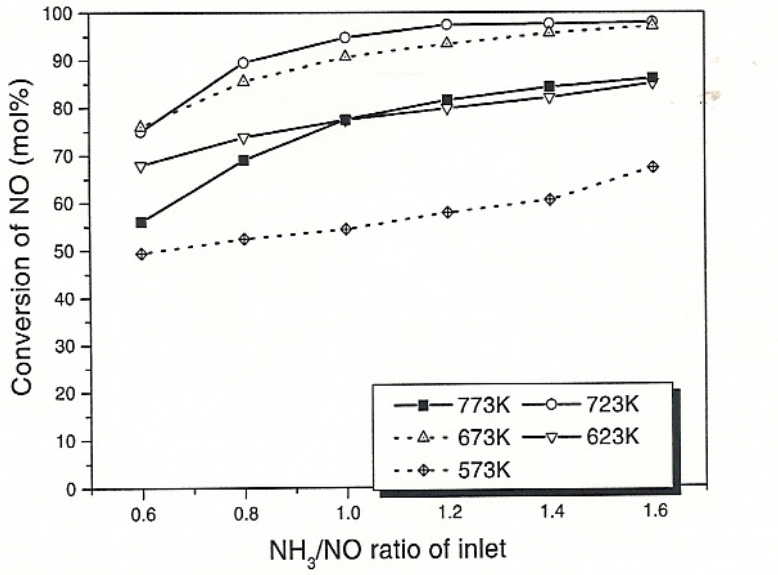

Figure 18. The correlation between NH_3/NO ratio of inlet and the conversion on NO at various reaction temperatures on V_2O_5-MoO_3-WO_3/TiO_2/Al_2O_3/cordierite-honeycomb. (SV = 6000 h^{-1}, oxygen ratio = 5%) [33].

NO_2 and N_2O production for SCR processes with ammonia over V/Ti based catalysts under the conditions of [NO] = 330 ppm, [NH_3] = 264 - 660 ppm, O_2 = 0 - 3.0%, space velocity = 7000 - 64000 h^{-1} were reported by Gupta [37]. An increase in oxygen concentration increases the production of NO_2 but decreases the production of N_2O [37]. The concentration of NO_2 was lower than approximately 5 ppm at reaction temperatures below 350ºC but increases steeply reaction temperatures above 350ºC [37]. The concentration of N_2O reaches a maximum at reaction temperatures between 350ºC and 400ºC, then decreases at higher temperatures.

When the NH_3-toNO ratio increases, the production of N_2O increases, but no significant effect is observed for NO_2 production [37]. An increase in space velocity decreases the production of N_2O and NO_2 [37]. The concentrations of NO_2 are obtained lower than 3 ppm. Concentrations lower than 3 ppm can be safely assumed to be an uncertainty or error in experimental measurement [37].

2.2 Pillared Interlayer Clay (PILC)-Based Catalysts

Pillared interlayer clay catalysts represent a new class of microporous materials that have found a wide range of potential applications in catalytic, adsorption and separation processes [38, 39]. Pillared interlayer clay catalysts are unique two-dimensional zeolite-like materials [39]. PILC catalysts have been extensively studied for selective catalytic reduction of NO_x with ammonia and hydrocarbons. The first results using PILC catalysts as superior catalysts for selective catalytic reduction of NO with ammonia were reported by Yang et al. in 1992 [40]. In their report, PILC catalysts with TiO_2, Fe_2O_3, Al_2O_3, ZrO_2, and Cr_2O_3, clusters showed very active in $DeNO_x$ process with ammonia. Apart from Cr_2O_3-PILC, all catalysts above exhibited resistant for SO_2 poisoning [40]. PILC catalysts were introduced as potential commercial catalysts.

PILC catalysts are prepared by exchanging the charge-compensation cations between the clay layers with larger inorganic hydroxy metal cations [41, 42, 43]. After heating, the intercalated species called metal polyoxycations are converted into the corresponding metal oxide clusters at high temperatures that are rigid enough not only to prevent the interlayer spaces from collapsing, but also to generate micropores larger than those of conventional zeolite catalysts [38, 39].

PILC-based catalysts show remarkable performance for selective catalytic reduction of NO_x with ammonia [42]. It was found that the catalytic activity for the SCR reaction increased in an order of Al_2O_3-PILC < ZrO_2-PILC < TiO_2-PILC < Fe_2O_3-PILC < Cr_2O_3-PILC [24, 40, 42]. Even though, Cr_2O_3-PILC catalysts exhibit the most catalytic activity, Cr_2O_3-PILC catalysts lost their activity in the presence of sulfur dioxide [42]. Among the PILC catalysts described above, titania-based PILC catalysts have outstanding characteristics: high thermal and hydrothermal stability, durability and large pore sizes [39]. Large pore sizes of TiO_2-PILC catalyst allow further incorporation of active species without hindering pore diffusion [39]. Also, the method of intercalating TiO_2 between the SiO_2 layers is the unique way of increasing surface area and acidity of the TiO_2 support [39]. A major characteristic of titania-based catalysts for the SCR reaction is their high resistance to SO_2 poisoning.

Ion-exchanged PILC catalysts performed better catalytic reactions than pure PILC catalysts for selective catalytic reduction of NO_x with ammonia. Among the ion-exchanged PILC catalysts, Fe-exchanged TiO_2-PILC obtained better catalytic activity than commercial V_2O_3+WO_3/TiO_2 catalysts [42, 43]. The catalytic activity on Fe-TiO_2-PILC catalysts was increased by the presence of H_2O and SO_2 which was attributed to an increase of surface acidity of the catalysts due to the formation of sulfate species of iron ions [42]. A promoter, Ce^{3+} that did not improve the catalytic activity for vanadia catalysts, was effective for Fe-TiO_2-PILC catalysts [42].

It is well known that the surface acidity is a significant factor for SCR of NO_x with ammonia [43]. The strong acidity is beneficial for the activation and adsorption of ammonia [43, 44]. The surface acid sites on TiO_2-PILC catalysts are different from those on TiO_2 catalysts [43]. Both Brønsted acid sites (V-OH) and Lewis acid sites (Ti-OH) exist on TiO_2-PILC, while only Lewis acid sites exist on TiO_2 [30, 40, 43, 45]. Both Brønsted and Lewis acid sites enhance the catalytic activity for the SCR reaction [16, 46]. The acidity and Brønsted and Lewis acid sites depend mainly on the starting clay, the preparation method and the exchanged cations [46].

Catalytic performance of PILC catalysts strongly depends on the conditions of intercalation process and the type of pillaring agent [41]. Catalytic activity of PILC catalysts in $DeNO_x$ process can be increased by their modification with different transition metals such as Cu, Fe and V [41]. However, the preparation method of transition metals affects catalytic performance of the SCR catalysts [41]. Among transition metals mentioned above, a few studies describing the preparation of Vanadium/PILC catalysts can be found in the literature [47]. One way of the preparation of Vanadium/PILC catalysts was introduced by M.A. Vicentr et al. [47]. In their report, various supported vanadium-containing catalysts were prepared by impregnation of both the natural and Al-pillared forms of a montmorillonite and a saponite with $NaVO_3$ precursor aqueous solutions [47]. As a result, no significant differences were found between montmorillonite-based and saponite-based catalysts, but the catalytic behavior of these two catalysts still merit to be investigated [47].

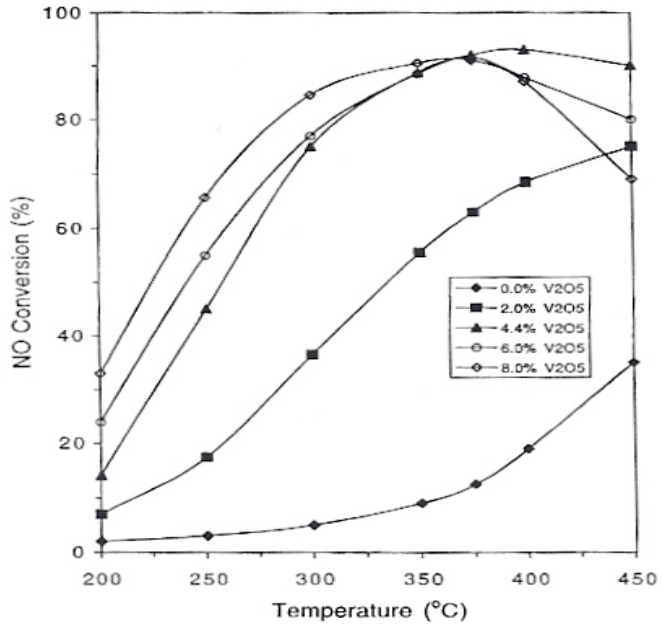

Figure 19. Catalytic activity for the SCR reaction on the 0 - 8.0% V_2O_5/TiO_2-PILC catalysts in the absence of H_2O and SO_2. Reaction conditions: 0.3 g catalyst, [NO] = $[NH_3]$ = 1000 ppm, $[O_2]$ = 2%, He = balance, total flow rate = 500 ml/min, and GHSV = 75000 h^{-1} [24].

2.2.1 Effect of Vanadium Loading

Figure 19 describes the catalytic activity for the SCR reaction on the 0 - 8.0% V_2O_5/TiO_2-PILC catalysts in the absence of H_2O and SO_2 under the conditions of 1000 ppm NO, 1000 ppm NH_3, 2% O_2, gas hourly space velocity (GHSV) of 75000 h^{-1}, and 0.3 g catalyst [24]. Pure TiO_2-PILC catalyst shows a low level of activity for NO reduction, but continues to increase for increasing reaction temperatures. NO conversion for 2.0% vanadium catalyst increases at 200 - 450ºC. Catalysts of vanadium loading of 4.4 - 8.0% obtain maximum NO reduction at 375 or 400ºC, and then NO conversion declines slightly for higher temperatures. Between the temperatures of 200 - 375ºC, NO conversion of all catalysts increases with an increase in vanadium loading from 0 to 8.0%. At the temperature above 375ºC, the highest NO conversion is obtained for the 4.4% V_2O_5/TiO_2-PILC catalyst.

The catalytic performance of various vanadium loading PILC-based catalysts for the selective catalytic reduction of NO with ammonia is summarized in table 2 [43]. The catalytic reactions were performed under the conditions of [NO] = 1000 ppm, [NH_3] = 1000 ppm, 2% oxygen concentrations, a catalyst sample of 0.3 g, balance He, total flow rate of 500 ml/min, gas hourly space velocity (GHSV) = 75000 h^{-1}, and in the absence of H_2O and SO_2 [43].

Pure TiO_2-PILC catalyst shows very low level of catalytic activity for NO conversion at reaction temperatures between 200 - 400ºC, while the catalytic activity of all cases of the vanadia-exchanged TiO_2-PILC catalysts is significantly enhanced under the same conditions. At reaction temperatures between 200 - 375ºC, the catalytic activities for NO conversion of VO-TiO_2-PILC catalysts between vanadium content of 2.1 - 3.5 wt% increase with increased reaction temperature and reach the maximum NO conversions at 375ºC. And then, NO conversions of all cases decreased slightly for higher reaction temperatures. The catalytic activities of all catalysts, except vanadium content of 13.2 wt%, increase with an increase in vanadium content.

VO(13)-TiO_2-PILC catalyst of 13.2 wt% vanadium content shows more active than pure TiO_2-PILC catalyst, but the catalytic activity for NO conversion is lowest among vanadia-exchanged catalysts. The reaction temperature of the maximum NO conversion of VO(13)-TiO_2-PILC is shifted toward lower temperature as compared with other vanadia-exchanged catalysts. The highest NO conversions among the catalysts are obtained on the VO(4)-TiO_2-PILC catalyst of 3.5 wt% vanadium content at overall reaction temperatures and found the maximum NO conversion (94.5%) at the reaction temperature 375ºC [43].

The comparison between VO-TiO_2-PILC catalysts and commercial 4.4% V_2O_5 + 8.2% WO_3/TiO_2 catalysts under the same conditions is also described in table 2 [43]. At the reaction temperatures between 350 - 400ºC, NO conversions of vanadium loading of 2.1 - 3.5 wt% and commercial catalysts show similar results, but N_2 selectivities of vanadium loading catalysts are better [43].

Table 2. Catalytic performance of VO-TiO_2-PILC catalysts [43].

Catalysts	V Content (wt%)	Temperature (ºC)	NO Conversion (%)	Selectivity (%)	
				N_2	N_2O
TiO_2-PILC	0	200	2.0	100	0
		250	3.2	100	0
		300	5.0	100	0
		350	9.0	100	0
		375	12.5	100	0
		400	19.0	100	0
VO(2)-TiO_2-PILC	2.1	200	12.0	100	0
		250	35.0	100	0
		300	65.0	100	0
		350	88.0	100	0
		375	93.0	100	0
		400	93.0	100	0
VO(3)-TiO_2-PILC	2.5	200	20.6	100	0
		250	47.8	100	0
		300	72.5	100	0
		350	89.3	100	0
		375	93.5	99.8	0.2
		400	93.0	99.6	0.4
VO(4)-TiO_2-PILC	3.5	200	34.3	100	0
		250	65.4	100	0
		300	86.0	100	0
		350	94.0	99.2	0.8
		375	94.5	98.8	1.2
		400	93.8	97.7	2.3
VO(13)-TiO_2-PILC	13.2	200	50.4	99.3	0.7
		250	65.3	99.0	1.0
		300	80.0	98.5	1.5
		350	85.0	97.0	3.0
		375	83.5	95.3	4.7
		400	70.0	92.3	7.7
4.4% V_2O_5 + 8.2% WO_3/TiO_2	4.4	350	92.2	97.2	2.8
		375	93.0	95.3	4.7
		400	90.5	91.8	8.2

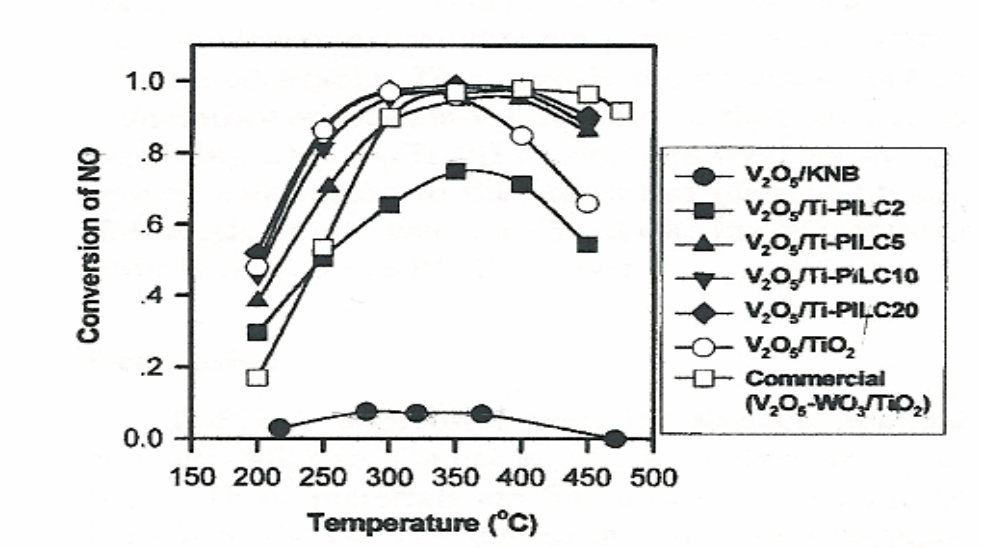

Figure 20. NO removal activity of V_2O_5/TiO_2-PILC catalysts with 1 - 20 mmol Ti/g of clay titanium content under the conditions of 500 ppm NO, 500 ppm NH_3, 5% O_2, and space velocity of 100,000 h^{-1} [25].

2.2.2 Effect of Reaction Temperature

Figure 20 represents the NO removal activity of V_2O_5/TiO_2-PILC with titanium content of 1 - 20 mmol Ti/g of clay [25]. The performances took place under the conditions of 500 ppm NO, 500 ppm NH_3, 5% O_2, and space velocity of 100,000 h^{-1} [25]. The maximum reaction temperature of a commercial V_2O_5-WO_3/TiO_2 catalyst is obtained at 350 - 400°C. For V_2O_5/TiO_2-PILC catalysts with varied titanium content, the maximum reaction temperatures are obtained approximately 350ºC. In addition, without any catalyst promoter such as WO_3, and MoO_3, V_2O_5/TiO_2-PILC catalysts reveal superior NO removal activity to a commercial V_2O_5-WO_3/TiO_2 catalyst, particularly in the range of the reaction temperature less than 350ºC [25]. This may be due to the peculiar physicochemical characteristics of Ti-PILC catalyst [25].

It is shown in many cases that the catalytic activity for NO conversion increases from 200 to 375 or 400ºC and obtains the maximum NO conversion at 375 or 400ºC. Then the catalytic activity decreases at higher temperatures as presented in figure 19, table 2 and figure 20.

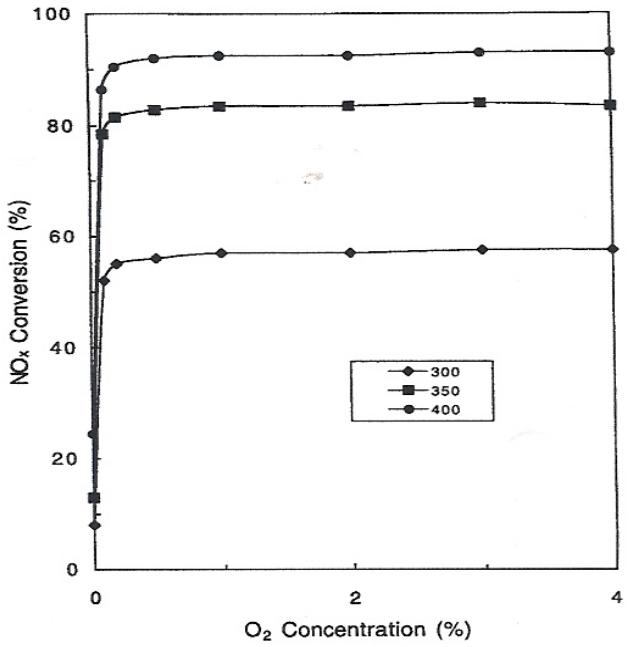

Figure 21. The effect of O_2 concentration on the catalytic activity for Fe(6)-TiO_2-PILC at different temperatures. Reaction conditions: 0.2 g catalysts, [NO] = [NH_3] = 1000 ppm, [O_2] = 0 - 4%, He balance, total flow rate = 500 ml/min, and GHSV = 113,000 l/hr [48].

2.2.3 Effect of Oxygen Concentration

Figure 21 describes the effect of oxygen concentration on the catalytic activity for Fe(6)-TiO_2-PILC catalysts at different temperatures under the conditions of 0.2 g catalysts, [NO] = [NH_3] = 1000 ppm, [O_2] = 0 - 4%, He = balance, total flow rate = 500 ml/min, and GHSV = 113,000 l/hr [48]. The catalytic activity for the SCR of NO with ammonia on Fe-TiO_2-PILC is very low at 300 - 400ºC in the absence of O_2 [48]. However, when very small amounts (0 - 0.3%) of oxygen are introduced in the reaction, the catalytic activity increased rapidly [48]. NO_x conversion for all cases in figure 21 stays almost steady after oxygen concentration of 0.5%. Long and Yang [48] also verified that oxygen contributes very important affects to the selective catalytic reduction of NO with ammonia.

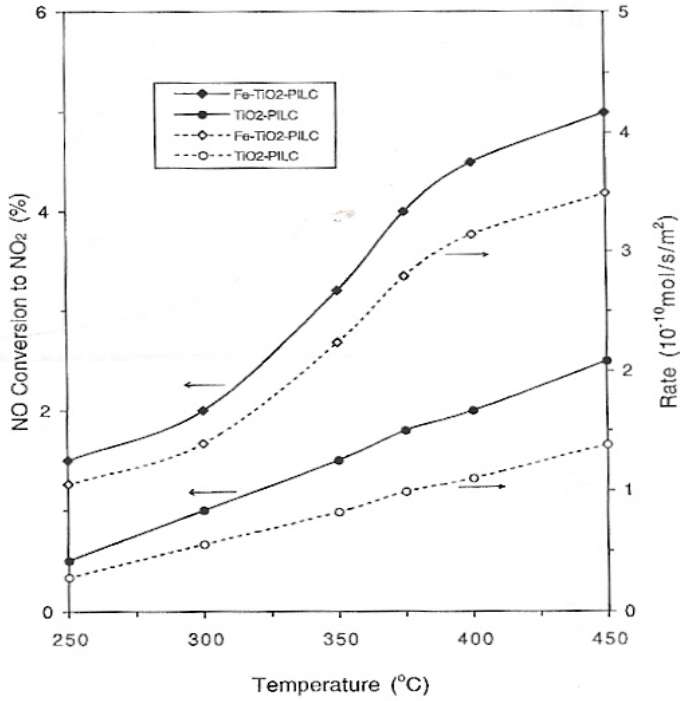

Figure 22. Oxidation activity of NO to NO_2 by oxygen on Fe-TiO_2-PILC and TiO_2-PILC catalysts for the SCR reaction under the conditions of 0.2 g of sample, 1000 ppm NO, 2% O_2, and total flow rate of 500 ml/min [49].

2.2.4 N_2O and NO_2 Production

In figure 22, the oxidation activity of NO to NO_2 by oxygen on Fe-exchanged TiO_2-PILC and pure TiO_2-PILC catalysts for the SCR of NO with ammonia is obtained [49]. The catalytic reactions were performed under the conditions of a catalyst sample of 0.2 g, [NO] = 1000 ppm, 2% oxygen concentration, and total flow rate of 500 ml/min [49]. The oxidation activity of NO to NO_2 on the pure TiO_2-PILC catalyst are obtained less than 2% in the ranges of the reaction temperature at 250 - 450ºC, while the Fe-TiO_2-PILC catalyst has higher oxidation activity under same conditions. This result indicates that iron ions on Fe-TiO_2-PILC catalysts affect the increasing of the oxidation reaction rate of NO to NO_2 as compared with the pure TiO_2-PILC catalysts [49].

Table 3. Oxidation of NO to NO_2 on Fe-TiO_2-PILC and sulfated Fe-TiO_2-PILC [50].

Catalysts	Temperature (ºC)	NO conversion to NO_2 (%)	Selectivity (%)		
			N_2	N_2O	NO
Fe-TiO_2-PILC-S (0%)	300	5.0	100	0	0
	350	6.0	82	1	17
	400	6.6	69	1	30
	450	6.9	78	1	21
Fe-TiO_2-PILC-S (0.7%)	300	5.1	100	0	0
	350	6.0	97	0	3
	400	6.2	84	2	14
	450	6.4	85	1	14
Fe-TiO_2-PILC-S (1.8%)	300	2.8	100	0	0
	350	2.9	100	0	0
	400	4.6	87	1	12
	450	4.9	87	1	12

The oxidation activity of NO to NO_2 by O_2 on Fe-TiO_2-PILC and sulfated Fe-TiO_2-PILC catalysts for the SCR of NO with ammonia is shown in table 3 [50]. The reactions occurred under the conditions of 0.1 g catalyst sample, 1000 ppm NO, 2% O_2, He = balance, total flow rate of 500 ml/min, and GHSV = 230,000 h^{-1} [50]. The NO conversion to NO_2 is enhanced with increased reaction temperature for all catalysts and reaches the maximum at the reaction temperature 450ºC. The oxidation activities of Fe-TiO_2-PILC without sulfur are higher than those of sulfated Fe-TiO_2-PILC catalysts for all range of reaction temperatures under the same conditions [50]. For sulfated Fe-TiO_2-PILC catalysts, the oxidation activity increases with decreasing sulfur content from 1.8 to 0.7% [50].

A few results describing N_2O concentration for selective catalytic reduction on NO with ammonia on PILC-based catalysts can be found in the literature. Long and Yang [43] reported briefly that much N_2O was formed at elevated reaction temperatures than 350ºC due to the oxidation of ammonia by O_2.

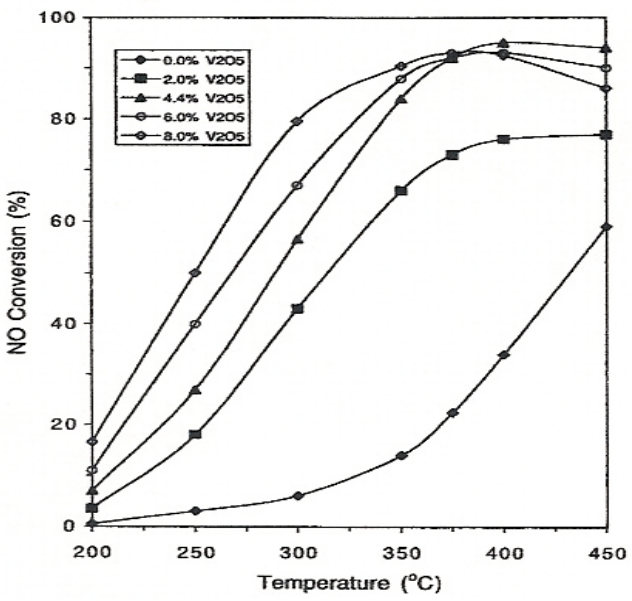

Figure 23. Catalytic activity on NO conversion for the SCR reaction on the 0 - 8.0% V_2O_5/TiO_2-PILC catalysts in the presence of H_2O and SO_2. Reaction conditions: [NO] =1000 ppm, [NH_3] = 1000 ppm, [O_2] = 2%, [H_2O] = 8%, [SO_2] = 1000 ppm, 0.3 g catalyst sample, He = balance, total flow rate = 500 ml/min, and gas hourly space velocity (GHSV) = 75000 h^{-1} [24].

2.2.5 Effect of H_2O and SO_2 Addition

Figure 23 presents the catalytic activity for the selective catalytic reduction of NO with ammonia on the 0 - 8.0% V_2O_5/TiO_2-PILC catalysts in the presence of H_2O and SO_2 [24]. The reactions took place under the same condition described in figure 19, but the only difference was the reaction in the presence of H_2O and SO_2. 8% H_2O and 1000 ppm of SO_2 was used to the catalytic reaction. From the compared results between figure 19 and figure 23, at low temperatures below 300ºC, the catalytic activity is decreased for all catalysts because the inhibition effect of H_2O at low reaction temperatures [24]. On the other hand, NO conversion increases slightly on the 0 - 8.0% V_2O_5/TiO_2-PILC catalysts at high reaction temperatures above 350ºC [24]. At the reaction temperature above 375ºC, the highest catalytic activity is obtained for the 4.4% V_2O_5/TiO_2-PILC catalyst which is the same result in figure 19.

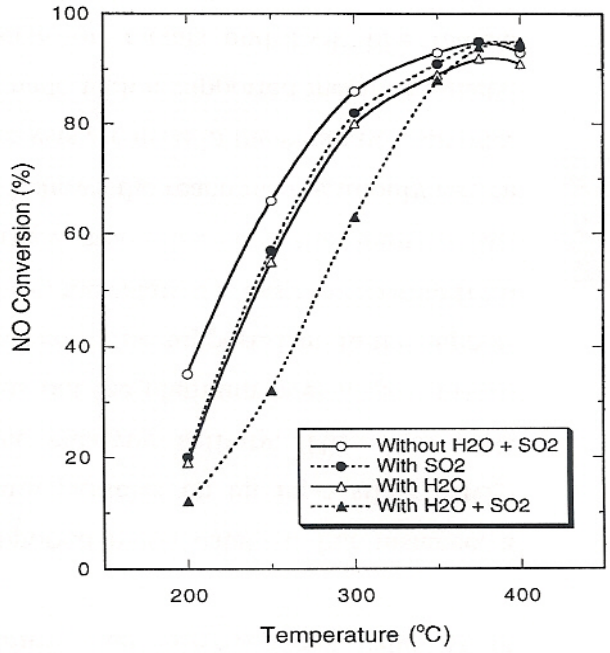

Figure 24. Effect of H_2O and SO_2 (separately and together) on the catalytic activity for the SCR of NO with ammonia on VO(4)-TiO_2-PILC (3.5 wt% vanadium). Reaction conditions: 0.3 g catalyst, [NO] = [NH_3] = 1000 ppm, [O_2] = 2%, [H_2O] = 8% (when used), [SO_2] = 1000 ppm (when used), He = balance, total flow rate = 500 ml/min, and GHSV = 75000 h^{-1} [43].

In figure 24, the effect of H_2O and SO_2 (separately and together) on the catalytic activity for the selective catalytic reduction of NO with ammonia on VO(4)-TiO_2-PILC (3.5 wt% vanadium) catalyst is presented [43]. NO conversion in the presence of H_2O and SO_2 shows the lowest level at reaction temperatures below 350ºC, while the difference of NO conversion among catalysts is negligible at the temperature above 375ºC [43]. At the temperature below 350ºC, NO conversion is increased in an order of the reaction in the presence of H_2O and SO_2 < in the presence of only H_2O < in the presence of only SO_2 < in the absence of H_2O and SO_2. No significant difference between the catalytic activities in the presence of only H_2O and only SO_2 is measured for all temperatures. The inhibition effect of H_2O occurs at reaction temperatures below 350ºC, but the inhibition effect of H_2O decreased with increasing temperature [43].

2.3 Summary and Conclusions

The effect of various parameters on the removal of NO for the SCR process was reviewed in this section. For both vanadia-based and pillared interlayer clay-based catalyst, every parameter had significant effects on NO reduction. The vanadium content was found to have a great influence on the SCR activity on NO reduction. With an increase in vanadium content, high NO reduction was obtained. The addition of WO_3 significantly improved the catalytic activity at low temperatures and broadened the temperature window of the maximum NO reduction. High NO reduction was determined in the presence of small amounts of oxygen concentration (from 0 to 1.0%), but a slight increase of NO reduction was observed from 1% to 7% oxygen concentration. Space velocity is, one of the most important factors for a catalytic design, is in inverse proportion to the volume of a catalyst. NO reduction improved with a decrease in space velocity or with an increase in the volume of the catalyst. Because NH_3-to-NO ratio affects NO removal and ammonia slip, it is one of the critical values for catalytic reactions. High NO reduction was obtained with an increase in NH_3-to-NO ratio, but the ammonia slip was increased as well. Therefore, NH_3-to-NO ratio should be between 0.9 and 1.0 to satisfy high NO reduction and low ammonia slip.

3. OBJECTIVES

The overall goal of the current research project is to investigate the selective catalytic reduction (SCR) of NO by ammonia over vanadia-based (V_2O_5-WO_3/TiO_2) and pillared interlayer clay-based (V_2O_5/Ti-PILC) catalysts.

The first part of this work is to obtain the effect of different parameters e.g. space velocities, temperatures, preheating, varying NH_3-to-NO feed ratio, and increasing inlet oxygen concentration over V_2O_5-WO_3/TiO_2 catalyst. Moreover, physical arrangements of a catalyst will be investigated under three cases over V_2O_5-WO_3/TiO_2 catalyst. The first case will be performed over 2 cm long monolithic catalyst samples (standard case). The second arrangement will be preformed over 2 cm long catalyst samples that are cut off 1 cm long each and stick together with 45° twist in the quartz-tube. The third arrangement will be tested over 2 cm long catalyst samples that are cut off 1 cm long each and placed 5 cm away each other with 45° twist in the quartz-tube. The purpose of the performance of the second and third cases is to minimize the 'slip' of gases. Thus hypothetically more reactions may be expected.

The second part of this work is to investigate the effect of vanadium coating, several NH_3-to-NO feed ratios and varying inlet oxygen concentration under the similar conditions over pillared interlayer clay-based (V_2O_5/Ti-PILC) catalysts.

The results of NO_x over vanadia-based (V_2O_5-WO_3/TiO_2) and pillared interlayer clay-based (V_2O_5/Ti-PILC) catalysts will then be compared to the results from previous experiments with vanadia-based (V_2O_5/TiO_2) and zeolite-based (Cu-ZSM-5) catalysts.

4. EXPERIMENTAL SYSTEMS AND DESCRIPTIONS

The experimental apparatus is composed of five distinct systems: (1) source of simulated exhaust gas, (2) mass flow controllers (MFC), (3) the furnace and reactor assembly with a catalyst sample in reaction zone, (4) a filtration system for undesirable particles from a catalyst, and (5) the output gas mixture analysis system (Fourier transform infrared spectrometer). Each of these systems is described in the following section.

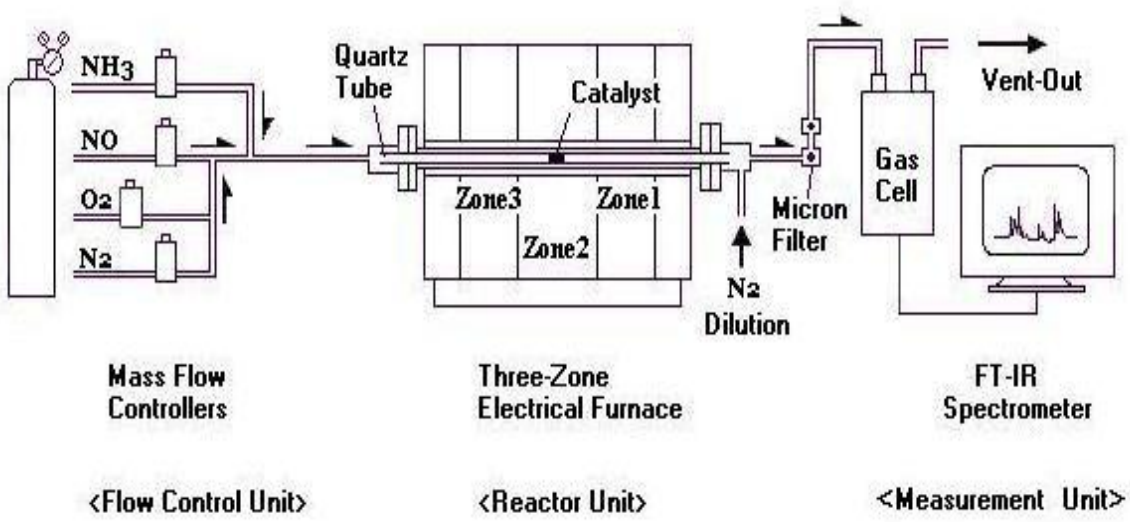

Figure 25. Schematic of the experimental apparatus used to perform NO removal.

4.1 Overview of the Experimental System

Figure 25 is a schematic of the experimental system. First, the mass flow controllers were calibrated individually with various gases (NO, NH_3, O_2 and N_2) and had accuracies ± 1.0% of full scale. This is described in more detail in Appendix A1. Gases from standard gas cylinders flowed into each MFC which controlled their concentrations and then were mixed together. The simulated mixture gas in a well-mixed form entered into the quartz-tube reactor inside the furnace.

Table 4. Concentrations of gas species in the standard gas cylinder used for experiments.

Species	Compositions in the cylinder	Purity	Supplier
NO	1.04% NO and 98.96% N_2	± 1%	Scott Specialty Gases, Inc.
NH_3	0.5207% NH_3 and 99.4793% N_2	± 1%	Scott Specialty Gases, Inc.
O_2	48.91% O_2 and 51.09% N_2	± 1%	Scott Specialty Gases, Inc.
N_2	100 % N_2	99.99%	Matheson Tri-Gas

The total flow rate of the simulated mixture was 1100 sccm (standard cubic centimeter per minute at O°C and 1 atm). A quartz tube (ID=20 mm, length=1.04 m) was placed in a three-zone electrical furnace that has an electronic temperature control unit. The variation of the temperature would be done in the range from the ambient temperature to 450°C with a temperature step of 50˚C or 100˚C. The catalyst sample was placed near the center of the quartz-tube (zone 2) along the length. By using different lengths of the catalyst sample, the space velocity can be varied. The output gas after reaction from the reactor was diluted by 5000 sccm of pure nitrogen gas and then passed through a 140 micron (μm) filter (to collect particulates, if any) and a 60 micron (μm) filter in sequence. The output gases of 6100 sccm included dilution gas flowed into the gas cell of the FTIR spectrometer where the composition of the simulated gas was analyzed. Necessary calibrations were completed to quantify the FTIR spectrum for each species, prior to the main experiments. Then, the gases were vented out to the atmosphere.

4.2 Source of Simulated Exhaust Gas

The compositions of the simulated gas were chosen based on the actual exhaust gas configurations of the general combustion. To avoid the inherent complexities of dealing with the exhaust gas from actual combustion sources, such as particulate emissions and transient irregularities in NO concentrations, this source of simulated exhaust gas was used.

Table 5. Mass flow controllers used for the experimental system.

MFC #	Manufacturer	Maximum flow capacity (sccm)	Gas used
1-3	MKS Instruments	200	NO/N_2
1-4	MKS Instruments	5000	N_2 (Dilution)
2-1	Precision Flow Devices	300	NH_3/N_2
2-2	Precision Flow Devices	300	O_2/N_2
2-4	Precision Flow Devices	1000	N_2 (Balance)

Each species was stored in the standard gas cylinder at pressures up to 2000 psi (pound per square inch). The concentrations of each gas species in the standard gas cylinder are listed in table 4. 1.04% NO, 0.5207% NH_3 and 48.91% O_2 in N_2, were used for this work. The pressure of the simulated gas stream was 40 psi by standard gas regulators. NO, balance N_2, and O_2 (if used) were mixed first to form the simulated exhaust gas stream, and ammonia was then injected into this simulated exhaust gas stream before entering the reactor system.

4.3 Mass Flow Controller (MFC)

As a means of controlling the flow of each constituent gas into the experimental system, five mass flow controllers were used (three of the PFD 401 series by Precision Flow Devices, Inc., and two of the MKS type 1179A by MKS Instruments). Table 5 shows the list of mass flow controllers used, MFC manufacturers, their maximum flow capacity (sccm) and used gases. MFC #1-4 and #2-4 were used for dilution N_2 of 5000 sccm and balance N_2, respectively. Figure 26 presents a diagram of the front panel controls of the MKS type 247D four-channel power supply/readout that connected to the MKS type mass flow controllers [17]. To set the desirable concentration of each species, select the MFC using the channel selector, lift up read/set point switch and then revolve the set point control.

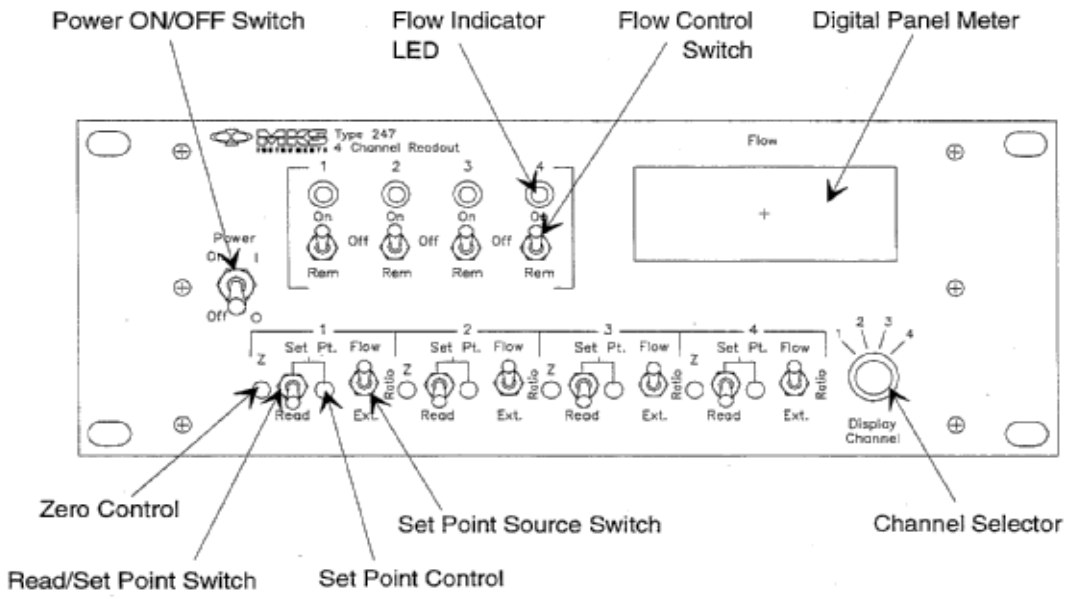

Figure 26. Front panel controls of MKS type 247D four-channel readout [17].

4.3.1 MFC Calibration Process

The gas flowing through the experimental system was collected in a glass flask. Initially, the glass flask was completely filled with water, which was displaced by the gas over time in ambient [51]. The time and displacement volume were measured, and the volume flow rate ($\dot{\forall}$) was obtained through the following equations [52]:

$$\dot{\forall} = \frac{\Delta \forall}{\Delta t} \equiv \frac{M_1 - M_2}{\rho_{H2O} \cdot t} \tag{4.1}$$

where M_1 and M_2 are weights of water at the beginning and the end.

To include the pressure difference from the changing water level in the glass flask during the displacement process, a correction term for the volume is required [51]:

$$\frac{\Delta \forall_{adjusted}}{\Delta t} = \left(\frac{P_0 - \rho_{H2O} \cdot gh}{P_0} \right) \left(\frac{T_0}{T} \right) \left(\frac{M_1 - M_2}{\rho_{H2O} \cdot t} \right) \tag{4.2}$$

The calibration procedures are described in more detail in Appendix A1.

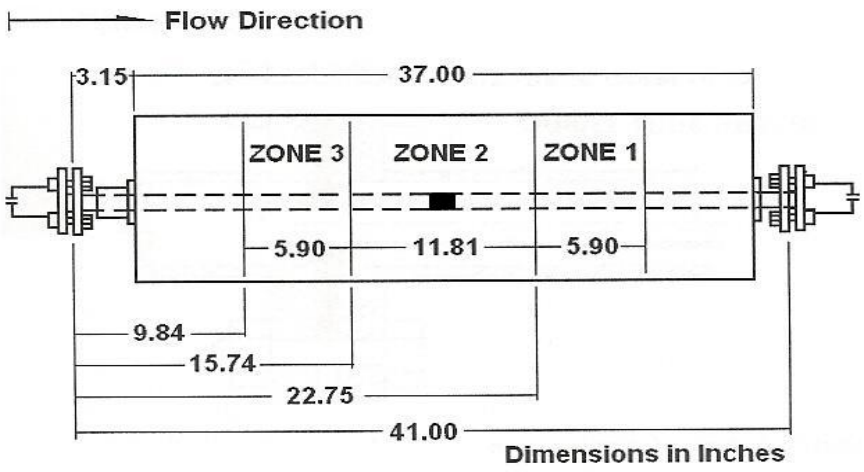

Figure 27. Schematic of the three-zone furnace system. All lengths in inches.

4.4 The Furnace and Reactor Assembly (Reaction Zone)

The simulated gas mixture flowing through the reactor was heated to reach desired temperatures by a three-zone furnace (Lindberg model number 54259), which has an electronic control unit (Lindberg model number 58475). Figure 27 represents the schematic of the three-zone furnace system. The initial and final heating zones of the furnace are 5.9 inches (15 cm) each long while the center zone is 11.81 inches (30 cm) in length. The energy produced by the heating zones is transferred to an Inconel 600 steel pipe in the entire length of the furnace. The quartz-tube reactor, which prevents catalytic reactions with the steel surface, is centrally located within the steel pipe. The reactor is 25.4 mm internal diameter tube of Inconel 600 which is 1.06 m long.

The steel pipe is threaded at both ends, and two 6.35 mm bolt flanges of 304 stainless steel are screwed on the ends as shown in figure 28 [53]. The quartz-tube is located in the center of the reactor with the support of graphite teflon gaskets made from Grafoil^{TM} sheets. The teflon gaskets were cut in annular shape with outer diameter greater than that of the steel pipe and internal diameter slightly smaller than that of the quartz-tube. The teflon gaskets seal the flanges on each end of the reactor. The temperature distribution in the furnace is described in more detail in Appendix A2.

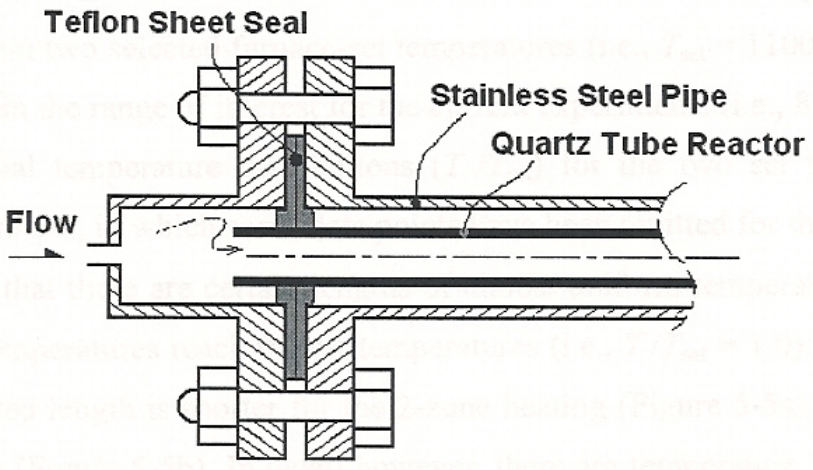

Figure 28. Teflon-sheet sealing between quartz-tube and steel tube [53].

The catalyst was placed near the center of the quartz-tube along the length where is in the middle of heating zone 2. To settle the catalyst sample in one place in the quartz-tube, a "dent" on the inside surface of the quartz-tube was made in the middle of heating zone 2. The dent is too small to change any conditions of the experiments.

4.4.1 Flow Regime

It is necessary to find whether the flow is laminar or turbulent for an internal flow in a circular tube (or pipe) for this work. In fully-developed region in a circular tube, the velocity distribution is parabolic as shown in figure 29 [53]. To determine laminar flow or turbulent flow, the Reynolds number must be obtained.

$$\mathrm{Re} = \frac{\rho VD}{\mu} = \frac{VD}{\nu} \tag{4.3}$$

where ρ is the fluid density (kg/m^3), μ is the dynamic viscosity (kg/sec·m), ν is kinematic viscosity (m^2/sec), V is the mean velocity of fluid, and D is the inside diameter of the quartz-tube. In general, the Reynolds number of laminar flow less than 2300.

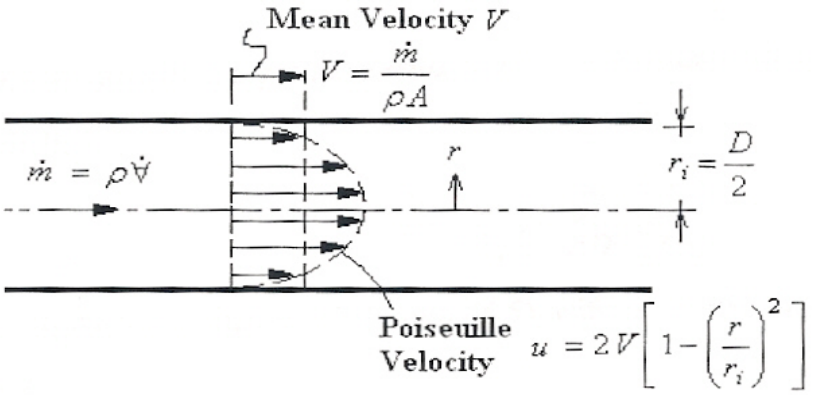

Figure 29. Fully-developed laminar velocity distribution in a circular tube [53].

Considering a gas mixture flowing through a quartz-tube of cross-sectional area (A), the mass flow rate and the mean velocity are

$$\dot{m} = \int_A (\rho u) dA = \rho A V \tag{4.4}$$

$$V = \frac{\dot{m}}{\rho A} = \frac{\dot{\forall}}{A} \tag{4.5}$$

where $\dot{\forall}$ is volume flow rate.

The initial volume flow rate ($\dot{\forall}_0$) in the reactor is 1100 sccm at atmosphere. P = P_0 and T_0 = ambient temperature (25°C) in this experiments. The volume flow rate depends on temperature.

$$\dot{\forall} = \dot{\forall}_0 \left(\frac{P_0}{P}\right)\left(\frac{T}{T_0}\right) = \dot{\forall}_0 \left(\frac{T}{T_0}\right) \tag{4.6}$$

$$V = \frac{\dot{\forall}}{A}\left(\frac{T}{T_0}\right) = \frac{4\dot{\forall}}{\pi D^2}\left(\frac{T}{T_0}\right) \tag{4.7}$$

Table 6. The percentages of each species in the simulated gas stream.

Species	Maximum capacity (sccm) and (MFC #)	MFC readout set points	Flow rate (sccm)	Percentage (%)
NO	200 (#1-3)	17.1	34.2	3.1
NH_3	300 (#2-1)	19.28 ~ 47.84	57.84 ~ 143.52	5.3 ~ 13.0
O_2	300 (#2-2)	0 ~ 22.51	0 ~ 67.53	0 ~ 6.1
N_2 (Balance)	1000 (#2-4)	81.87 ~ 98.57	818.7 ~ 985.7	75 ~ 90

Table 7. The Reynolds number at various temperatures for the current study.

Temperature (T)	Volume flow rate ($\dot{\forall}_0$) (sccm)	Diameter (D) (cm)	Kinematic viscosity (ν) of N_2 (m^2/sec)	Reynolds #
Ambient (25˚C)	1100	2.0	15.5×10^{-6}	75.3
450˚C	1100	2.0	70.43×10^{-6}	40.2

Therefore, the Reynolds number is

$$\mathrm{Re} = \frac{4\dot{\forall}_0}{\pi D \nu}\left(\frac{T}{T_0}\right) \tag{4.8}$$

For the current performances, the temperature varied from the ambient temperature (25˚C) to 450˚C, and the inner diameter of the quartz-tube was 2 cm. The thermodynamic properties of the simulated gas mixture were assumed to be those of pure nitrogen due to the high percentage of N_2 (balance) concentration in the simulated gas (at least 75 and 90% maximum as listed in table 6).

Table 7 shows the maximum and minimum Reynolds number for the current study. Figure 30 presents the Reynolds number as a function of the reaction temperature. Using the equation (4.8), the Reynolds numbers were calculated at constant volume flow rate and tube diameter. The Reynolds number was the greatest at ambient temperature (25˚C), and declined with an increase in reaction temperature.

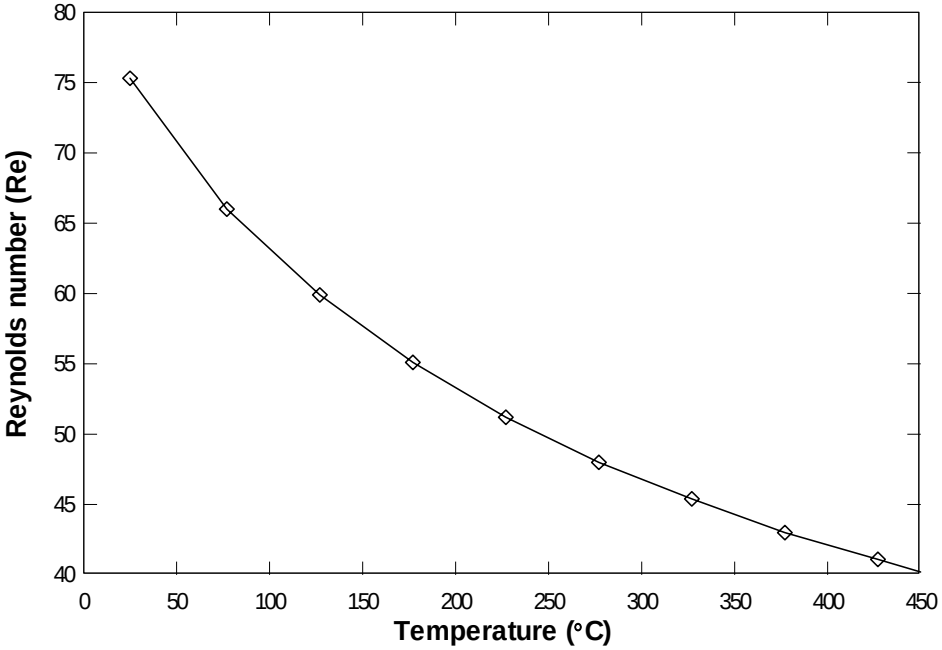

Figure 30. The Reynolds number as a function of the reaction temperature.

4.4.2 Catalyst Samples

The experiments were performed on two catalyst samples: vanadia-based (V_2O_5-WO_3/TiO_2) and PILC-based (V_2O_5/Ti-PILC) catalyst samples. Figure 31 shows (a) V_2O_5-WO_3/TiO_2 and (b) V_2O_5/Ti-PILC monolithic honeycomb catalyst samples. V_2O_5-WO_3/TiO_2 catalyst samples have smaller and more cells per cross-section area than V_2O_5/Ti-PILC samples. More details about suppliers and specifications for the two catalyst samples are listed in Appendix 3.

The catalyst samples were carefully handled because of their toxic components to inhale or swallow. Both original samples from suppliers were too big to be used for the current experiments. To obtain desirable space velocity, the sample had to be carefully cut off to make a snug fit into the quartz-tube as shown in figure 32.

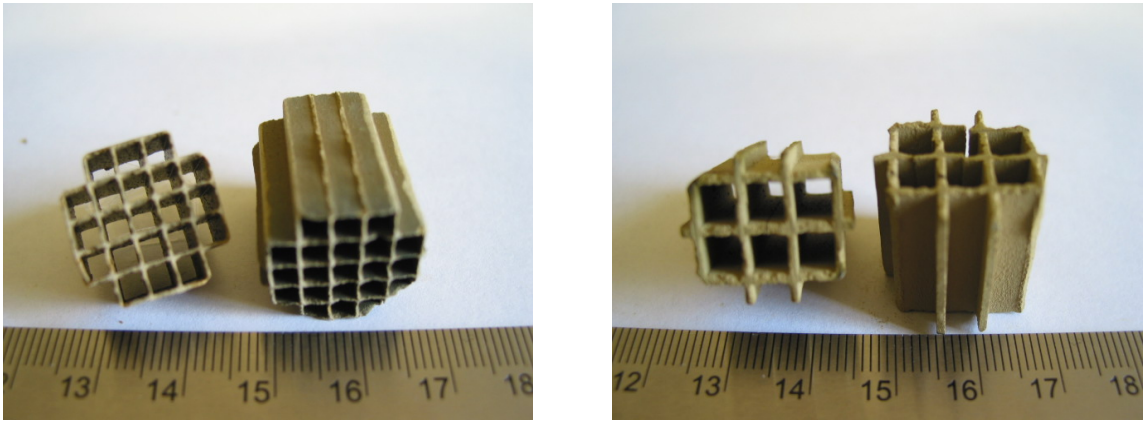

(a) (b)

Figure 31. Samples of (a) V_2O_5-WO_3/TiO_2 and (b) V_2O_5/Ti-PILC catalysts.

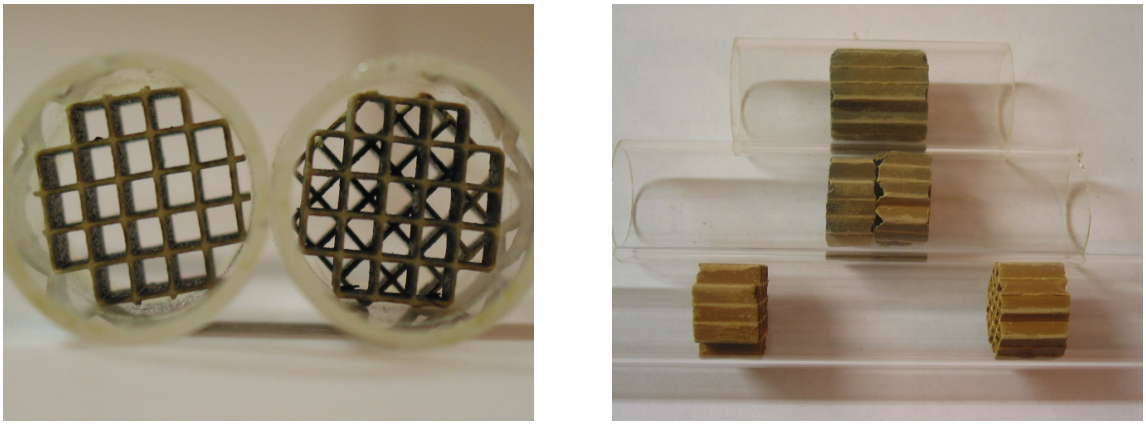

(a)
Cross-section areas

(b)
Arrangements

Figure 32. Different arrangements (or twist conditions) of V_2O_5-WO_3/TiO_2 catalysts.

Figure 32 presents different arrangements (or twist conditions) for V_2O_5-WO_3/ TiO_2 catalyst samples. Figure 32 (a) shows cross-section areas for a twist and a standard case. The left catalyst is for the standard case, and the right catalyst is for the twist case. Much more cells are shown because of twist of two catalysts. Figure 32 (b) shows the different arrangements for a standard, a twist, and a twist and separate case from the top.

A 2 cm long monolithic catalyst was used for the standard case. For the twist case, a 2 cm long catalyst was cut off 1 cm long each and stick together with 45° twist in the quartz-tube. For the twist and separate case, a 2 cm long catalyst was cut off 1 cm long each and placed 5 cm away each other with 45° twist in the quartz-tube. The purpose of the twist performance is to reduce the 'slip' of gases on the catalyst surface. To minimize the 'slip' of gases past the catalyst surface, two methods were tested. One was to make a snug fit for V_2O_5-WO_3/TiO_2 samples into the quartz-tube and to retain the 'wings' on the surface of the V_2O_5/Ti-PILC samples as shown in figure 31 (b). The other method was to use the "twist condition" of the catalysts as shown in figure 32 (a). The purpose of the performance of minimizing the 'slip' of gases was to increase more reactions on the catalyst surface.

V_2O_5/Ti-PILC catalyst and the vanadium coating procedures were provided by Postech Environmental Catalysis Laboratory (PECL) [54] in Korea. The vanadium coating procedures to coat vanadium on the catalyst surface is explained in more detail in Appendix A4. After 0.57 wt% vanadium (analyzed by Neutron Activation Analysis) were coated on the catalyst surface, the catalyst samples were dried at 100°C. Then, the samples were calcined at 500°C in flowing oxygen for 20 hours to decompose the ammonium salts into oxides [24, 31].

Space velocity is defined as the ratio of the total gas flow rate to the catalyst volume, expressed in per-hour. At a constant gas flow rate, space velocity is inversely proportional to catalyst volume such that increasing catalyst volume corresponds to decreasing space velocity. Table 8 lists space velocities used for 1 cm and 2 cm long samples. It was assumed that the same space velocity was used for the separate catalyst because the total length of two catalysts was as long as that of the one-piece catalyst.

Table 8. Space velocities calculation for the current experiments.

Catalyst length (cm)	Tube Diameter (cm)	Catalyst volume (cm^3)	Space velocity (h^{-1})
1	2	3.142	21000
2 (standard)	2	6.283	10500
1 + 1 (separate)	2	6.283	10500

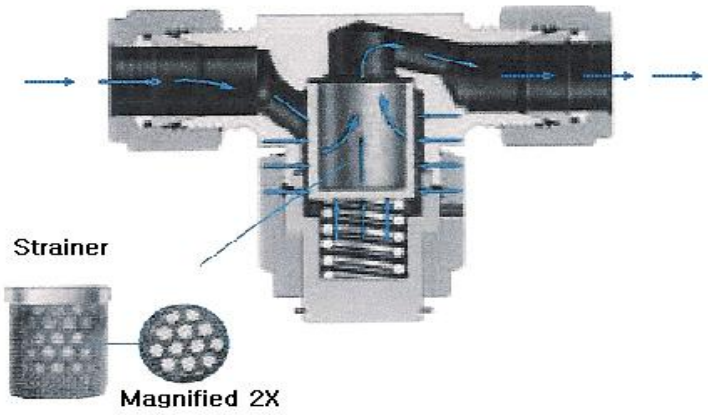

Figure 33. A sectional diagram of a tee type filter and a strainer [55].

$$\text{Space Velocity}\,(h^{-1}) = \frac{\text{Total Flow Rate}}{\text{Catalyst Volume}}$$

Table 9. Filtration systems for the current experiments.

Filter size	Body material	Part #	Type
140 micron	stainless steel	SS-4FT-140	Tee type
60 micron	stainless steel	SS-4FT-60	Tee type

4.5 The Filtration System

A filtration system to filter out unexpected impurities such as particles from a catalyst was placed between the electrical furnace and FTIR spectrometer as shown in figure 33 [55]. After reactions occurred in the furnace, the output gas diluted 5000 sccm of pure nitrogen passed through two tee type filters which were 140 micron (μm) and 60 micron (μm) filters in sequence as listed in table 9. The filtration system was replaced worn strainers with new ones provided by Swagelok Company [55] before the experiment.

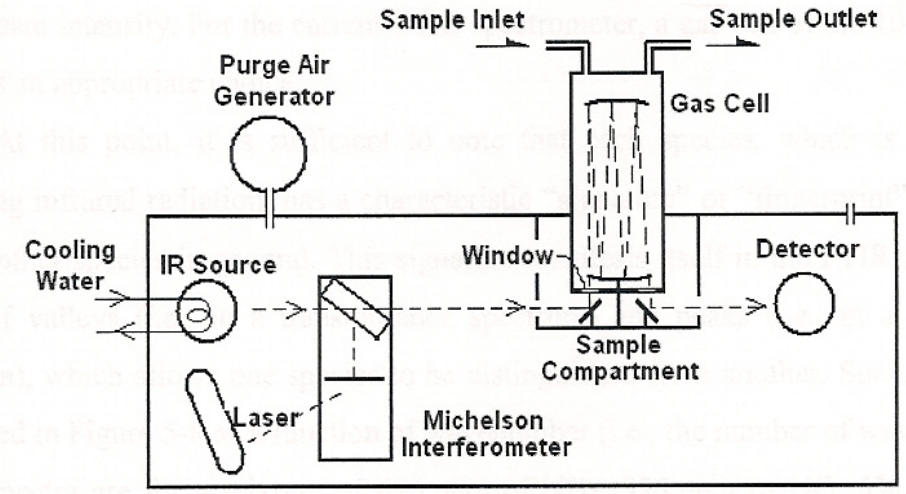

Figure 34. Schematic of FTIR spectrometer and the gas cell [53].

4.6 The Output Gas Analysis System (Fourier Transform Infrared Spectrometer)

After reactions occurred, to determine the concentration of the various species exiting in the reactor, a Fourier transform infrared (FTIR) spectrometer was used. Figure 34 shows the schematic of FTIR spectrometer, a gas cell and a purge gas generator [53].

The current Bio-Rad FTIR (FTS-60A) is equipped with He-Ne laser and a liquid nitrogen-cooled MCT (Mercury-Cadmium-Tellurium) detector which works in the range of wavenumber of 4000 to 400 cm^{-1}. Figure 35 shows a simple system of an IR spectrometer, in which infrared radiation emitted from a source passes through a sample that absorbs the radiation. The remaining radiation which has not been absorbed by the sample is transmitted to a detector which transfers data to a data processing device. Bio-Rad WinIR-pro version 2.96 software was used to collect data from FTIR for the current experiment. To determine which frequencies have been absorbed by the sample, the data processing device analyzes the transmitted radiation by means of IR spectrum. To operate the FTIR spectrometer properly, three coolants were used: the liquid nitrogen, water and ambient air. Water and ambient air flowed inside FTIR all the time, and the liquid nitrogen should be recharged in MCT detector daily for the experiments.

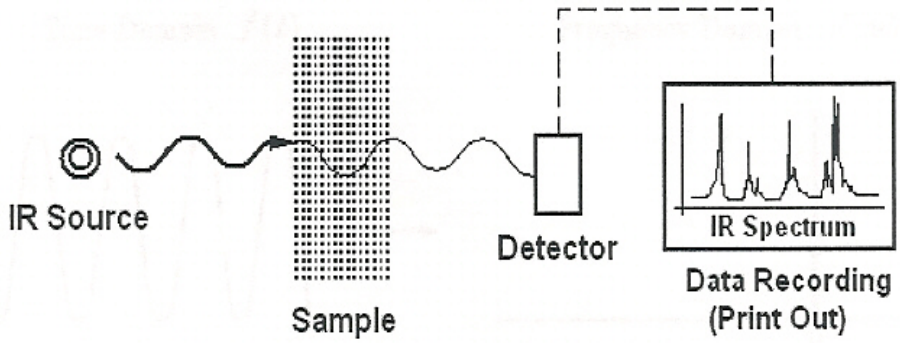

Figure 35. Simple representation of IR spectrometer [53].

After dilution, the total simulated mixture gas stream of 6100 sccm entered into the cylindrical-shape gas cell (Permanently Aligned Long Path cell) as shown in figure 34. Two beam splitters of both top and bottom in the gas cell create 10 meters of optical path, folded in a volume of 2.3 liters and analyze the output gas compositions. After the simulated mixture was analyzed in the gas cell, it vented out to the atmosphere.

Since the gas cell is made out of KBr crystal, which is sensitive to ambient air conditions, a purge gas generator is used to ensure proper air conditions. The purge gas generator is utilized to purge unwanted CO_2 and water vapor from the IR beam paths.

More details about various components of FTIR spectrometer, Permanently Aligned Long Path cell, and the purge gas generator are reported by Baek [53].

The calibration procedure and obtaining method of data for the different species used in the experiments for FTIR spectrometer are described in more detail by Park [17] and Baek [53].

5. EXPERIMENTAL PROCEDURES AND OBSERVATIONS

Prior to describing the actual experimental procedures, the standard conditions of the current experiment are provided. The total flow rate of the simulated mixture in the quartz-tube was 1100 sccm (standard cubic centimeter per minute at 0°C and 1 atm), regulated by the mass flow controllers. This standard condition is consistent with former studies completed by Gupta [37].

5.1 Procedures for Performing Experiments

First of all, to stabilize the flow rate from the mass flow controllers, the MFCs and the four-channel power supply/readout needed to be turned on at least two hours before the experiment begins. Liquid nitrogen, used as a coolant for the FTIR spectrometer, was added to the MCT detector. The whole system was tested for leakage before the main experiment everyday. MFC #1-4 and #2-4 which controlled the balance and dilution nitrogen were switched on to take a background scan with the FTIR. The background scan must be taken for each experiment. After obtaining the background scan, the other species were flowed.

The set points of each mass flow controller were determined using an Excel spreadsheet, which included the calibration data for each specific mass flow controller. The set points of the mass flow controllers were double-checked to ensure the flow of the correct quantities of each component in the mixture. During the complete time of the experiments, the furnace remained on all the time to ensure thermal stability. The temperature of the furnace was increased by a temperature step of 50°C or 100°C from the ambient temperature (25°C) to 450°C.

After taking the last reading at 450°C, the flow of all species except N_2 was stopped. Only the balance nitrogen of 1100 sccm flowed till the remaining gases of NO, NH_3 and O_2 in the system were gone. The heated reactor needed to cool back to the ambient temperature, which normally took about 5 hours with compressed air assistance.

Table 10. The average time to obtain the final value for each reaction temperature.

Reaction Temperature (°C)	Average time to obtain the final value (mins)	
	V_2O_5-WO_3/TiO_2 samples	V_2O_5/Ti-PILC samples
Ambient	94	134
100	79	-
150	83	124
200	67	92
250	63	-
300	50	66
350	42	26
400	37	57
450	44	57

5.2 Procedures for Data Collection

To process the data of a FTIR scan, Bio-Rad WinIR-pro version 2.96 software was used. The scans of the output gas in the FTIR gas cell were taken after steady state of both NO and NH_3 was established. To determine whether the steady state condition was reached, scans of the FTIR were repeatedly taken. The values of the last 25 scans fluctuated within the error ranges of ± 0.5 ppm were considered to be in the steady state condition. Then, the average value of the last 25 scans was obtained, and the final value, the closest value to the average value, was determined at the reaction temperature.

The average times to obtain the final values for each temperature are listed in table 10. The average time is decreasing with an increase in the reaction temperature. In the beginning of the experiments at lower temperatures, it took a very long time (~ 134 mins) to reach the steady state, and the high NH_3 concentration was responsible for that. The lowest values of the average time for V_2O_5-WO_3/TiO_2 at 400°C and V_2O_5/Ti-PILC at 350°C were corresponding to the occurrence of the maximum NO reduction and 100% NH_3 conversion. After collecting the final scan for every single reaction temperature, the concentration data was plotted as a function of the reaction temperature.

5.3 Experimental Uncertainty and Error Range

Performing the experiments under the exact same condition was very hard. The background scan by the FTIR spectrometer was different for every single experiment. The experimental results could be different under the same experimental conditions because of the different background scan. The background scan by the FTIR spectrometer was easily affected by the temperature of surroundings (or room temperature), the weather condition and the gas condition in a cylinder. (1) The room temperature varied slightly (~ 3°C) all the time because of the air conditioning and the frequent opening and closing of the door. (2) The background scan on a rainy day was different from the results on a sunny day (affected by humidity). (3) The different condition of nitrogen (N_2) in a cylinder (could occur during the recharging process of a gas) affected the background scan.

To investigate the range of uncertainty of the NO and NH_3 concentrations, three cases of catalyst arrangements under similar reaction conditions were selected. Figure 36 shows NO reduction as a function of the reaction temperature over V_2O_5-WO_3/TiO_2 for the conditions of [NO] = [NH_3] = 330 ppm, heating area of zones 2 + 3 (preheating case), 0.5% O_2, and SV = 10500 h^{-1}. Among several oxygen concentrations (0 ~ 3.0%), the results of 0.5% O_2 (figure 36) showed the largest difference between the average case and each case for NO reduction. The maximum difference between the average case and the third case is approximately 6.5% (or 21.5 ppm) at 400°C, and it is also the maximum difference among all results in figure 36. Therefore, the uncertainty for the NO reduction is at most ± 6.5%. For many cases, the uncertainty was much less than ± 6.5%. Figure 37 shows NH_3 conversion as a function of the reaction temperature for 3.0% O_2. Among several oxygen concentrations (0 ~ 3.0%), the results of 3.0% O_2 (figure 37) showed the largest uncertainty for NH_3 conversion. For the temperature of 150°C, the difference between the average case and the second case is approximately 5.7% (18.15 ppm), while the difference for the other temperatures is less than 3% (10 ppm). Therefore, the uncertainty of the NH_3 conversion is at most ± 3.0%. For many cases, the uncertainty of the NH_3 conversion was much less than ± 3.0%.

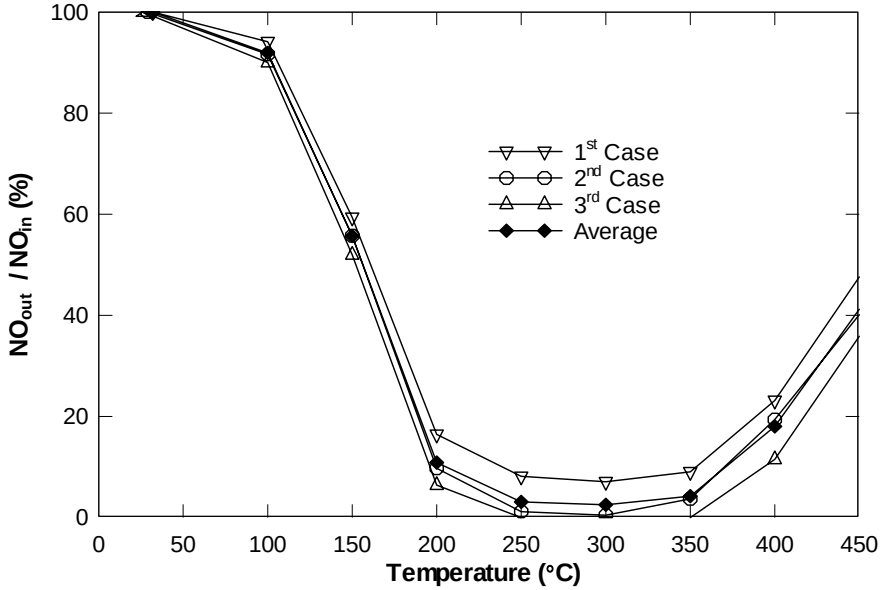

Figure 36. NO reduction as a function of the reaction temperature over V_2O_5-WO_3 /TiO_2. Reaction conditions: [NO] = 330 ppm, [NH_3] = 330 ppm, 0.5% O_2, heating area of zones 2 + 3 (preheating case), and SV = 10500 h^{-1}.

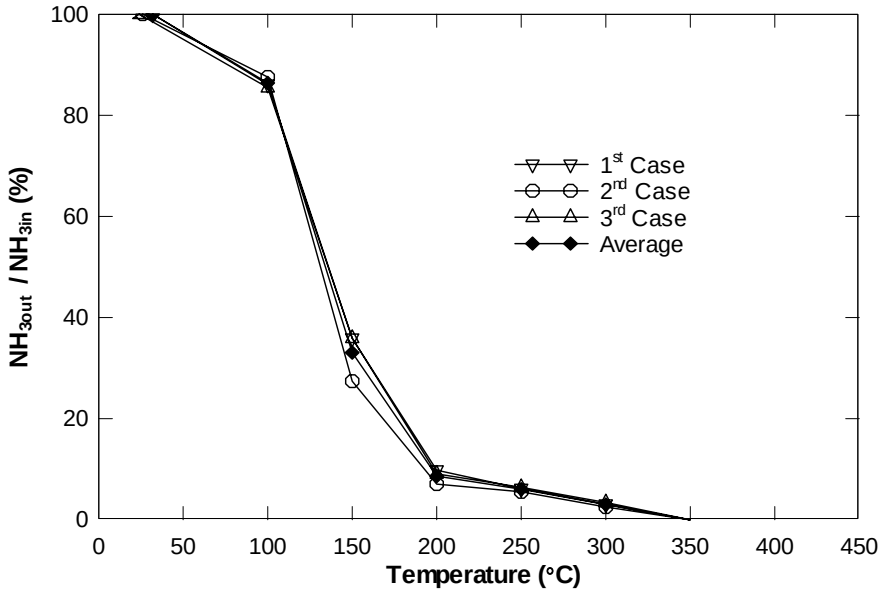

Figure 37. NH_3 conversion as a function of the reaction temperature over V_2O_5-WO_3 /TiO_2. Reaction conditions: [NO] = 330 ppm, [NH_3] = 330 ppm, 3.0% O_2, heating area of zones 2 + 3 (preheating case), and SV = 10500 h^{-1}.

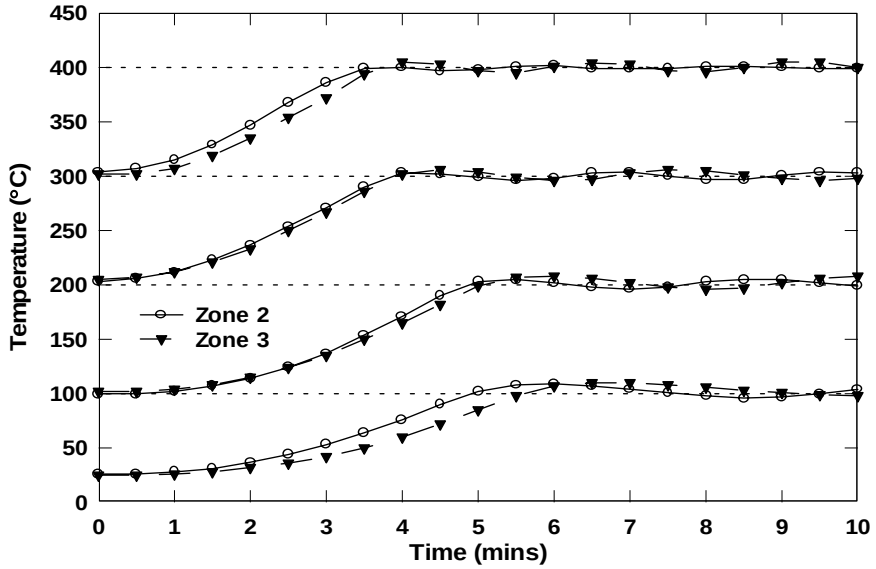

Figure 38. The transition of the reaction temperature as a function of time for the heating zone 2 and zone 3 of the furnace by the temperature step of 100°C.

5.4 Temperature Increase of the Furnace

The reaction temperature of the furnace was increased by the temperature step of 50°C or 100°C from the ambient temperature (approximately 25°C) to 450°C for every single experiment. Figure 38 shows the transition of the temperature of the furnace for the heating zone 2 and zone 3 by the temperature step of 100°C. The heating zones 2 and 3 were heated simultaneously (preheating case). After the final values of NO and NH_3 concentrations were obtained at ambient, the temperature was increased to 100°C. Five minutes later, the temperature reached 100°C and remained constant with only slight fluctuation. To get the final species values at 100°C, more than an hour is required as listed in table 10. Again, after final concentrations were obtained at 100°C, the reaction temperature was increased to 200°C. Five minutes later, the temperature reached 200°C and remained constant with only slight fluctuation. The time to reach the next temperature reduces for higher temperatures. In general, the temperature of zone 2 reaches the set temperature 30 seconds or a minute earlier than the temperature of zone 3.

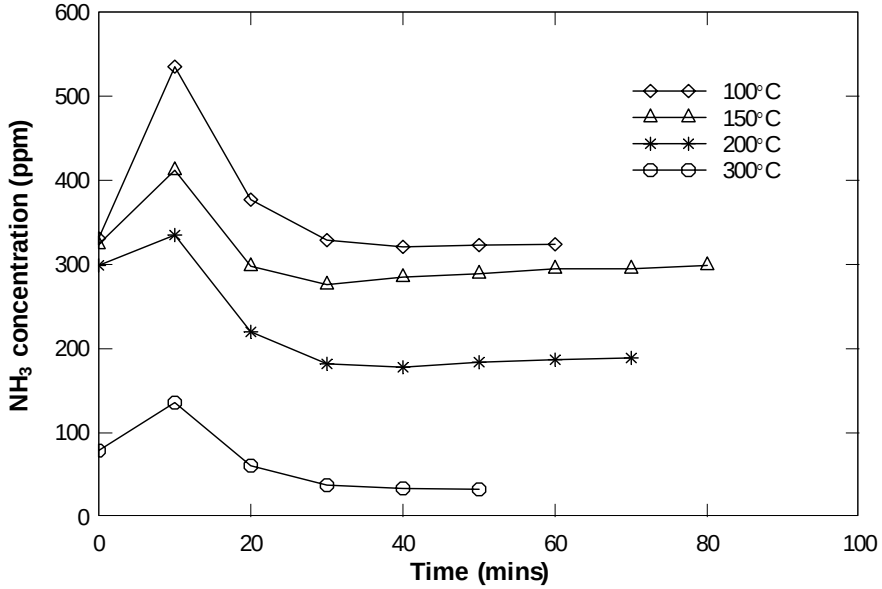

Figure 39. NH_3 concentration as a function of time at different reaction temperatures over V_2O_5-WO_3/TiO_2. Reaction conditions: [NO] = 330 ppm, [NH_3] = 330 ppm, 0.1% O_2, heating area of zone 2, and SV = 21000 h^{-1}.

5.5 Observation of NH_3 Concentration

Prior to running the main experiments, each reading normally took around 20 - 25 minutes to reach steady state during the NO calibration process. On the other hand, it took up to an hour to stabilize during the NH_3 calibration. In the main experiment as well as the calibration process, NH_3 needed a longer time to stabilize than NO.

After the background scan, all species (such as 330 ppm of NO, 330 ppm of NH_3, 0 - 3.0% O_2, balance N_2, and dilution N_2 of 5000 sccm) flowed through the system. Initially when the gas species started to flow, the catalyst sample apparently absorbed mostly ammonia. Thus, the concentration of NH_3 in the output gases very gradually increased up to 330 ppm (initial NH_3 concentration) at the ambient temperature. This is the reason that the average time at the ambient temperature was the longest one as listed in table 10.

Figure 39 represents the NH_3 concentrations as a function of time at various reaction temperatures over V_2O_5-WO_3/TiO_2 under the reaction conditions of [NO] = 330 ppm, [NH_3] = 330 ppm, 0.1% O_2, heating area of zone 2, and SV = 21000 h^{-1}. Every

time the reaction temperature of the furnace was increased by the temperature step of 50°C or 100°C, a sudden 'burst' of ammonia concentration was detected by FTIR spectrometer. Though the NH_3 concentration of 330 ppm was metered through the MFC, it was measured around 550 ppm or even up to 1300 ppm (for an NH_3-to-NO ratio of 2.0 at SV = 10500 h^{-1}). The concentration declined after it reached the maximum level around 10 minutes after the experiment started. The sudden 'burst' was most obvious for the lower reaction temperatures. The maximum levels of the NH_3 concentration were all different at various reaction temperatures. These phenomena were observed for every single experiment. Considering figure 38 and figure 39 together, the time region between 0 and 10 minutes, reaction temperatures increase and stabilize. That is to say, the temperature of 100°C increases to 200°C within 5 minutes and stabilizes, and NH_3 concentration increase during this moment. More details concerning these observations will be provided in Chapter 6, Experimental Results and Discussion.

5.6 Observation of NO Concentration

Figures 40 and 41 show the NO concentrations as a function of time at various reaction temperatures over V_2O_5-WO_3/TiO_2 under the reaction conditions of 0% O_2 and heating area of zone 2 and under the reaction conditions of 0.5% O_2 and heating area of zones 2 + 3 (preheating case), respectively. Unlike ammonia species, the concentrations of NO were decreased as soon as the reaction temperature increased as shown in figure 40. A sudden decrease of NO concentration was detected and was also greater at lower reaction temperatures. At higher reaction temperatures in figure 41, the concentration of NO was increased for the case of 0.5% O_2. More detail will be discussed in the Chapter 6, Experimental Results and Discussion.

To determine the final scan, not only the NO concentration should be stabilized, but also the NH_3 concentration should reach the steady state. When the ammonia concentration was completely gone (i.e., 100% NH_3 conversion), the final scan depended only on the NO condition.

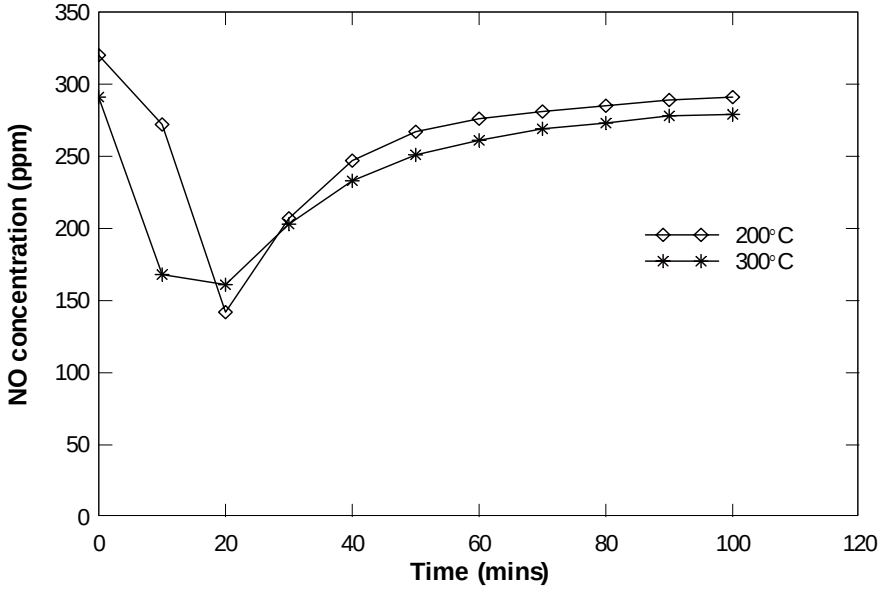

Figure 40. NO concentration as a function of time at different reaction temperatures over V_2O_5-WO_3/TiO_2. Reaction conditions: [NO] = 330 ppm, [NH_3] = 330 ppm, 0% O_2, heating area of zone 2, and SV = 21000 h^{-1}.

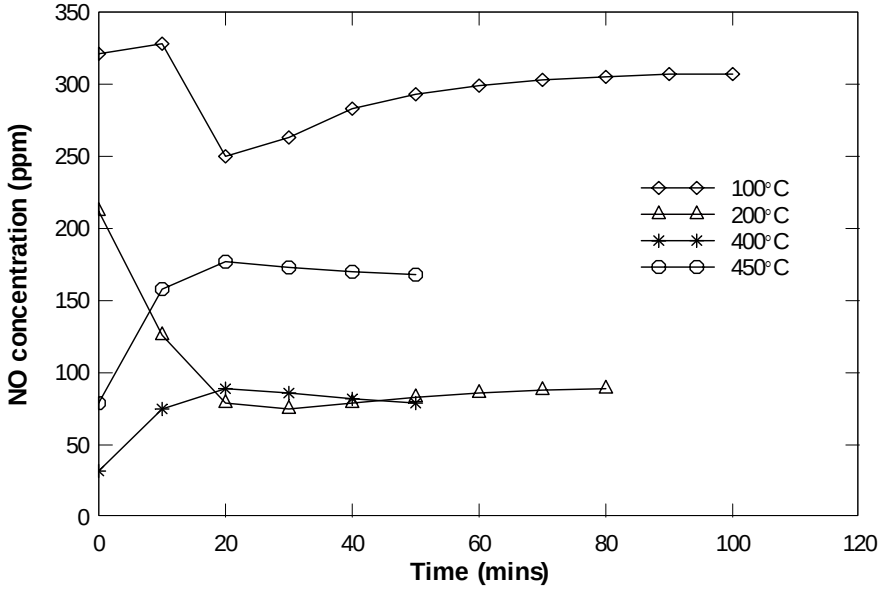

Figure 41. NO concentration as a function of time at different reaction temperatures over V_2O_5-WO_3/TiO_2. Reaction conditions: [NO] = 330 ppm, [NH_3] = 330 ppm, 0.5% O_2, heating area of zones 2 + 3 (preheating case), and SV = 21000 h^{-1}.

6. EXPERIMENTAL RESULTS AND DISCUSSION

The results obtained for the selective catalytic reduction (SCR) of NO with ammonia as the reducing agent over vanadia-based (V_2O_5-WO_3/TiO_2) and pillared interlayer clay-based (V_2O_5/Ti-PILC) monolithic honeycomb catalysts are presented and discussed. As a preface to this section, lines in all figures used to connect data points are only for the purpose of helping the reader differentiate one set of data from another. In all the following figures, NO reduction is defined as the ratio of the output NO concentration (as measured by the FTIR) to the input NO concentration (as metered through the MFC) in percentage form. Similarly, NH_3 conversion is defined as the ratio of the output NH_3 concentration to the input NH_3 concentration in percentage form. Therefore, higher NO reduction or higher NH_3 conversion means more NO or NH_3 removal from the exhaust.

6.1 Vanadia-Based (V_2O_5-WO_3/TiO_2) Catalysts

The selective catalytic reduction (SCR) of nitric oxide (NO) with ammonia over V_2O_5-WO_3/TiO_2 monolithic honeycomb catalysts has been widely investigated. Some results in this paper are already well investigated, but some of them have not been studied yet. The results are presented and discussed case by case for the different reaction conditions.

Table 11 summarizes the experimental cases performed on V_2O_5-WO_3/TiO_2 catalysts in the current study. Three physical arrangements of the catalyst samples were tested. These are explained in more detail in Chapter 4: Experimental Systems and Descriptions. Two space velocities of 10500 h^{-1} (a sample of 2 cm in length) and of 21000 h^{-1} (a sample of 1 cm in length) were used. The number of heating zones activated included zones 2 and 3 (preheating case) were mainly performed and some cases of heating area of zone 2. The NH_3-to-NO ratio was 0.8, 1.0 and 2.0 ([NO] = 330 ppm, [NH_3] = 264 ppm, 330 ppm, and 660 ppm, respectively). Four different oxygen concentrations of 0, 0.1, 0.5, and 3.0% were tested for all cases over V_2O_5-WO_3/TiO_2 catalysts.

Table 11. The experimental cases performed on V_2O_5-WO_3/TiO_2 catalysts.

Catalysts condition	Space velocity (h^{-1})	Heating area	NH_3-to-NO ratio	Oxygen concentration (%)
Standard arrangement	21000	Zone 2	1.0 ([NO] = 330 ppm $[NH_3]$ = 330 ppm)	0 0.1 0.5 3.0
		Preheating (zone 2 + 3)	1.0	0 0.1 0.5 3.0
Standard arrangement	10500	Zone 2	1.0	0 0.1 0.5 3.0
		Preheating (zone 2 + 3)	0.8 ([NO] = 330 ppm $[NH_3]$ = 264 ppm)	0 0.1 0.5 3.0
			1.0 ([NO] = 330 ppm $[NH_3]$ = 330 ppm)	0 0.1 0.5 3.0
			2.0 ([NO] = 330 ppm $[NH_3]$ = 660 ppm)	0 0.1 0.5 3.0
Second arrangement	10500	Preheating (zone 2 + 3)	1.0	0 0.1 0.5 3.0
Third arrangement	10500	Preheating (zone 2 + 3)	1.0	0 0.1 0.5 3.0

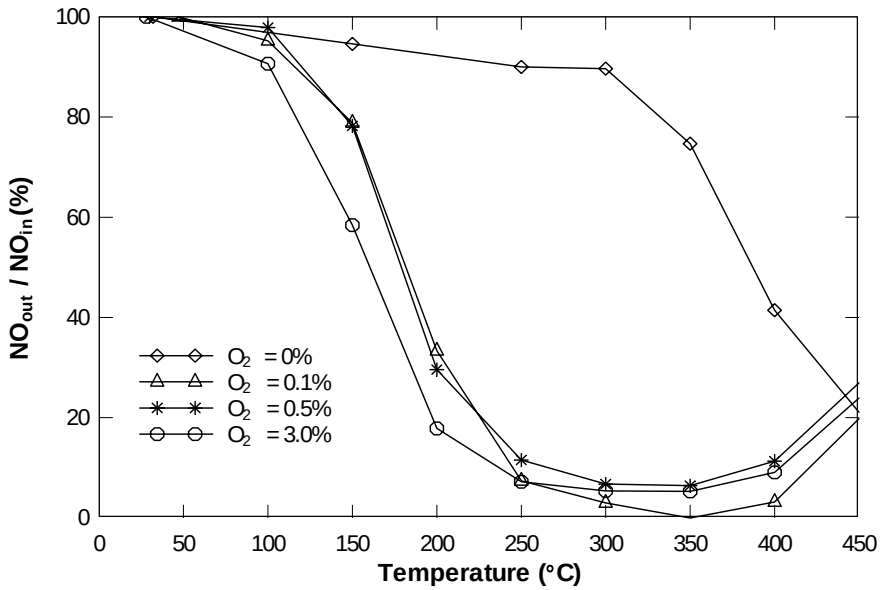

Figure 42. NO reduction as a function of the reaction temperature at various oxygen concentrations over V_2O_5-WO_3/TiO_2. Reaction conditions: [NO] = 330 ppm, [NH_3] = 330 ppm, 0 - 3.0% O_2, heating area of zone 2, and SV = 10500 h^{-1}.

6.1.1 Effect of Reaction Temperature

Figures 42 and 43 describe NO reduction and NH_3 conversion, respectively, as a function of the reaction temperature at various oxygen concentrations for the conditions of [NO] = [NH_3] = 330 ppm, heating area of zone 2, and SV = 10500 h^{-1}.

In figure 42, NO reductions of 88% or more are achieved for reaction temperatures between 250 and 400°C for all cases in the presence of oxygen. Thus, the temperature window of almost 150°C is determined for NO reduction of 88% or more. The maximum NO reductions are obtained at the reaction temperature of 350°C for all cases in the presence of oxygen. After NO reduction reaches the maximum value, the concentration of NO increases at higher reaction temperatures.

In figure 43, NH_3 conversions over 87% are obtained at the reaction temperatures above 250°C for all cases in the presence of oxygen. NH_3 conversions lower than 3% (or 10 ppm) are detected at the reaction temperature of approximately 350°C and is near zero for 400 or 450°C.

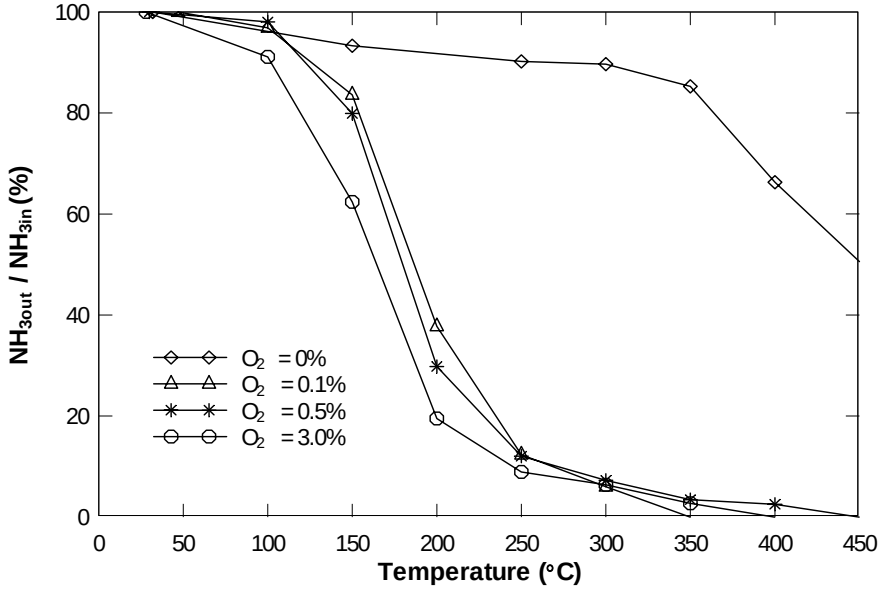

Figure 43. NH_3 conversion as a function of the reaction temperature at various oxygen concentrations over V_2O_5-WO_3/TiO_2. Reaction conditions: [NO] = 330 ppm, [NH_3] = 330 ppm, 0 - 3.0% O_2, heating area of zone 2, and SV = 10500 h^{-1}.

Figures 44 and 45 present NO reduction and NH_3 conversion, respectively, as a function of the reaction temperature at various oxygen concentrations at a space velocity of 21000 h^{-1}. Catalytic reactions take place for the conditions of [NO] = [NH_3] = 330 ppm and heating area of zone 2.

In figure 44, NO reductions of 88% or more are successfully found at the reaction temperature between 300 and 400°C for all cases in the presence of oxygen. Thus, the temperature window of 100°C is obtained for NO reduction of 89% or more achieved. After NO reductions reaches the maximum value obtained at the reaction temperature of 350°C, the concentration of NO increases at higher reaction temperatures for all cases in the presence of oxygen.

In figure 45, NH_3 conversions over 87% are obtained at the reaction temperatures above 300°C for all cases in the presence of oxygen. The conversions of NH_3 are completely removed or lower than 3% (or 10 ppm) at the reaction temperature of 400°C. The choice of the percentages (i.e., 88 and 87%) is purely based on convenience.

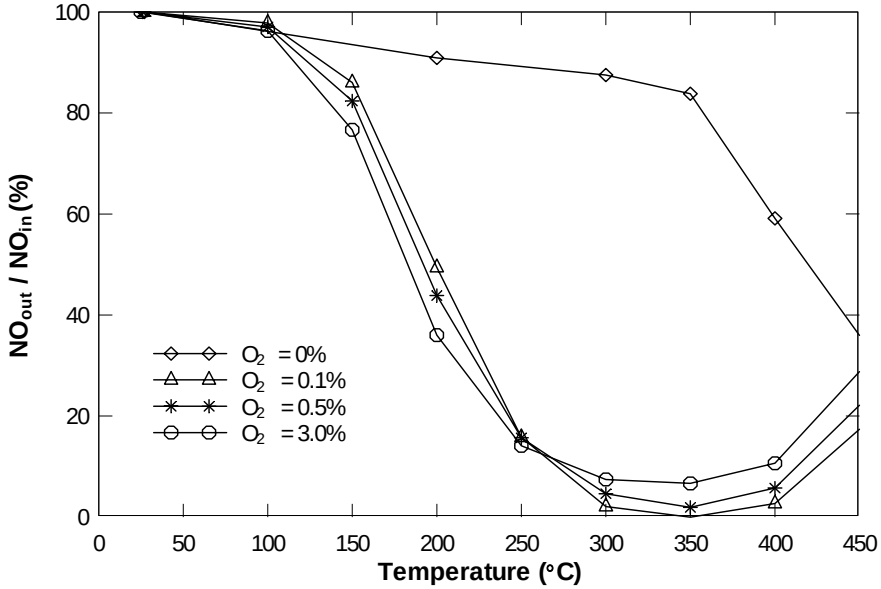

Figure 44. NO reduction as a function of the reaction temperature at various oxygen concentrations over V_2O_5-WO_3/TiO_2. Reaction conditions: [NO] = 330 ppm, [NH_3] = 330 ppm, 0 - 3.0% O_2, heating area of zone 2, and SV = 21000 h^{-1}.

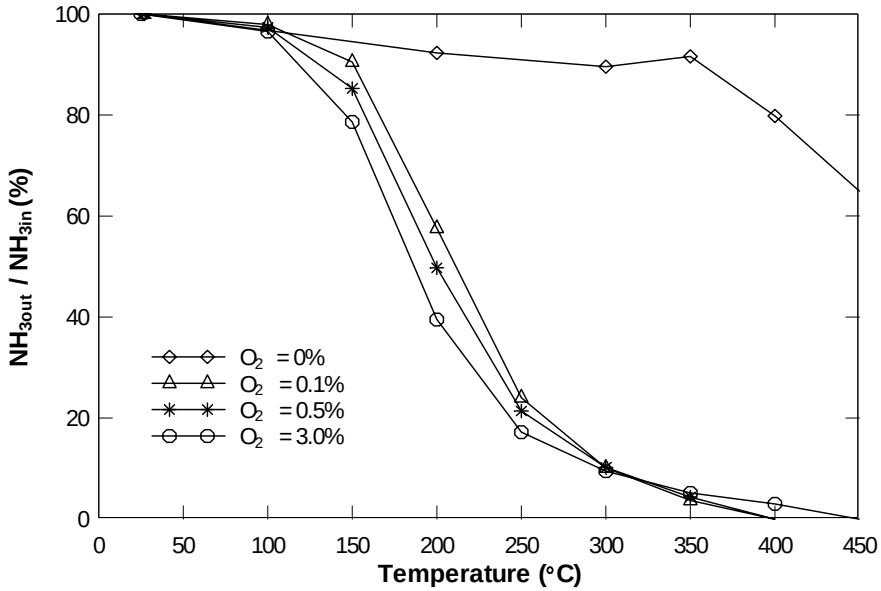

Figure 45. NH_3 conversion as a function of the reaction temperature at various oxygen concentrations over V_2O_5-WO_3/TiO_2. Reaction conditions: [NO] = 330 ppm, [NH_3] = 330 ppm, 0 - 3.0% O_2, heating area of zone 2, and SV = 21000 h^{-1}.

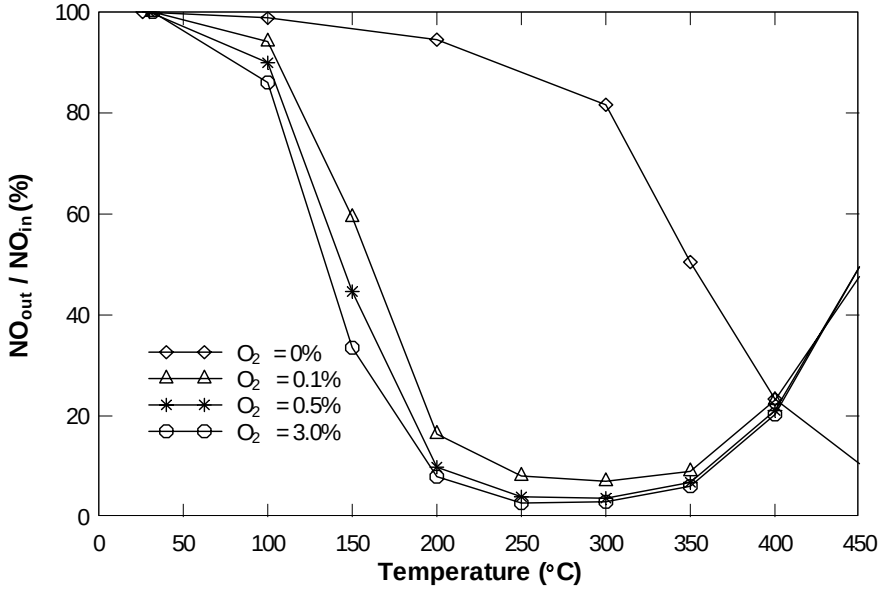

Figure 46. NO reduction as a function of the reaction temperature at various oxygen concentrations over V_2O_5-WO_3/TiO_2. Reaction conditions: [NO] = 330 ppm, [NH_3] = 330 ppm, 0 - 3.0% O_2, heating area of zones 2 + 3 (preheating case), and SV = 10500 h^{-1}.

6.1.2 Effect of Oxygen Concentration

Figure 46 shows NO reductions as a function of the reaction temperature at various inlet oxygen concentrations (the amount metered into reactor along with other gas species, on a molar percentage basis) for heating area of zones 2 + 3 (preheating case). Recall that results without preheating (zone 2 only) were shown in figure 42

For both figures, very low catalytic activities of NO reduction are obtained in the absence of oxygen, but high NO reductions are achieved in the presence of even small amounts of oxygen. However, the increase of oxygen concentration from 0.1 to 3.0% has no great influence to NO reduction.

In figure 42, the result of the oxygen concentration of 0.1% shows the best NO reduction at the temperatures above 250°C. In figure 46, higher NO reduction is found with an increase in oxygen concentration for the entire temperature range, and the result of 3.0% O_2 is the best performance for the preheating case. NO reductions over 83% are achieved for reaction temperatures between 200 and 350°C in the presence of oxygen.

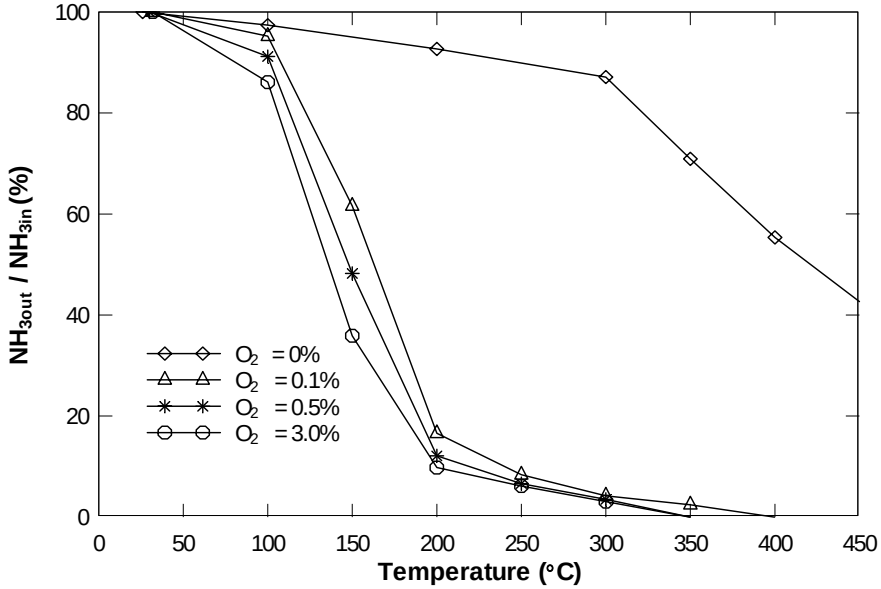

Figure 47. NH_3 conversion as a function of the reaction temperature at various oxygen concentrations over V_2O_5-WO_3/TiO_2. Reaction conditions: [NO] = 330 ppm, [NH_3] = 330 ppm, 0 - 3.0% O_2, heating area of zones 2 + 3 (preheating case), and SV = 10500 h^{-1}.

Figure 47 shows NH_3 conversions as a function of the reaction temperature at various inlet oxygen concentrations under the same conditions including heating area of zones 2 + 3 (preheating case). Figure 43 shows results for only zone 2 heating.

For both figures, it is observed that high conversions of ammonia are successfully achieved in the presence of small amounts of oxygen, while very poor NH_3 conversions are obtained in the absence of oxygen in the entire temperature window. The presence of small amounts of oxygen concentration facilitates the oxidation of ammonia. Though higher NH_3 conversion is obtained with an increase in oxygen concentration from 0.1 to 3.0%, the differences are small.

The result of the oxygen concentration of 3.0% in both figures shows the best NH_3 conversion for the entire temperature range. The lowest reaction temperature for 100% NH_3 conversion is from 350 to 400°C, depending on the oxygen concentration. NH_3 conversions over 87% are obtained at the reaction temperatures above 200°C in the presence of oxygen.

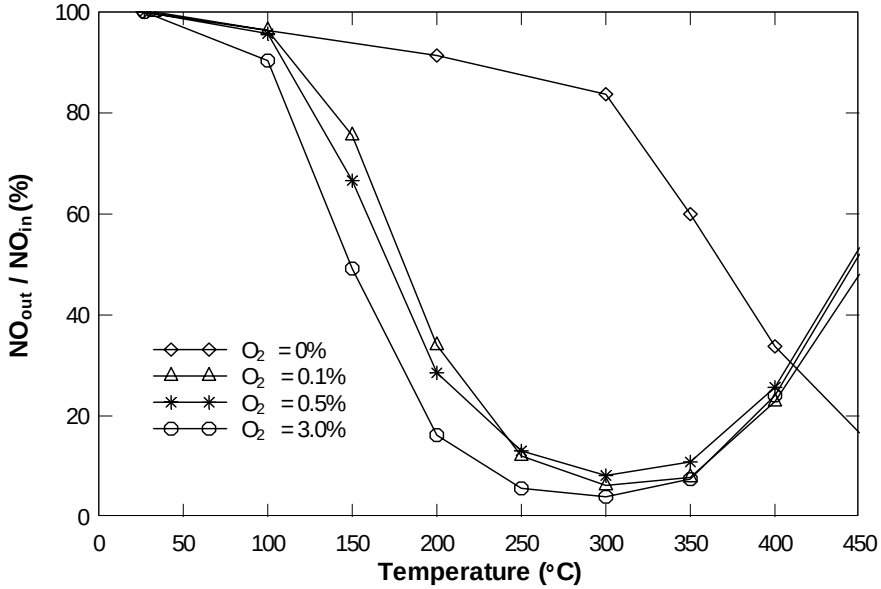

Figure 48. NO reduction as a function of the reaction temperature at various oxygen concentrations over V_2O_5-WO_3/TiO_2. Reaction conditions: [NO] = 330 ppm, [NH_3] = 330 ppm, 0 - 3.0% O_2, heating area of zones 2 + 3 (preheating case), and SV = 21000 h^{-1}.

Figure 48 shows NO reductions as a function of the reaction temperature for various inlet oxygen concentrations for the heating area of zone 2 + 3 (preheating case) for SV = 21000 h^{-1}. Recall that results of zone 2 heating were shown in figure 44. The space velocity used in figure 42 (zone 2) and figure 46 (preheating), was 10500 h^{-1}.

The results in the absence and presence of oxygen in figure 44 and 48 are very similar to the previous results as shown in figure 42 and 46. High catalytic activities of NO reduction are obtained in the presence of oxygen, whereas NO reduction is very low in the absence of oxygen. The increase of oxygen concentration from 0.1 to 3.0% has a modest influence on the NO reduction.

In figure 44, for reaction temperatures above 300°C, the result of the 0.1% O_2 case shows the best NO reduction among the results in the presence of oxygen. In figure 48, in contrast, the result of 3.0% O_2 shows the best NO reduction among the results in the presence of oxygen for the entire temperature range. NO reductions over 83% are obtained for reaction temperatures between 250 and 350°C in the presence of oxygen.

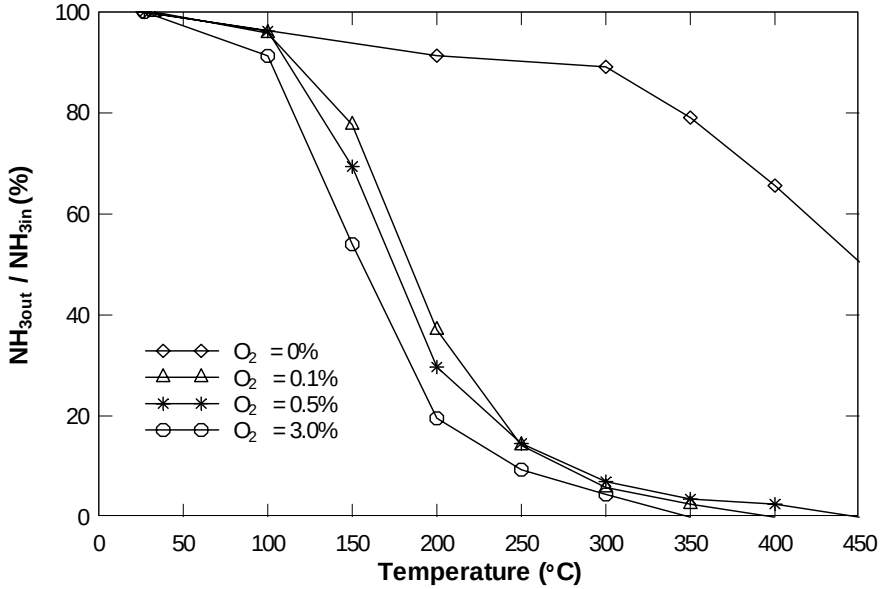

Figure 49. NH_3 conversion as a function of the reaction temperature at various oxygen concentrations over V_2O_5-WO_3/TiO_2. Reaction conditions: [NO] = 330 ppm, [NH_3] = 330 ppm, 0 - 3.0% O_2, heating area of zones 2 + 3 (preheating case), and SV = 21000 h^{-1}.

Figure 49 shows NH_3 conversions as a function of the reaction temperature at various inlet oxygen concentrations for the heating area of zone 2 + 3 (preheating case) for SV = 21000 h^{-1}. Recall that results of zone 2 heating were shown in figure 45. The space velocity used in figure 43 (zone 2) and figure 47 (preheating), was 10500 h^{-1}.

The results which are determined in the absence and presence of oxygen are very similar to previous results in figure 43 and 47. High NH_3 conversions are performed in the presence of oxygen. The presence of small amounts of oxygen facilitates the oxidation of ammonia. The difference of NH_3 conversions as the oxygen concentration is increased from 0.1% to 3.0% is negligible. Low NH_3 conversion is observed in the absence of oxygen.

The result of 3.0% O_2 shows the best NH_3 conversion for the entire temperature range in figure 49. The lowest reaction temperature of 100% NH_3 conversion found is between about 350 and 450°C, depending on the oxygen concentration. NH_3 conversions over 87% are obtained at the temperatures above 250°C in the presence of oxygen.

Table 12. The reaction temperatures of the maximum NO reduction.

Oxygen concentration (%)	Temperature of maximum NO reduction (°C)			
	SV = 10500 h^{-1}		SV = 21000 h^{-1}	
	Zone 2	Preheating	Zone 2	Preheating
0	450	450	450	450
0.1	350	300	350	300
0.5	350	300	350	300
3.0	350	250	350	300

Table 13. The lowest reaction temperatures of 100% NH_3 conversion.

Oxygen concentration (%)	Lowest temperature of 100% NH_3 conversion (°C)			
	SV = 10500 h^{-1}		SV = 21000 h^{-1}	
	Zone 2	Preheating	Zone 2	Preheating
0	-	-	-	-
0.1	350	400	400	400
0.5	450	350	400	450
3.0	400	350	450	350

Table 12 lists the reaction temperatures of the maximum NO reduction at various oxygen concentrations with SV = 10500 h^{-1} and 21000 h^{-1} in different heating areas. For both space velocity in the presence of oxygen, the maximum NO reduction occurs at 350°C for the heating area of zone 2 and at 250 and 300°C for the heating area of zones 2 + 3 (preheating case). The increase of the heating area decreases the temperature for the maximum NO reduction.

Table 13 lists the lowest temperatures of 100% NH_3 conversion at various oxygen concentrations with space velocity of 10500 h^{-1} and 21000 h^{-1}. Any specific order of the reaction temperature with an increase in oxygen concentration is not observed.

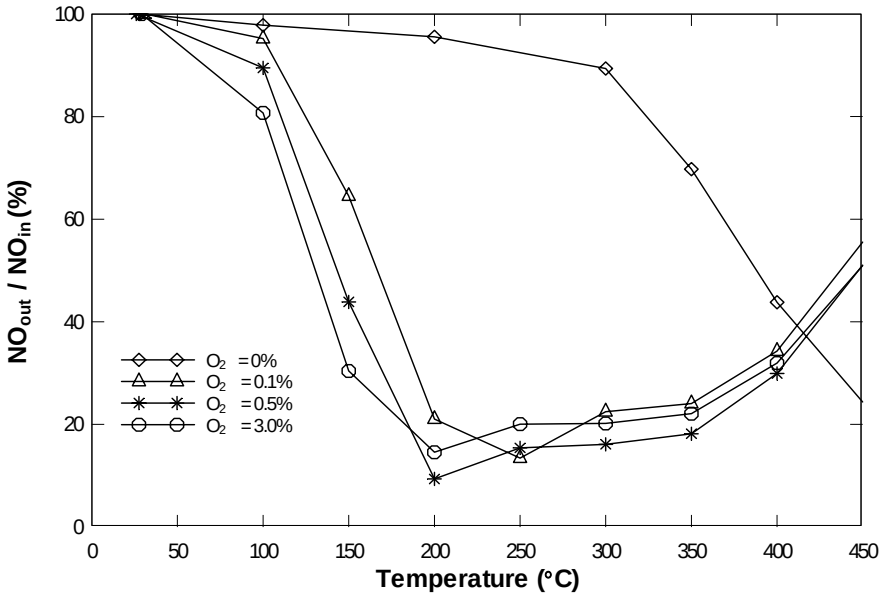

Figure 50. NO reduction as a function of the reaction temperature at various oxygen concentrations over V_2O_5-WO_3/TiO_2. Reaction conditions: NH_3-to-NO ratio = 0.8 ([NO] = 330 ppm, [NH_3] = 264 ppm), 0 - 3.0% O_2, heating area of zones 2 + 3 (pre-heating case), and SV = 10500 h^{-1}.

6.1.3 Effect of NH_3-to-NO Ratio

Figures 50 to 53 show NO reductions and NH_3 conversions as functions of the reaction temperature at various oxygen concentrations. The variation in the inlet ammonia concentration from 264 to 660 ppm results in the variation of NH_3-to-NO ratio from 0.8 to 2.0, respectively. These results are for the conditions of [NO] = 330 ppm, 0 - 3.0% O_2, heating area of zones 2 + 3 (preheating case), and SV = 10500 h^{-1}.

Figure 50 presents the effect of low ammonia concentration on NO reduction, corresponding to an NH_3-to-NO ratio of 0.8. For reaction temperatures above 200°C, the highest NO reduction is for 0.5% O_2, and the maximum NO reduction is obtained approximately 90% for 200°C. Except for only one point (for 0.5% O_2 at 200°C), NO reductions over 88% are not obtained in the entire reaction temperature range.

In figure 51, conversions of ammonia lower than 3% (or 10 ppm) are found for reaction temperatures above 250°C in the presence of oxygen.

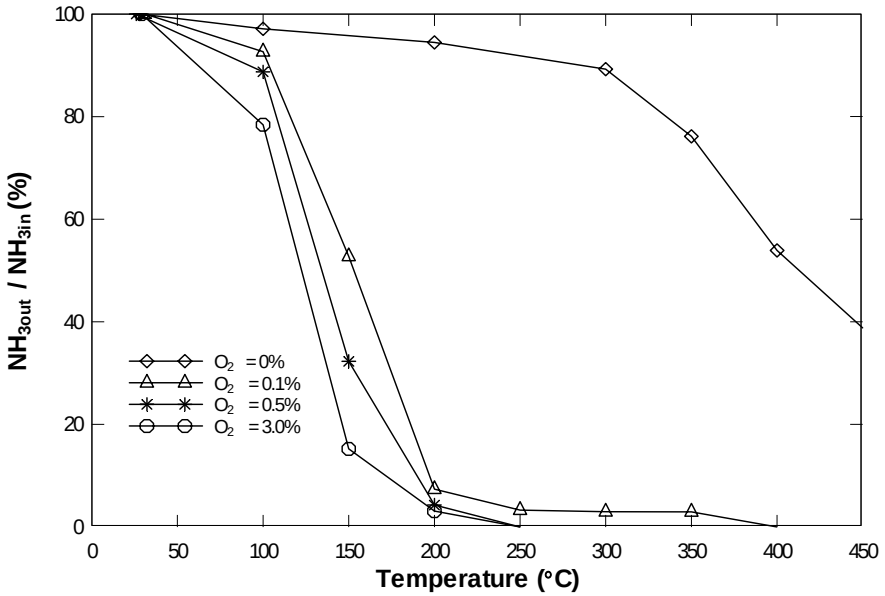

Figure 51. NH_3 conversion as a function of the reaction temperature at various oxygen concentrations over V_2O_5-WO_3/TiO_2. Reaction conditions: NH_3-to-NO ratio = 0.8 ([NO] = 330 ppm, [NH_3] = 264 ppm), 0 - 3.0% O_2, heating area of zones 2 + 3 (preheating case), and SV = 10500 h^{-1}.

In figure 52, the effect of high ammonia concentration on NO reduction, corresponding to an NH_3-to-NO ratio of 2.0 is illustrated. The results for all cases in the presence of oxygen indicate relatively high NO reductions. NO reductions over 92% are obtained for reaction temperatures from 200°C to 400°C (except for a point of 0.1% O_2 at 200°C). For temperatures above 200°C, the results of NO reduction for 3.0% O_2 are lower than those for 0.1% O_2. The highest NO reduction is found at 0.5% O_2 at reaction temperatures above 200°C, and a maximum NO reduction is obtained of near 100% at the temperatures between 250°C and 350°C.

The effect of high ammonia concentration on NH_3 conversion is determined in figure 53. The results in the presence of oxygen are very different from others presented before. NH_3 concentration drops quite slowly at low temperatures. At the reaction temperature of 300°C, NH_3 conversion was found approximately 90% or more in the previous cases, but only 70% NH_3 conversion is obtained for this case.

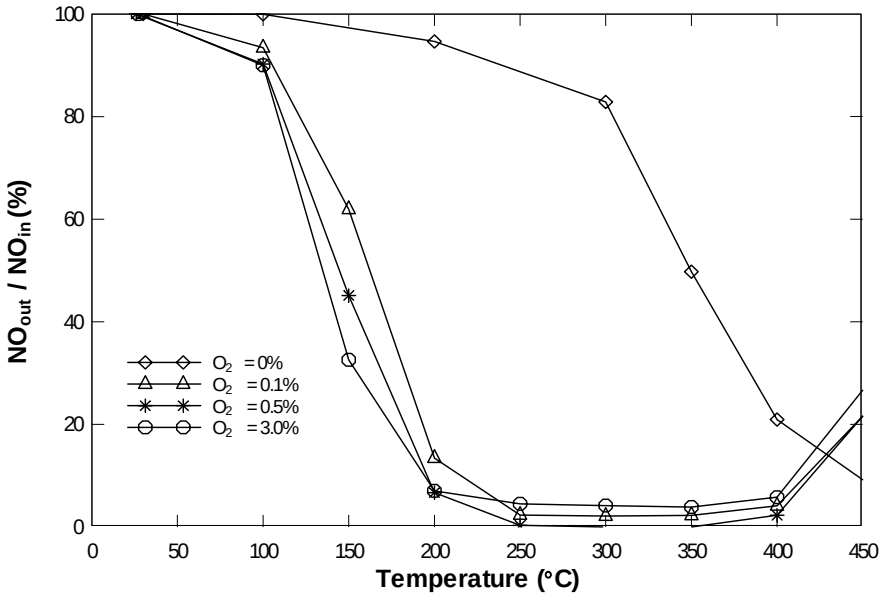

Figure 52. NO reduction as a function of the temperature at various oxygen concentrations over V_2O_5-WO_3/TiO_2. Reaction conditions: NH_3-to-NO ratio = 2.0 ([NO] = 330 ppm, [NH_3] = 660 ppm), 0 - 3.0% O_2, preheating case, and SV = 10500 h^{-1}.

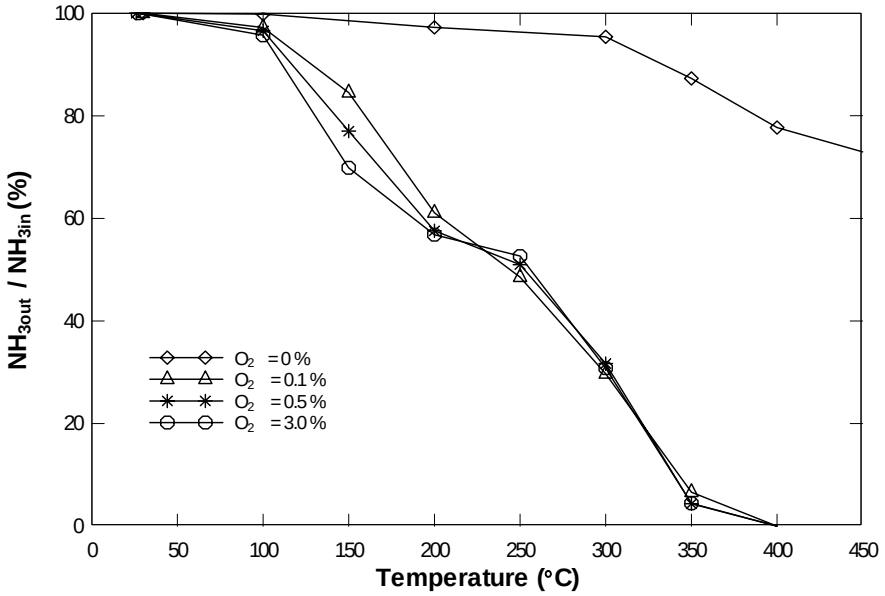

Figure 53. NH_3 conversion as a function of the temperature at various oxygen concentrations over V_2O_5-WO_3/TiO_2. Reaction conditions: NH_3-to-NO ratio = 2.0 ([NO] = 330 ppm, [NH_3] = 660 ppm), 0 - 3.0% O_2, preheating case, and SV = 10500 h^{-1}.

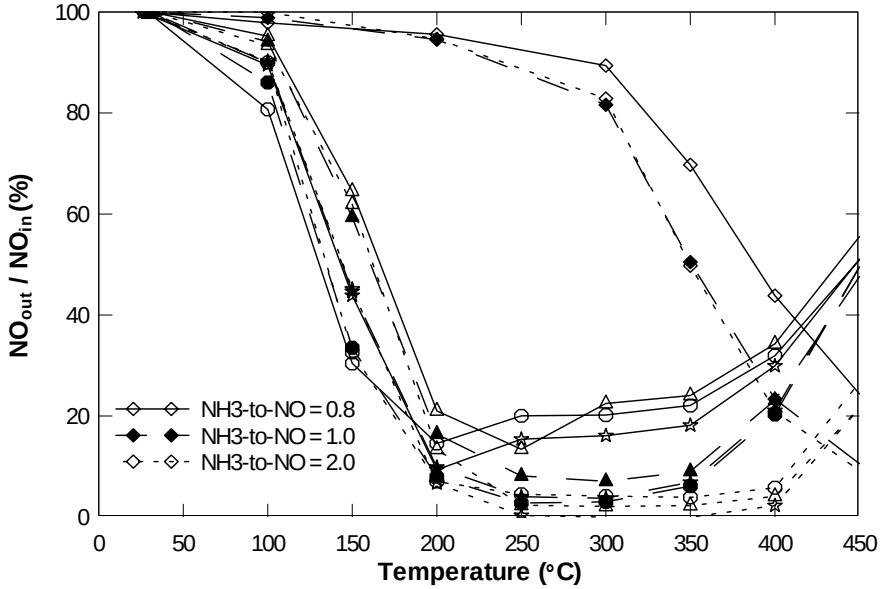

Figure 54. NO reduction as a function of the reaction temperature at various NH_3-to-NO ratios over V_2O_5-WO_3/TiO_2. Reaction conditions: 0 - 3.0% O_2, preheating case, SV = 10500 h^{-1}, and NH_3-to-NO ratio = 0.8 (solid lines with open symbols), 1.0 (broken lines with closed symbols), and 2.0 (dashed lines with open symbols).

Figures 54 and 55 present combinations of the previous results for variations of NH_3-to-NO ratio. For the reduction of NO, the results in figures 50, 46 and 52 are combined together into figure 54. Likewise, the results of NH_3 conversion in figures of 51, 47 and 53 are combined together into figure 55. These results are for NH_3-to-NO ratios of 0.8 (solid lines with open symbols), 1.0 (broken lines with closed symbols), and 2.0 (dashed lines with open symbols). The symbols indicate oxygen concentrations of 0% (◇), 0.1% (△), 0.5% (☆), and 3.0% (O).

Figure 54 describes the effect of the variation of NH_3-to-NO ratio on NO reduction as a function of the reaction temperature. For reaction temperatures below 200°C, no great difference is observed with an increase in NH_3-to-NO ratio at the same oxygen concentration (for the cases with non-zero oxygen). However, for reaction temperatures above 200°C, noticeable increase of NO reduction is observed with an increase in NH_3-to-NO ratio in the presence of oxygen. NO reductions increase with an increase in NH_3-to-NO ratio.

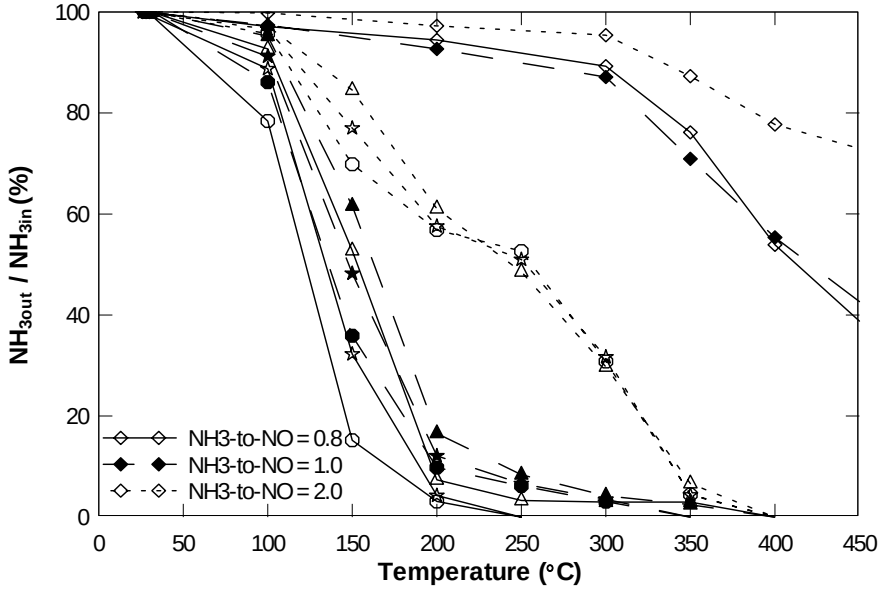

Figure 55. NH_3 conversion as a function of the reaction temperature at various NH_3-to-NO ratios over V_2O_5-WO_3/TiO_2. Reaction conditions: 0 - 3.0% O_2, preheating case, SV = 10500 h^{-1}, and NH_3-to-NO ratio = 0.8 (solid lines with open symbols), 1.0 (broken lines with closed symbols), and 2.0 (dashed lines with open symbols).

Figure 55 shows the effect of the variation of NH_3-to-NO ratio on NH_3 conversion as a function of the reaction temperature. NH_3 conversion is decreased with an increase in NH_3-to-NO ratio in the presence of oxygen. At temperatures below 200°C, the results of NH_3-to-NO ratios of 0.8 and 1.0 are observed the considerable difference, and NH_3 conversion dropped rapidly. Otherwise, NH_3 conversion of NH_3-to-NO ratio of 2.0 decreases very slowly in the entire temperature range. At the temperature of 300°C, NH_3 conversions of NH_3-to-NO ratios of 0.8 and 1.0 are obtained lower than 4.5% (or 15 ppm), whereas NH_3 conversion of NH_3-to-NO ratio of 2.0 is obtained 31.7% (or 209 ppm). NH_3 conversions of NH_3-to-NO ratio of 0.8 (above 250°C) and 1.0 (above 350°C) at 0.1% O_2 are obtained approximately 97% or more. Though the conversions are not 100%, they could be considered 100% due to the possible error of the experimental condition. If so, the complete NH_3 conversions are obtained at the reaction temperatures of 250, 350 and 400°C for NH_3-to-NO ratios of 0.8, 1.0 and 2.0, respectively. The temperature of 100% NH_3 conversion increases with an increase in NH_3-to-NO ratio.

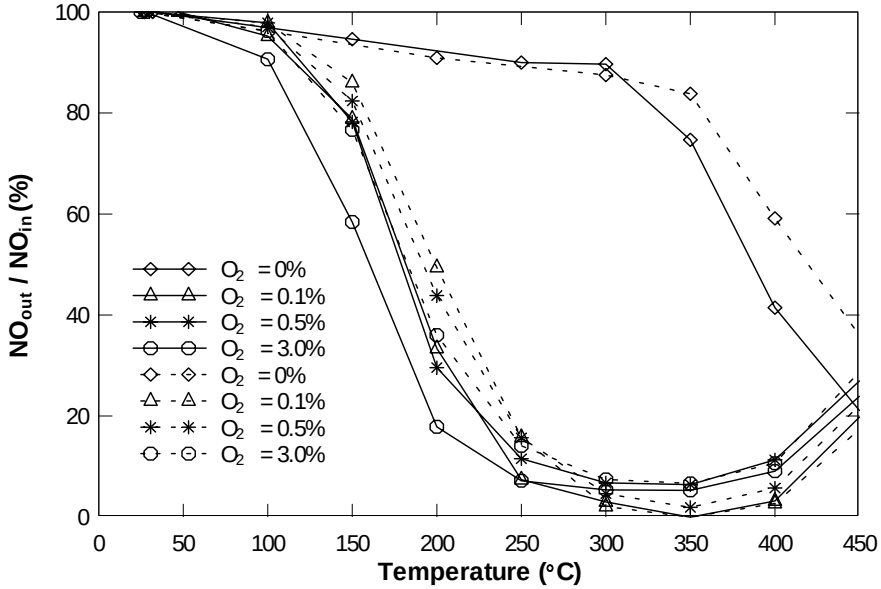

Figure 56. NO reduction as a function of the reaction temperature at various space velocities over V_2O_5-WO_3/TiO_2. Reaction conditions: [NO] = 330 ppm, [NH_3] = 330 ppm, zone 2 heated, 0 - 3.0% O_2, and SV = 10500 h^{-1} (solid line) and 21000 h^{-1} (broken line).

6.1.4 Effect of Space Velocity

Space velocity is defined as the ratio of the total gas flow rate to the catalyst volume, expressed in per-hour. At a constant gas flow rate, space velocity is inversely proportional to catalyst volume such that increasing catalyst volume corresponds to decreasing space velocity. The experimental conditions are [NO] = 330 ppm, [NH_3] = 330 ppm, the oxygen concentration of 0 - 3.0%, and heating areas of zone 2 and zone 2 + 3 (preheating case).

Figure 56 shows NO reduction as a function of the reaction temperature at various space velocities for heating area of zone 2. The solid lines are for the space velocity of 10500 h^{-1} and the broken lines are for the space velocity of 21000 h^{-1}. The decrease of space velocity leads the results of NO reduction shift toward lower reaction temperature. In the presence of oxygen, higher NO reduction is found at the reaction temperatures below 300°C with a decrease in space velocity. On the other hand, the differences of NO reductions at the reaction temperatures above 300°C are modest.

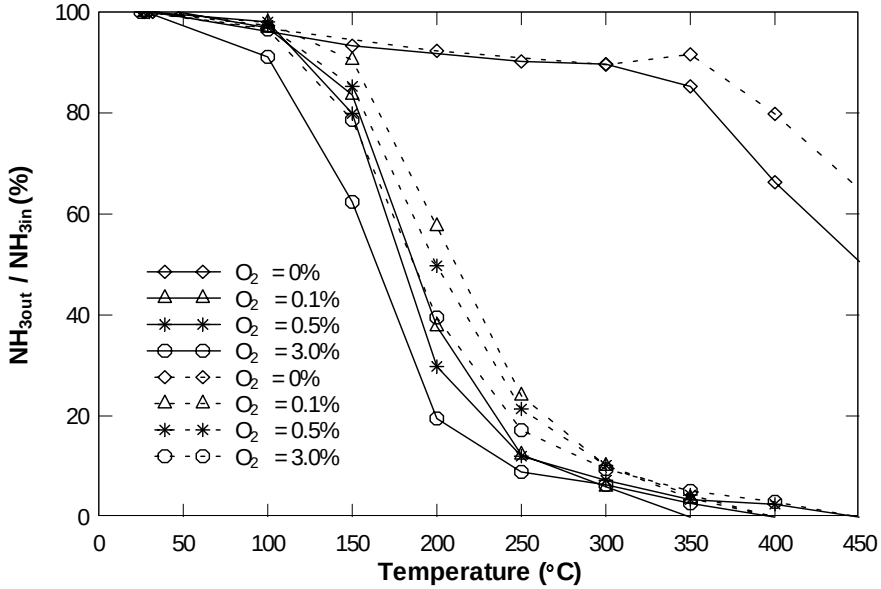

Figure 57. NH_3 conversion as a function of the reaction temperature at various space velocities over V_2O_5-WO_3/TiO_2. Reaction conditions: [NO] = 330 ppm, [NH_3] = 330 ppm, zone 2 heated, 0 - 3.0% O_2, and SV = 10500 h^{-1} (solid line) and 21000 h^{-1} (broken line).

Table 14 lists the maximum NO reduction at various space velocities in the heating area of zone 2 over V_2O_5-WO_3/TiO_2. It is found that the difference of the maximum NO reduction between two space velocities is lower than 4.5% (approximately 15 ppm) in the presence of oxygen. 100% NO reduction takes place with oxygen concentration of 0.1% for both cases, but the results of 0.1% O_2 does not performed the best NO reduction in the entire reaction temperature range. The oxygen concentrations of the highest maximum NO reduction and the best NO reduction in the entire temperature range are not identical for the heating area of zone 2.

In figure 57, NH_3 conversion as a function of the reaction temperature at various space velocities is described. Better catalytic activity of NH_3 conversion is detected in the entire temperature range with a decrease in space velocity. The decrease of space velocity causes the same NH_3 conversion to shift toward lower temperatures. The result for the 3.0% O_2 case, given by the solid line with open circle symbols, is the best conversion of NH_3 in the entire temperature range for a space velocity of 10500 h^{-1}.

Table 14. Maximum NO reduction at various space velocities for different heating areas.

Oxygen concentration (%)	Maximum NO reduction (%)			
	Zone 2		Preheating	
	SV = 10500 h^{-1}	SV = 21000 h^{-1}	SV = 10500 h^{-1}	SV = 21000 h^{-1}
0	78.9	64	89.5	83.3
0.1	100	100	92.9	93.7
0.5	93.6	98.1	96.2	91.8
3.0	94.7	93.3	97.2	96

Table 15. The lowest reaction temperatures for NH_3 concentrations lower than 10 ppm.

Oxygen concentration (%)	Lowest temperature (°C) of NH_3 concentration < 10 ppm (or 3%)			
	Zone 2		Preheating	
	SV = 10500 h^{-1}	SV = 21000 h^{-1}	SV = 10500 h^{-1}	SV = 21000 h^{-1}
0	-	-	-	-
0.1	350	400	350	350
0.5	400	400	350	400
3.0	350	400	300	350

Table 15 lists the lowest reaction temperatures for NH_3 concentrations lower than 10 ppm (or less than 3% conversion) with the two types of heating over a V_2O_5-WO_3/ TiO_2 catalyst. No certain order of the results with an increase in oxygen concentration is observed. However, it should be noticed that the reaction temperatures increase with an increase in space velocity for both heating areas.

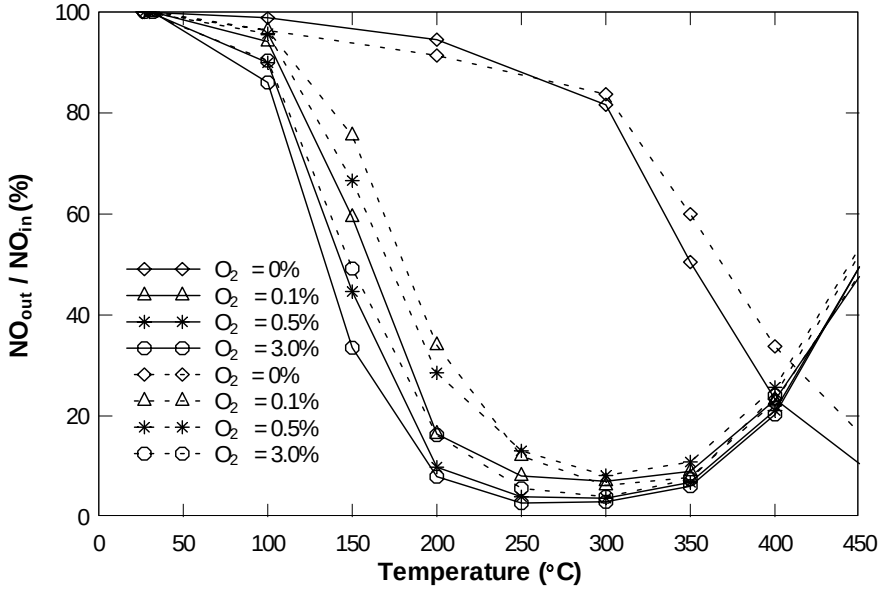

Figure 58. NO reduction as a function of the reaction temperature at various space velocities over V_2O_5-WO_3/TiO_2. Reaction conditions: [NO] = 330 ppm, [NH_3] = 330 ppm, preheating case, 0 - 3.0% O_2, and SV = 10500 h^{-1} (solid line) and 21000 h^{-1} (broken line).

Figure 58 describes NO reduction under the same conditions used in figure 56, except for the heating area of zones 2 + 3 (preheating case). Similar results are observed. The result of NO reduction shifts toward lower reaction temperature with a decrease in space velocity. Higher NO reduction is found in the presence of oxygen for all temperatures for the lower space velocity.

Table 14 also lists the maximum NO reduction at various space velocities in the preheating area. It is found that the difference of the maximum NO reduction between two space velocities is lower than 4.4% (approximately 14 ppm) in the presence of oxygen. The highest NO reduction takes place with the oxygen concentration of 3.0% for both cases, and also the best NO reduction occurs with the oxygen concentration of 3.0% in the entire reaction temperature range. The oxygen concentrations of the highest maximum NO reduction and the best NO reduction for the entire reaction temperature range are identical for the preheating area.

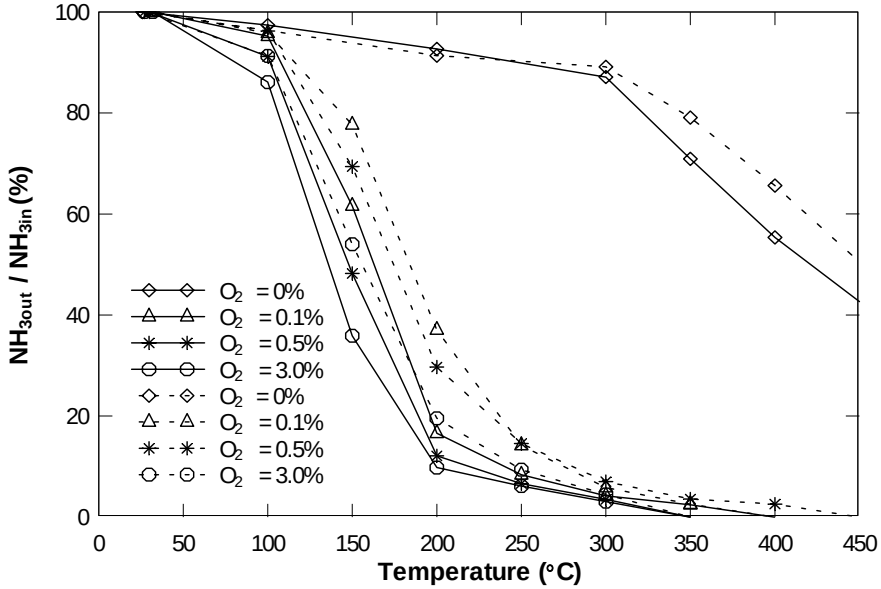

Figure 59. NH_3 conversion as a function of the reaction temperature at various space velocities over V_2O_5-WO_3/TiO_2. Reaction conditions: [NO] = 330 ppm, [NH_3] = 330 ppm, preheating case, 0 - 3.0% O_2, and SV = 10500 h^{-1} (solid line) and 21000 h^{-1} (broken line).

In figure 59, NH_3 conversion as a function of the reaction temperature at various space velocities under the same conditions used in figure 57, except for the heating area of zones 2 + 3 (preheating case), is described. Similar results are observed. NH_3 conversion shifts toward lower temperatures with a decrease in space velocity. Higher NH_3 conversion is determined with a decrease in space velocity for the entire reaction temperature range. The result for the 3.0% O_2 case, indicated by a solid line with open circle symbols, is found the best conversion of NH_3 at a space velocity of 10500 h^{-1}. In the presence of oxygen, higher NH_3 conversion is found at temperatures below 250°C with a decrease in space velocity. On the other hand, the differences of NH_3 conversion at temperatures above 300°C are very slight.

Table 15 lists the lowest reaction temperatures obtained for NH_3 concentrations lower than 10 ppm (or less than 3% conversion) in preheating area. No certain order of the results with an increase in oxygen concentration is observed. However, the reaction temperatures are increased with an increase of space velocity.

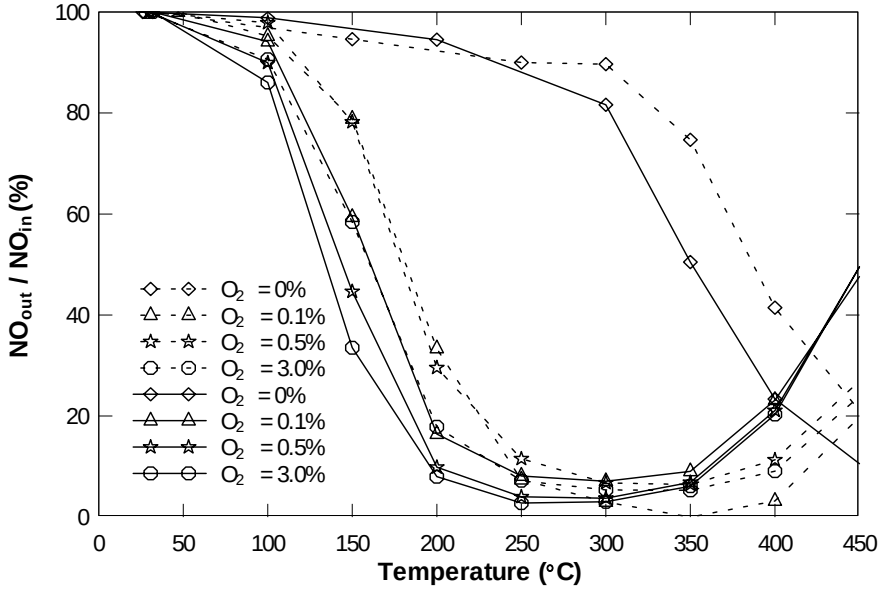

Figure 60. NO reduction as a function of the reaction temperature at various heating areas over V_2O_5-WO_3/TiO_2. Reaction conditions: [NO] = [NH_3] = 330 ppm, 0 - 3.0% O_2, SV = 10500 h^{-1}, and heating areas of zone 2 (broken line) and preheating (solid line).

6.1.5 Effect of Heating Area

NO reductions (figure 60) and NH_3 conversions (figure 61) at various heating areas for the conditions of [NO] = 330 ppm, [NH_3] = 330 ppm, 0 - 3.0% O_2, and SV = 10500 h^{-1} are illustrated. Two heating areas of zone 2 and zone 2 + 3 (preheating case) are tested. In figure 60, NO reductions over 88% are successfully achieved at temperatures between 250°C and 400°C for the zone 2 case and 83% or more between 200°C and 350°C in the presence of oxygen for the preheating case. The choice of the percentages (i.e., 88 and 83%) is purely based on convenience. The temperature ranges of 150°C are determined for both heating areas. For temperatures below 300°C, better results of NO reduction are obtained in preheating area. On contrast, higher NO reductions are found for the zone 2 case above 300°C, and the difference between two NO reductions are more significant. The results are shifted toward lower reaction temperatures with an increase in heating area from zone 2 to zone 2 + 3. It indicates that the temperature of the simulated gas in the preheating case is higher than in the case of zone 2 only.

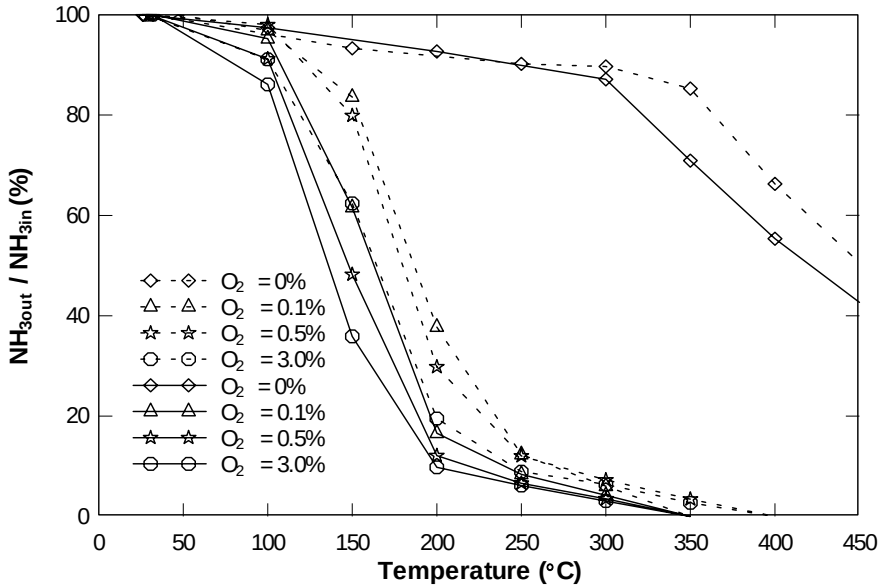

Figure 61. NH_3 conversion as a function of the reaction temperature at various heating areas over V_2O_5-WO_3/TiO_2. Reaction conditions: [NO] = [NH_3] = 330 ppm, 0 - 3.0% O_2, SV = 10500 h^{-1}, and heating areas of zone 2 (broken line) and preheating (solid line).

Figure 61 shows that NH_3 conversions over 83% were obtained at the reaction temperature of 200°C with the preheating case, while 87% or more at 250°C for zone 2 case (no preheating) for a SV = 10500 h^{-1}. The results of the preheating case (solid line) demonstrated slightly better catalytic activity of NH_3 conversion and shifted toward lower reaction temperatures than those of the case of zone 2 (without preheating).

Figure 62 shows NO reductions over 88% were found for temperatures between 300°C and 400°C for the zone 2 case and over 83% between 250°C and 350°C in the presence of oxygen for the preheating case (zone 2 + 3) at SV = 21000 h^{-1}. Thus, a temperature range of about 100°C is obtained for both heating cases. The temperature range of NO reduction of 83% or more are 50°C wider for the cases of SV = 10500 h^{-1}.

In figure 63, NH_3 conversions of 83% or more are achieved at 250°C for preheating, while 87% or more at 300°C for zone 2 over SV = 21000 h^{-1}. In general, the reaction temperatures of the preheating cases are lower than those of the zone 2 cases (without preheating) and more NH_3 conversion took place.

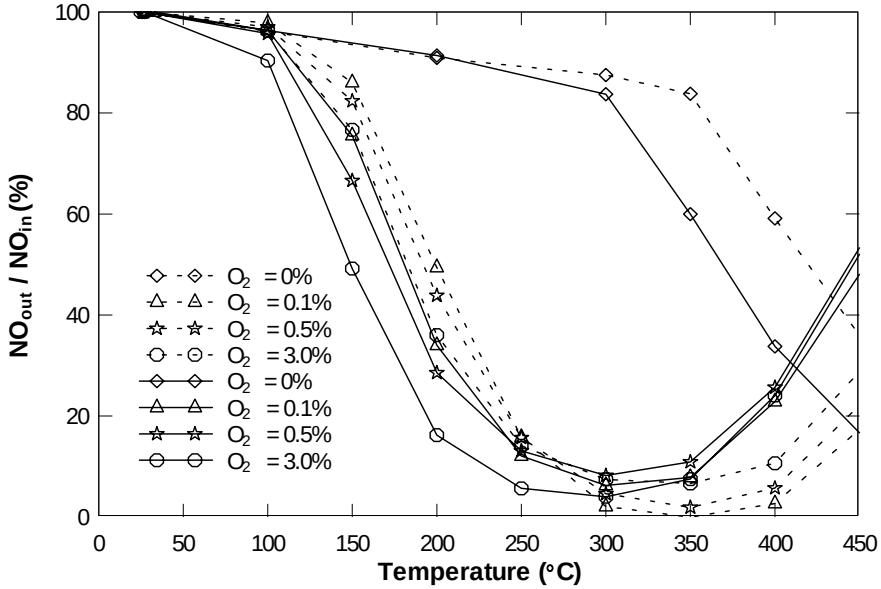

Figure 62. NO reduction as a function of the temperature at various heating areas over V_2O_5-WO_3/TiO_2. Reaction conditions: [NO] = [NH_3] = 330 ppm, 0 - 3.0% O_2, SV = 21000 h^{-1}, and heating areas of zone 2 (broken line) and preheating (solid line).

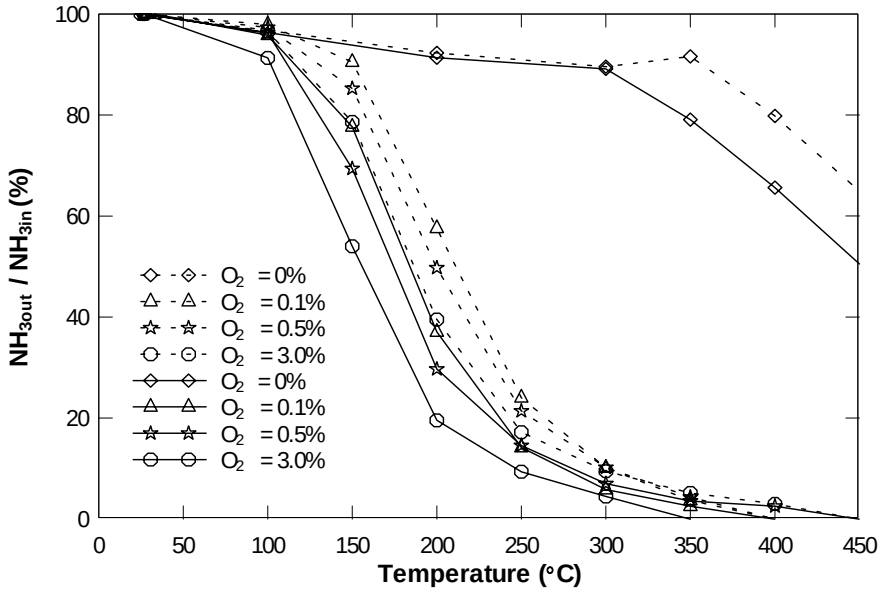

Figure 63. NH_3 conversion as a function of the temperature at various heating areas over V_2O_5-WO_3/TiO_2. Reaction conditions: [NO] = [NH_3] = 330 ppm, 0 - 3.0% O_2, SV = 21000 h^{-1}, and heating areas of zone 2 (broken line) and preheating (solid line).

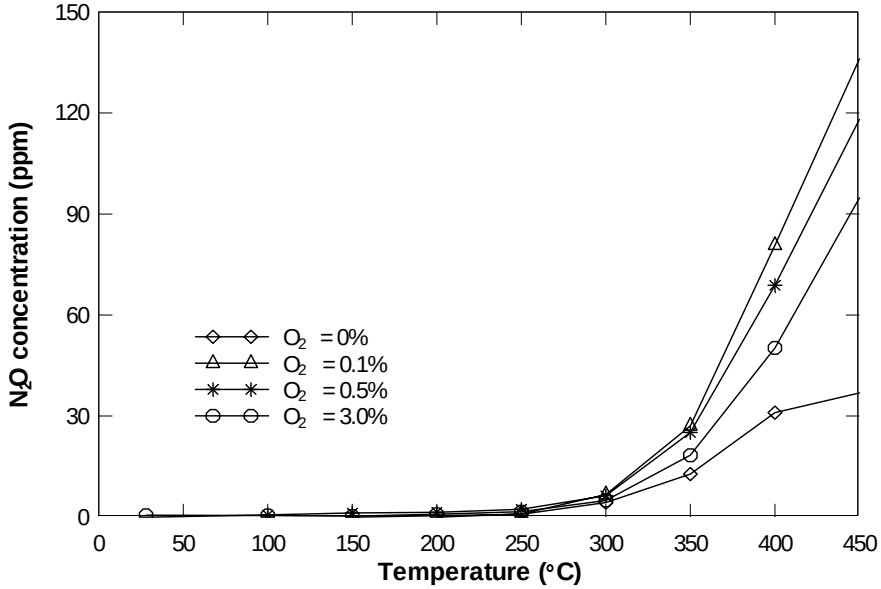

Figure 64. N_2O concentration as a function of the reaction temperature at various oxygen concentrations over V_2O_5-WO_3/TiO_2. Reaction conditions: [NO] = 330 ppm, [NH_3] = 330 ppm, 0 - 3.0% O_2, heating area of zone 2, and SV = 10500 h^{-1}.

6.1.6 N_2O and NO_2 Production

The production of nitrous oxide (N_2O) and nitrogen dioxide (NO_2) for the selective catalytic reduction of NO with ammonia over V_2O_5-WO_3/TiO_2 catalysts are presented in this section. The results of NO_2 and N_2O production are explained case by case for the different reaction conditions listed in table 11. The reactions occur for the conditions of [NO] = [NH_3] = 330 ppm and oxygen concentrations of 0 to 3.0%. The different parameters of the conditions are listed in each explanation.

Figures 64 and 65 show the production of N_2O and NO_2, respectively, as a function of the reaction temperature at various oxygen concentrations for the conditions of heating area of zone 2, and SV = 10500 h^{-1}. In figure 64, N_2O concentrations of 5 ppm or less appear for reaction temperatures below about 250°C, and increase steeply at higher temperatures for all cases. In the presence of oxygen, N_2O concentrations decrease with an increase in oxygen concentration. The maximum concentration of N_2O is approximately 136 ppm at the reaction temperature of 450°C at 0.1% O_2.

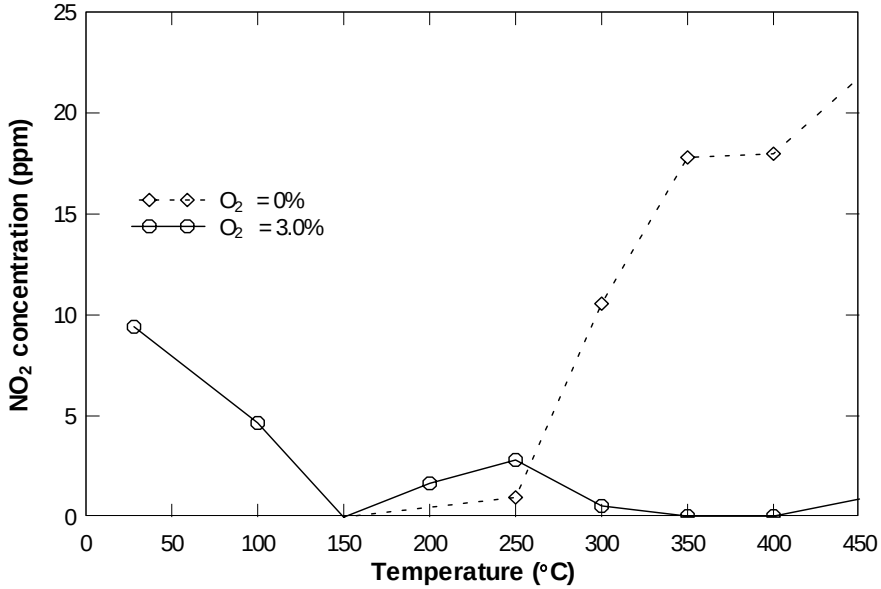

Figure 65. NO_2 concentration as a function of the reaction temperature at various oxygen concentrations over V_2O_5-WO_3/TiO_2. Reaction conditions: [NO] = 330 ppm, [NH_3] = 330 ppm, 0 - 3.0% O_2, heating area of zone 2, and SV = 10500 h^{-1}.

In figure 65, NO_2 concentrations at only 0 and 3.0% O_2 are shown. No concentrations of NO_2 were detected from the experiments at 0.1 and 0.5% O_2. The maximum concentration of NO_2 is approximately 22 ppm at the highest temperature at 0% O_2.

Figures 66 and 67 show the production of N_2O and NO_2, respectively, as a function of the reaction temperature at various oxygen concentrations for the conditions of preheating case and SV = 10500 h^{-1}. Figure 66 presents that no N_2O concentration appears for reaction temperatures below about 200°C. N_2O concentration increases rapidly for higher temperatures. In the presence of oxygen, N_2O concentrations decrease with an increase in oxygen concentration. The maximum N_2O production is approximately 160 ppm at 0.1% O_2. NO_2 production for only 0.1 and 3.0% O_2 cases is shown in figure 67. NO_2 concentrations at 0 and 0.5% O_2 were not detected in these experiments. NO_2 production at 3.0% O_2 is zero for reaction temperatures below 400°C. The maximum concentration of NO_2 is about 7 ppm at the reaction temperature of 250°C at 0.1% O_2. In this case, the production of NO_2 is modest (less than 7 ppm).

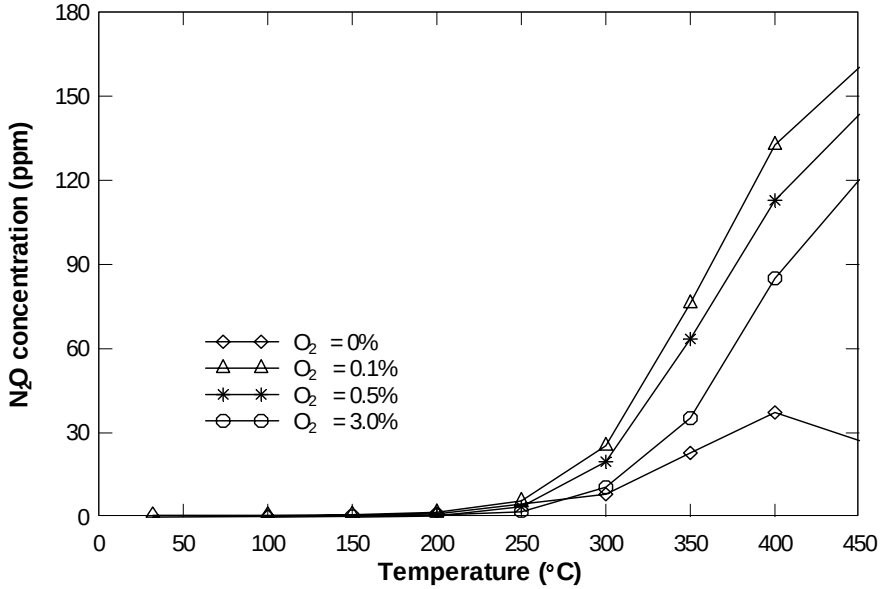

Figure 66. N_2O concentration as a function of the reaction temperature at various oxygen concentrations over V_2O_5-WO_3/TiO_2. Reaction conditions: [NO] = 330 ppm, [NH_3] = 330 ppm, 0 - 3.0% O_2, preheating case, and SV = 10500 h^{-1}.

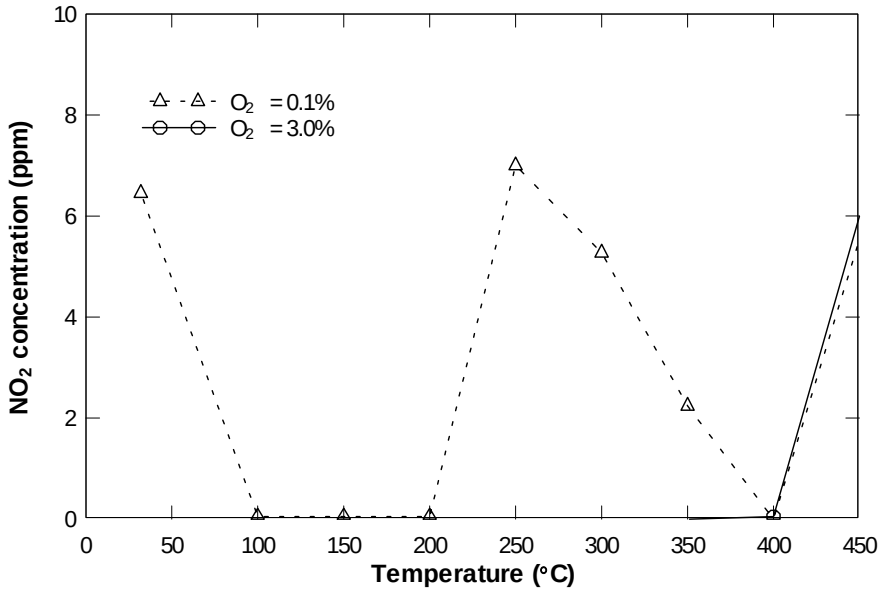

Figure 67. NO_2 concentration as a function of the reaction temperature at various oxygen concentrations over V_2O_5-WO_3/TiO_2. Reaction conditions: [NO] = 330 ppm, [NH_3] = 330 ppm, 0 - 3.0% O_2, preheating case, and SV = 10500 h^{-1}.

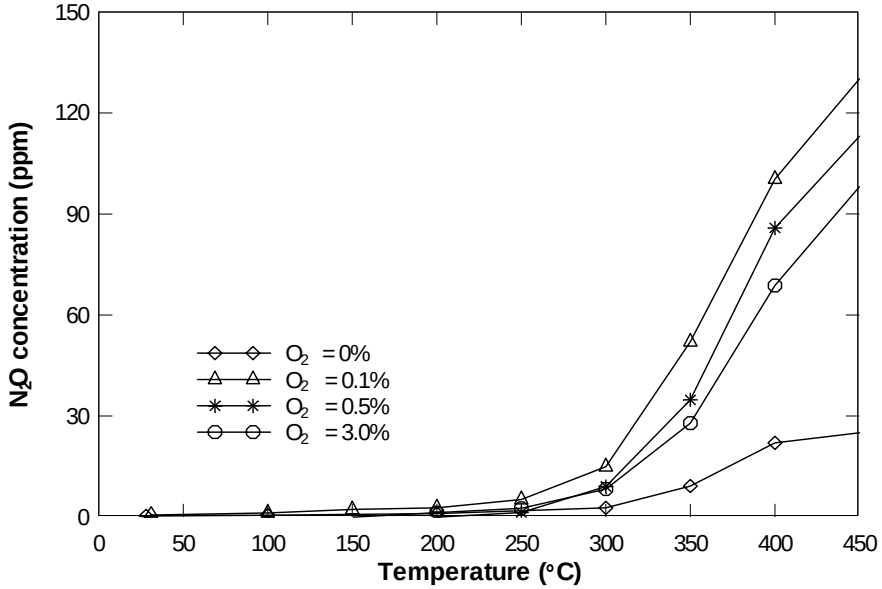

Figure 68. N_2O concentration as a function of the reaction temperature at various oxygen concentrations over V_2O_5-WO_3/TiO_2. Reaction conditions: [NO] = 330 ppm, [NH_3] = 264 ppm (NH_3-to-NO ratio = 0.8), 0 - 3.0% O_2, preheating case, and SV = 10500 h^{-1}.

Figures 68 and 69 illustrate the production of N2O and NO2 concentrations, respectively, as a function of the reaction temperature at various oxygen concentrations for the conditions of [NH_3] = 264 ppm (corresponding to NH_3-to-NO ratio of 0.8), heating area of zones 2 + 3 (preheating case), and SV = 10500 h^{-1}.

Figure 68 presents that N_2O concentrations increase sharply at higher reaction temperatures above 300°C in the presence of oxygen. The maximum production of N_2O is approximately 130 ppm at the reaction temperature of 450°C at the oxygen concentration of 0.1%. In the presence of oxygen, the concentrations of N_2O decrease with an increase in oxygen concentration.

In figure 69, the results of NO_2 production at the oxygen concentration of only 0 and 0.1% O_2 are shown. The production of NO_2 at 0.5 and 3.0% O_2 did not occur in these experiments. The maximum concentration of NO_2 is approximately 39 ppm at the reaction temperature of 200°C at 0.1% O_2.

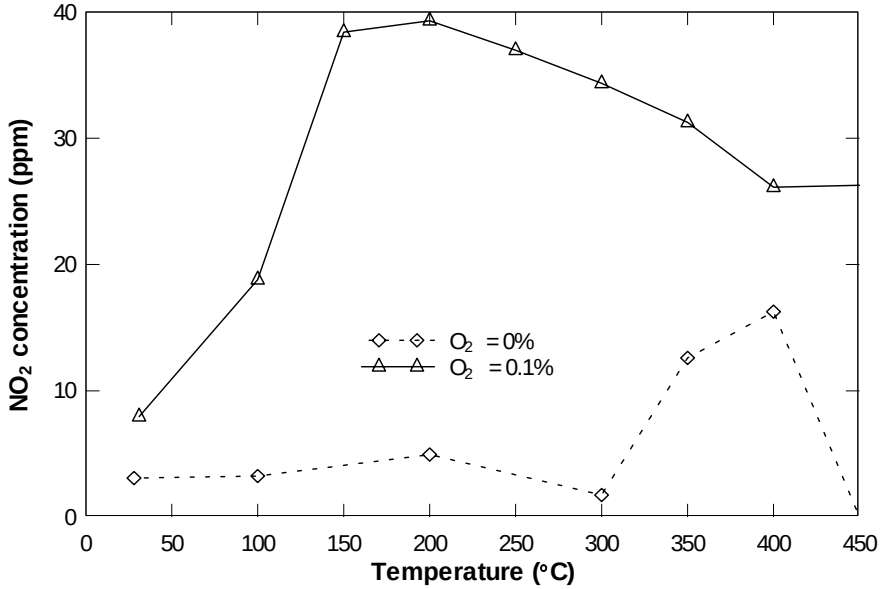

Figure 69. NO_2 concentration as a function of the reaction temperature at various oxygen concentrations over V_2O_5-WO_3/TiO_2. Reaction conditions: [NO] = 330 ppm, [NH_3] = 264 ppm (NH_3-to-NO ratio = 0.8), 0 - 3.0% O_2, preheating case, and SV = 10500 h^{-1}.

Figures 70 and 71 represent the production of N2O and NO2 concentrations, respectively, as a function of the reaction temperature at various oxygen concentrations for the conditions of [NH_3] = 660 ppm (corresponding to NH_3-to-NO ratio = 2.0), heating area of zones 2 + 3 (preheating case), and SV = 10500 h^{-1}.

In figure 70, N_2O concentrations over 5 ppm appear at the reaction temperature of 250°C and increase steeply at higher reaction temperatures in the presence of oxygen. The maximum concentration of N_2O is approximately 300 ppm at the reaction temperature of 450°C at 0.1% O_2, and the results are the highest values among all N_2O production. In the presence of oxygen, N_2O concentrations decrease with an increase in oxygen concentration.

In figure 71, the results of NO_2 production at the oxygen concentration of only 0% O_2 are shown. The production of NO_2 at 0.1, 0.5 and 3.0% O_2 was not detected from the experiments. The maximum concentration of NO_2 is approximately 19 ppm at the reaction temperature of 200°C at 0.1% O_2.

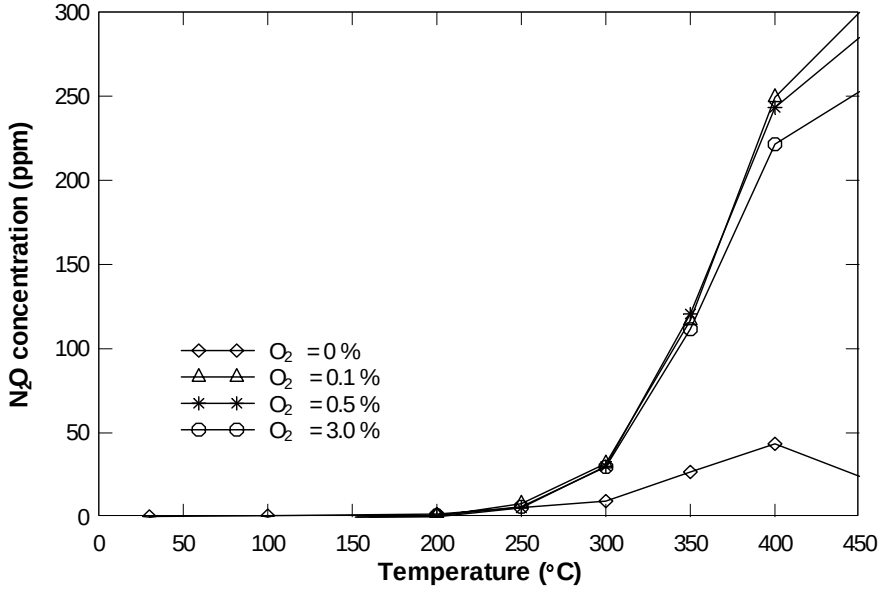

Figure 70. N_2O concentration as a function of the reaction temperature over V_2O_5-WO_3/TiO_2. Reaction conditions: [NO] = 330 ppm, [NH_3] = 660 ppm (NH_3-to-NO ratio = 2.0), 0 - 3.0% O_2, preheating case, and SV = 10500 h^{-1}.

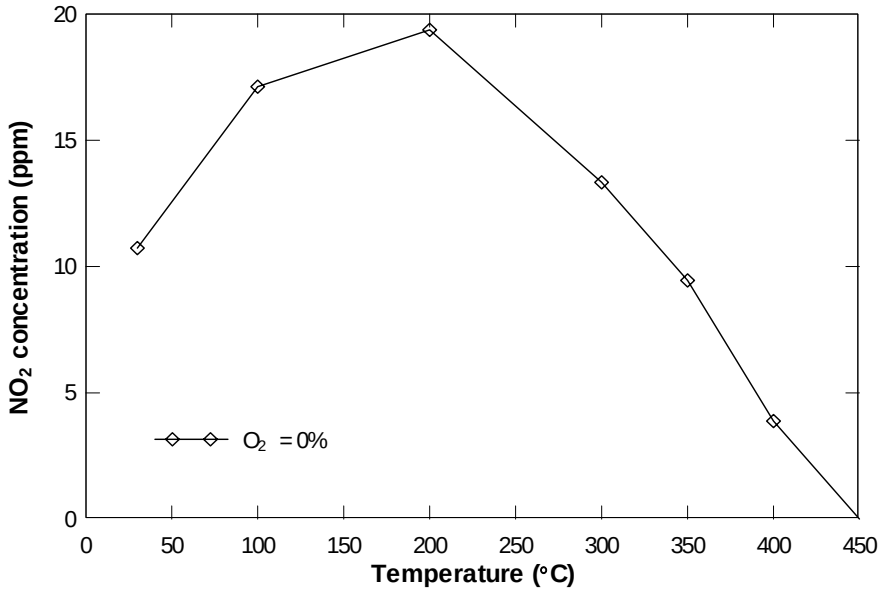

Figure 71. NO_2 concentration as a function of the reaction temperature over V_2O_5-WO_3/TiO_2. Reaction conditions: [NO] = 330 ppm, [NH_3] = 660 ppm (NH_3-to-NO ratio = 2.0), 0 - 3.0% O_2, preheating case, and SV = 10500 h^{-1}.

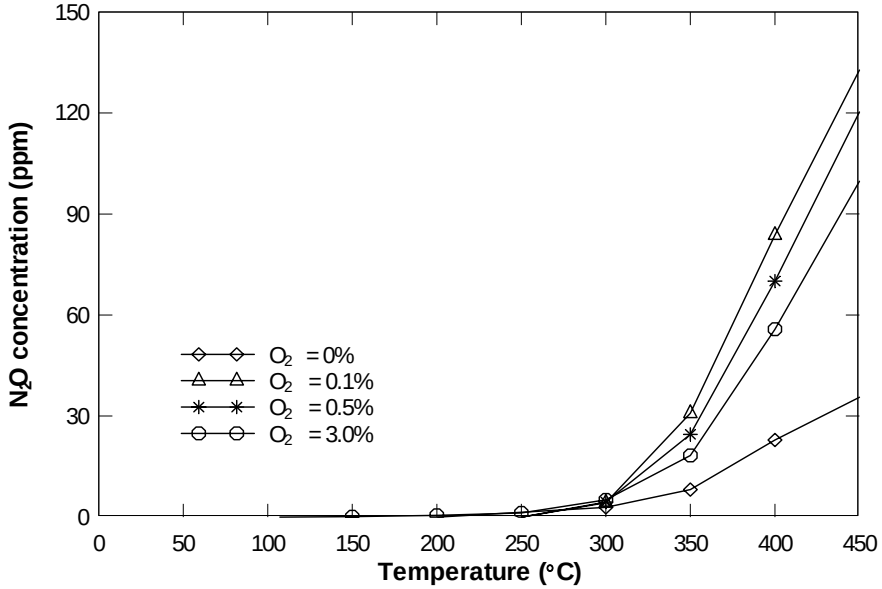

Figure 72. N_2O concentration as a function of the reaction temperature at various oxygen concentrations over V_2O_5-WO_3/TiO_2. Reaction conditions: [NO] = 330 ppm, [NH_3] = 330 ppm, 0 - 3.0% O_2, heating area of zone 2, and SV = 21000 h^{-1}.

Figure 72 describes N_2O production as a function of the reaction temperature at various oxygen concentrations for the conditions of the heating area of zone 2, and SV = 21000 h^{-1}. N_2O concentrations of 5 ppm or less appear for temperatures below 300°C and then increase at higher temperatures in the presence of oxygen. The maximum concentration of N_2O obtained is approximately 133 ppm at 0.1% O_2. In the presence of oxygen, N_2O concentrations decrease with an increase in oxygen concentration. No concentration of NO_2 is produced for this condition.

Figures 73 and 74 represent the production of N_2O and NO_2 concentrations, respectively, as a function of the reaction temperature at various oxygen concentrations for the conditions of preheating case and SV = 21000 h^{-1}. Similar results are obtained for the production of N_2O, and the maximum value obtained is approximately 151 ppm at 0.1% O_2, as shown in figure 73. NO_2 production at 0.1% O_2 is only shown in figure 74. No NO_2 production at 0, 0.5 and 3.0% O_2 occurred from the experiments. The maximum NO_2 concentration is approximately 3.3 ppm at 33°C at 0.1% O_2.

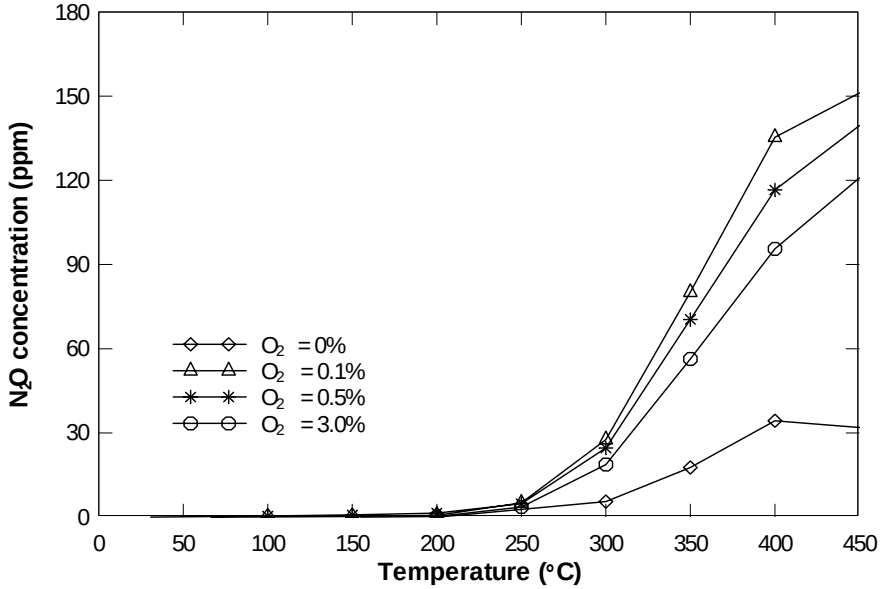

Figure 73. N_2O concentration as a function of the reaction temperature at various oxygen concentrations over V_2O_5-WO_3/TiO_2. Reaction conditions: [NO] = 330 ppm, [NH_3] = 330 ppm, 0 - 3.0% O_2, preheating case, and SV = 21000 h^{-1}.

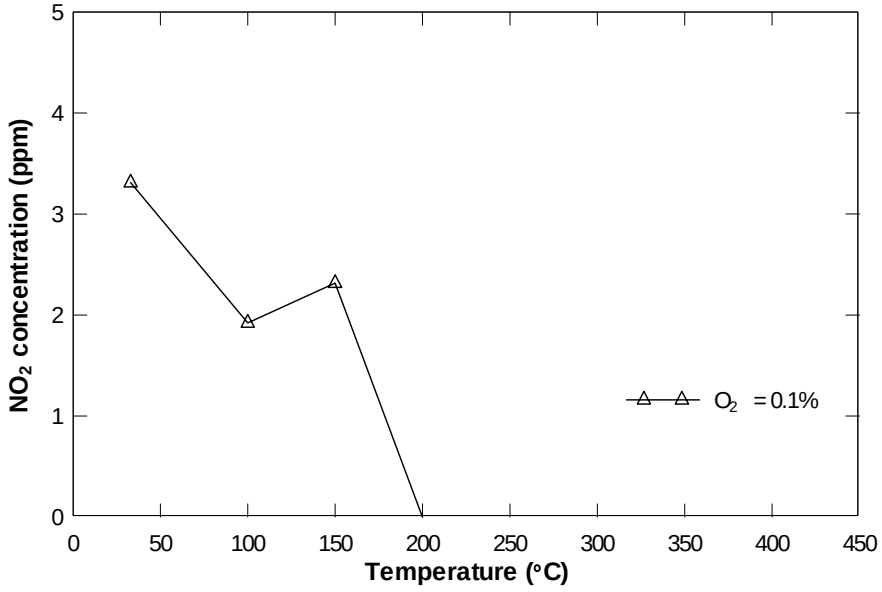

Figure 74. NO_2 concentration as a function of the reaction temperature at various oxygen concentrations over V_2O_5-WO_3/TiO_2. Reaction conditions: [NO] = 330 ppm, [NH_3] = 330 ppm, 0 - 3.0% O_2, preheating case, and SV = 21000 h^{-1}.

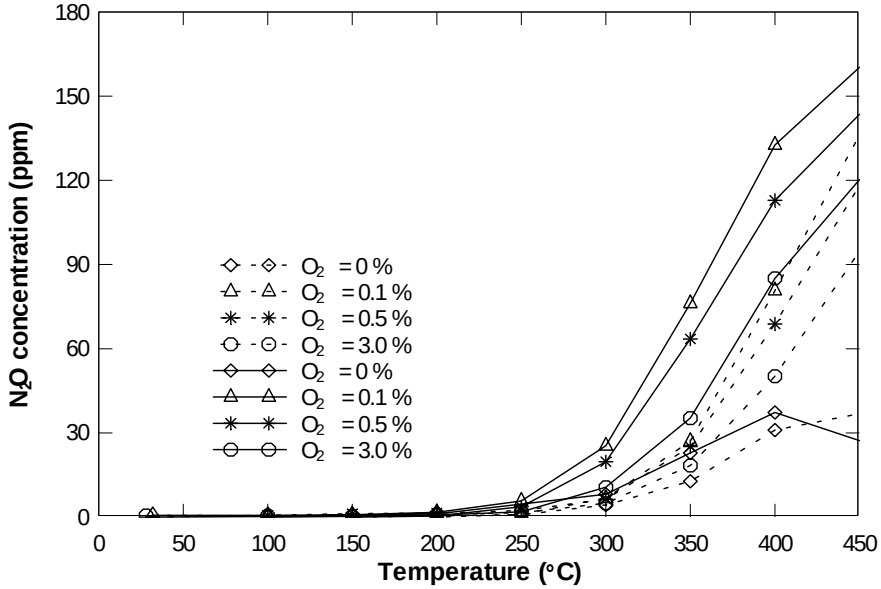

Figure 75. N_2O concentration as a function of the reaction temperature at various heating areas over V_2O_5-WO_3/TiO_2. Reaction conditions: [NO] = [NH_3] = 330 ppm, 0 - 3.0% O_2, SV = 10500 h^{-1}, and heating areas of zone 2 (broken line) and preheating (solid line).

To understand the various effects of the heating area, NH_3-to-NO ratio and space velocity on N_2O production, results presented before are combined together and explained.

Figure 75 (a combination of figures 64 and 66) presents the effect of the heating area on N_2O production for the condition of space velocity of 10500 h^{-1}. The production of N_2O increases with an increase in heating area from zone 2 to zones 2 and 3 in the presence of oxygen. The difference of the maximum N_2O production at 0.1% O_2 is 24 ppm.

Figure 76 (a combination of figures 72 and 73) shows the effect of the heating area on N_2O production at SV = 21000 h^{-1}. The similar result which the production of N_2O increases with an increase in heating area in the presence of oxygen is observed. The difference of the maximum N_2O production at 0.1% O_2 is 18 ppm.

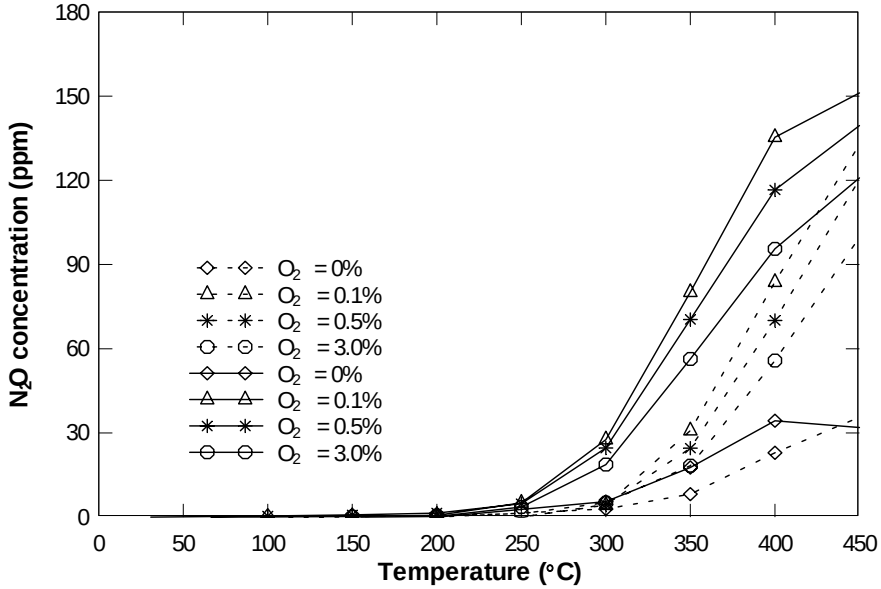

Figure 76. N_2O concentration as a function of the reaction temperature at various heating areas over V_2O_5-WO_3/TiO_2. Reaction conditions: [NO] = [NH_3] = 330 ppm, 0 - 3.0% O_2, SV = 21000 h^{-1}, and heating areas of zone 2 (broken line) and preheating (solid line).

Results from figure 66, 68 and 70 are combined into figure 77 to illustrate the effect of NH_3-to-NO ratio on the production of N_2O at SV = 10500 h^{-1}. The production of N_2O decreases with a decrease in NH_3-to-NO ratio for all cases. The difference of the maximum N_2O production at NH_3-to-NO ratio between 0.8 and 2.0 at 0.1% O_2 is 170 ppm.

Figure 78 (a combination of figures 64 and 72) presents the effect of variation in the space velocity on the production of N_2O in the heating area of zone 2. The change of the space velocity does not have a significant influence on the production of N_2O concentration.

Results form figures 66 and 73 are combined into figure 79 to show the effect of variation in the space velocity on the production of N_2O for the preheating case (zone 2 + 3). Again, no great effect for the various space velocities on the production of N_2O concentration is observed.

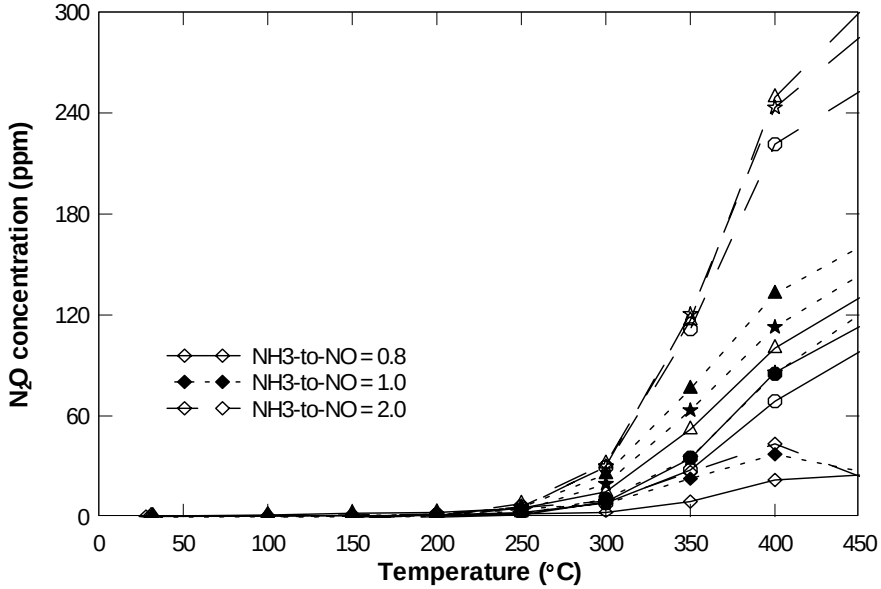

Figure 77. N_2O concentration as a function of the temperature at various NH_3-to-NO ratios over V_2O_5-WO_3/TiO_2. Reaction conditions: 0 - 3.0% O_2, preheating case, SV = 10500 h^{-1}, and NH_3-to-NO ratio = 0.8 (solid lines with open symbols), 1.0 (dashed lines with closed symbols), and 2.0 (broken lines with open symbols).

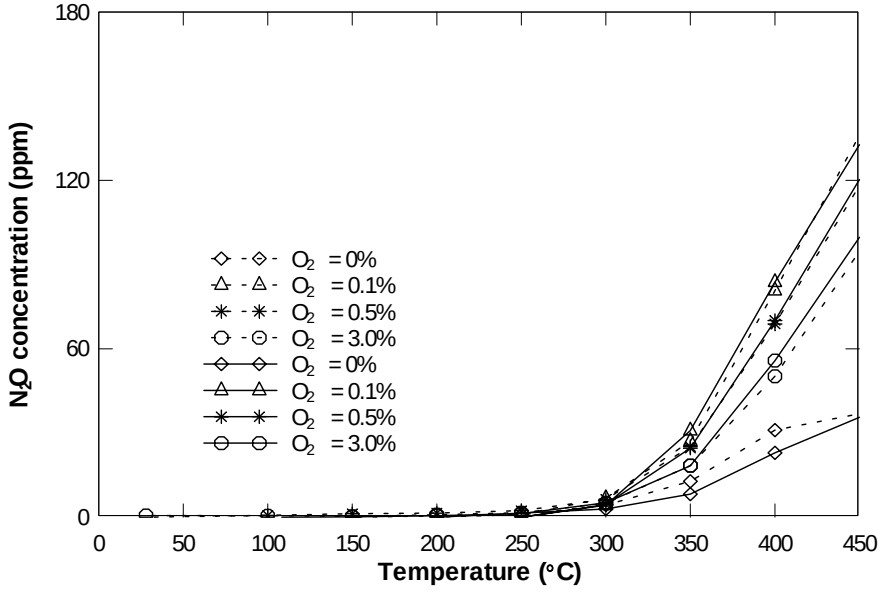

Figure 78. N_2O concentration as a function of the temperature at various space velocities over V_2O_5-WO_3/TiO_2. Reaction conditions: [NO] = [NH_3] = 330 ppm, zone 2 heated, 0 - 3.0% O_2, and SV = 10500 h^{-1} (broken line) and 21000 h^{-1} (solid line).

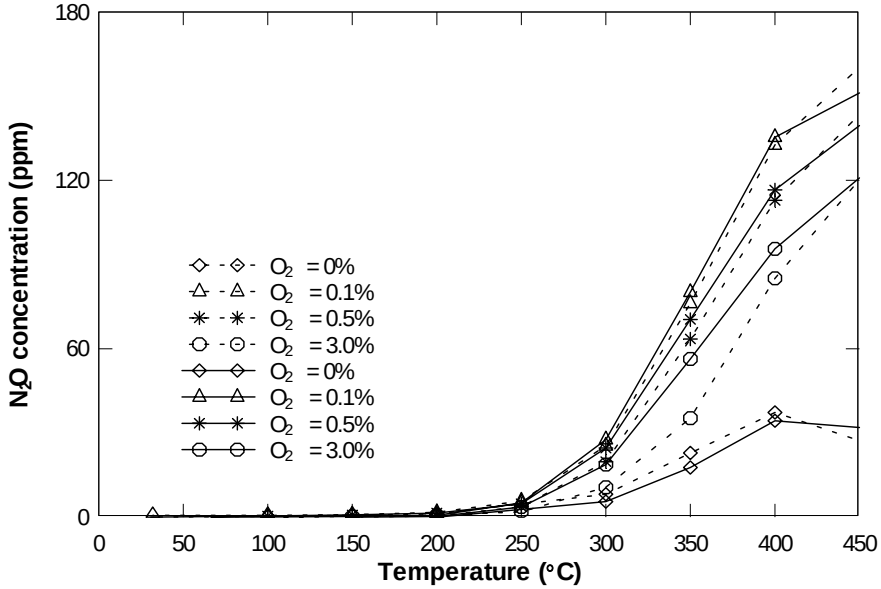

Figure 79. N_2O concentration as a function of the reaction temperature at various space velocities over V_2O_5-WO_3/TiO_2. Reaction conditions: [NO] = [NH_3] = 330 ppm, preheating case, 0 - 3.0% O_2, and SV = 10500 h^{-1} (broken line) and 21000 h^{-1} (solid line).

6.1.7 Effect of Different Arrangements of a Catalyst

So far, all catalysts used in these experiments were single monolith honeycomb samples (standard case). In this section, however, different arrangements of V_2O_5-WO_3/TiO_2 catalyst samples are used as shown in figure 32. Two cases were performed, which were the sample conditions of “twist only” and “both twist and separate”. Figure 32 (a) shows 2 cm long twist samples that were cut off 1 cm long each and placed together with 45° twist in the quartz-tube as a second arrangement. Figure 32 (b) shows a 45° twist and 5 cm separated sample that were cut off 1 cm long each and placed 5 cm away from each other with 45° twist in the quartz-tube as a third arrangement. The purpose of different arrangements of catalyst samples was to reduce the ‘slip’ of gases past the catalyst surface. Therefore, hypothetically, more reactions and better results were expected. The catalytic reactions occurred for the conditions of [NO] = [NH_3] = 330 ppm, preheating area, 0 - 3.0% O_2, and SV = 10500 h^{-1} (2 cm in length). The results are compared to the results of the standard case.

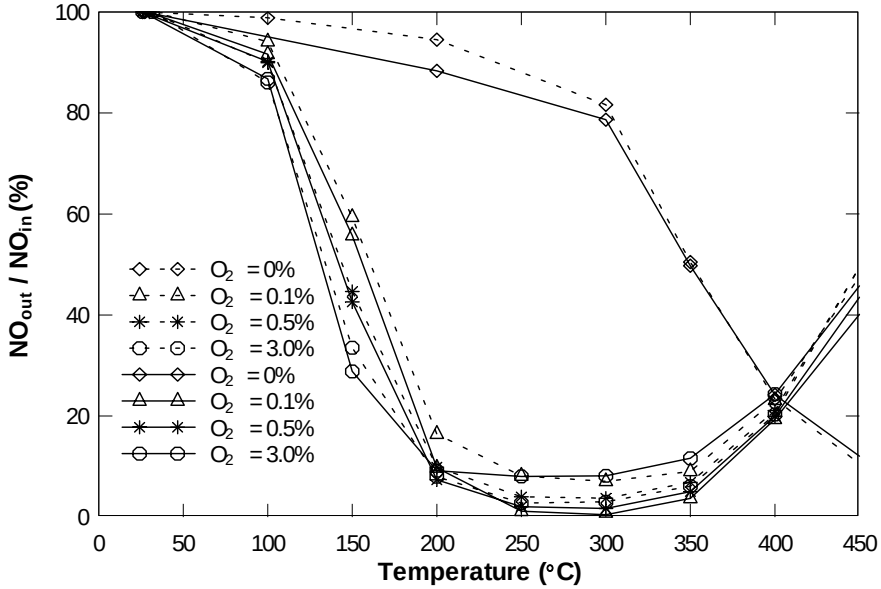

Figure 80. NO reduction as a function of the reaction temperature for arrangements of the catalyst. Reaction conditions: [NO] = [NH_3] = 330 ppm, preheating case, 0 - 3.0% O_2, a standard case (broken line), and a second arrangement case (solid line).

6.1.7 1. Effect of a Second Arrangement (45° Twist) of a Catalyst

In figures 80 to 83, the results are presented the standard case (broken lines) and the second arrangement case (solid lines) of the catalyst sample. Figure 80 describes NO reduction as a function of the reaction temperature over a 45° twist V_2O_5-WO_3/TiO_2 catalyst (second arrangement case). The results of the standard case are from the figure 46. NO reductions at 3.0% O_2 (second arrangement case) are shown worse than those of the standard case, however, the results at 0.1 and 0.5% O_2 (second arrangement case) show better than those of the standard case. NO reductions at 0.1% O_2 case show considerably higher results than those of the standard case.

In figure 81, the effect of a second arrangement catalyst (45° twist) on NH_3 conversion is observed. The results of the standard case are from the figure 47. NH_3 conversions at 3.0% O_2 of the second arrangement case show the best among the all results. NH_3 conversions of the second arrangement case are shown a little higher than those of the standard case for the entire reaction temperature range.

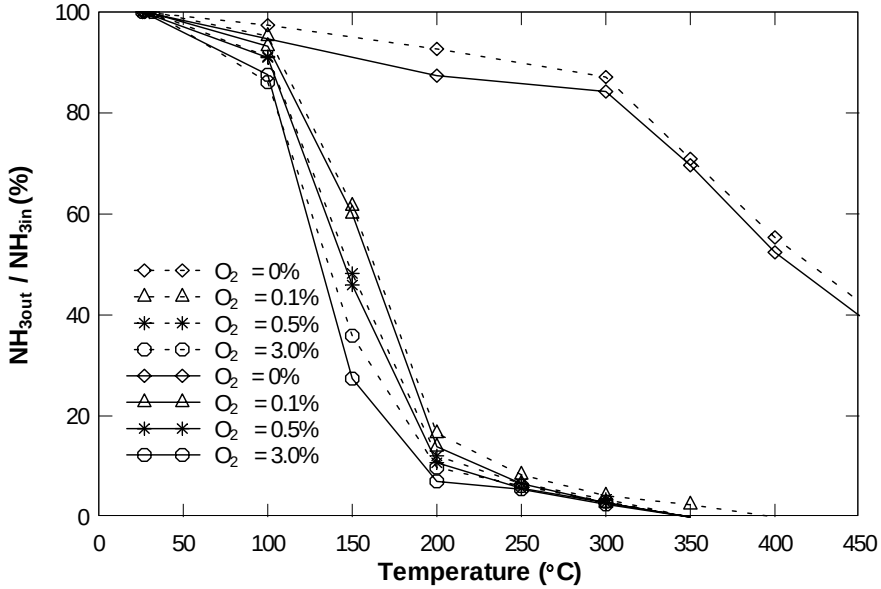

Figure 81. NH_3 conversion as a function of the reaction temperature for arrangements of the catalyst. Reaction conditions: [NO] = [NH_3] = 330 ppm, preheating case, 0 - 3.0% O_2, a standard case (broken line), and a second arrangement case (solid line).

Figure 82 illustrates N_2O concentration as a function of the reaction temperature over a 45° twist V_2O_5-WO_3/TiO_2 catalyst (second arrangement case). The results of the standard case are from the figure 66. Not much change is observed between two results for the entire reaction temperature range.

In figure 83, the effect of a 45° twist catalyst (second arrangement case) on NO_2 production as a function of the reaction temperature is observed. The results of the standard case are from the figure 67. Much NO_2 concentrations are produced for the second arrangement case for the entire temperature range. The maximum NO_2 production was obtained approximately 48 ppm at 3.0% O_2 at 450°C.

As a consequence of the second arrangement case, NO reduction and NH_3 conversion were generally found slight higher than those of the standard case. The result of N_2O production showed no significant change for the entire reaction temperature range. The results of the second arrangement case show even much higher production of NO_2 concentration.

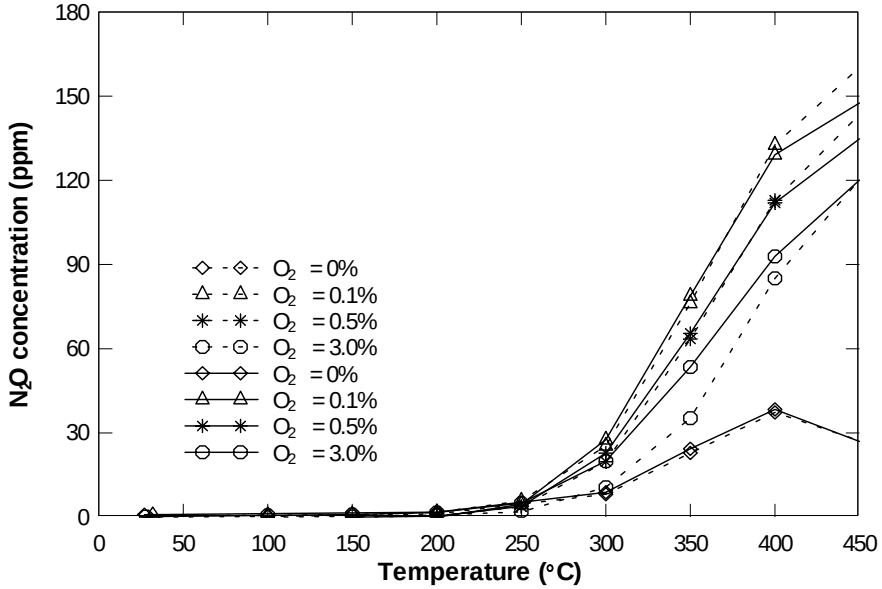

Figure 82. N_2O concentration as a function of the temperature for arrangements of the catalyst. Reaction conditions: [NO] = [NH_3] = 330 ppm, preheating case, 0 - 3.0% O_2, a standard case (broken line), and a second arrangement case (solid line).

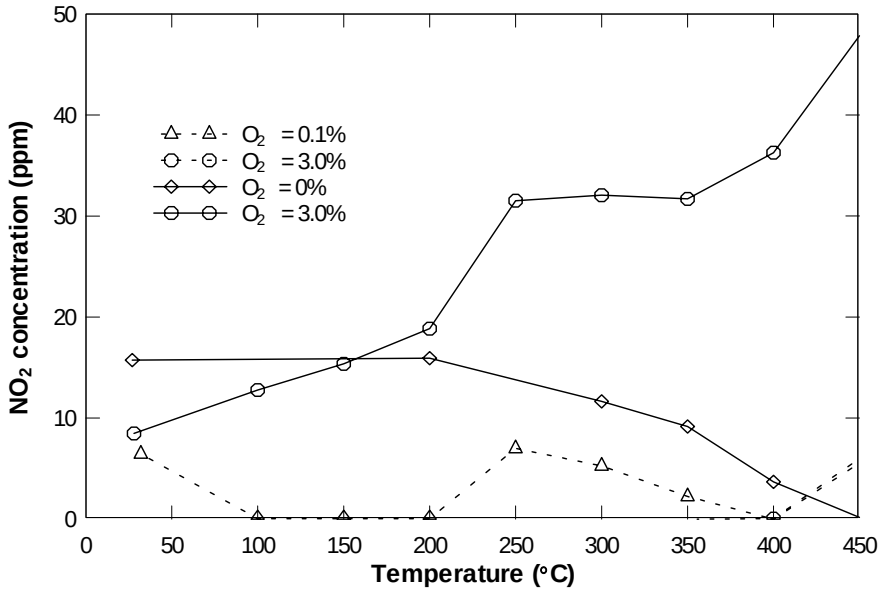

Figure 83. NO_2 concentration as a function of the temperature for arrangements of the catalyst. Reaction conditions: [NO] = [NH_3] = 330 ppm, preheating case, 0 - 3.0% O_2, a standard case (broken line), and a second arrangement case (solid line).

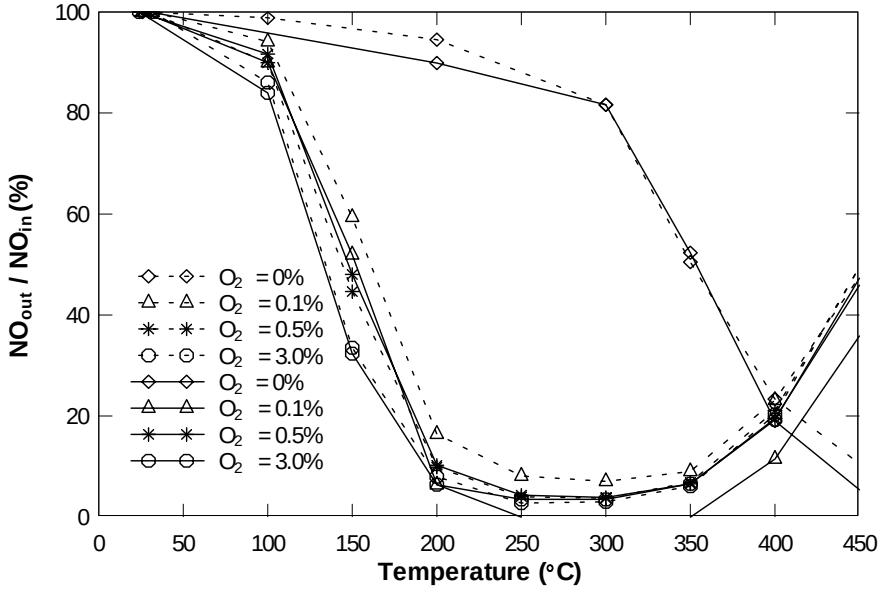

Figure 84. NO reduction as a function of the temperature for arrangements of the catalyst. Reaction conditions: [NO] = [NH_3] = 330 ppm, preheating case, 0 - 3.0% O_2, a standard case (broken line), and a third arrangement case (solid line).

6.1.7.2 Effect of a Third Arrangement (45° Twist and 5 cm Separate) of a Catalyst

Figure 84 presents NO reduction as a function of the reaction temperature over a 45° twist and 5 cm separate V_2O_5-WO_3/TiO_2 catalyst (third arrangement case). The results of the standard case are from figure 46. For the entire reaction temperature range, NO reductions of 0.1% O_2 for the third arrangement case are observed considerably higher results, whereas, the other results show much less difference.

Figures 85 and 86 show the effect on NH_3 conversion and N_2O production, respectively for the third arrangement case. The results of the standard case are from the figure 47 for NH_3 conversion and figure 66 for N_2O production. No great change is observed for the entire temperature range for both results.

As a consequence of the third arrangement case, no remarkable result was observed, except for the result of 0.1% O_2. It should be noticed that no NO_2 concentration was produced from the reaction. In general, the results do not sufficiently support the idea that alternative physical arrangements method yield better results.

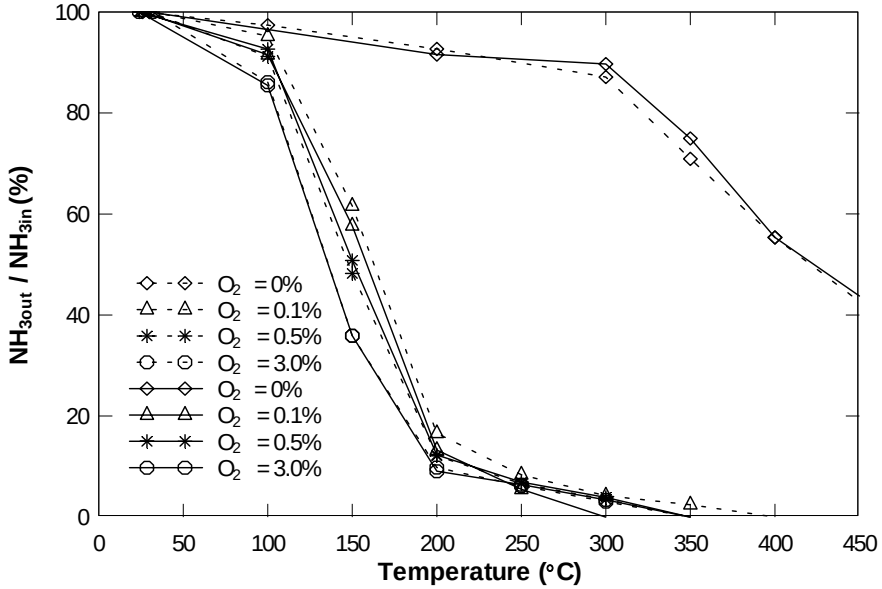

Figure 85. NH_3 conversion as a function of the temperature for arrangements of the catalyst. Reaction conditions: [NO] = [NH_3] = 330 ppm, preheating case, 0 - 3.0% O_2, a standard case (broken line), and a third arrangement case (solid line).

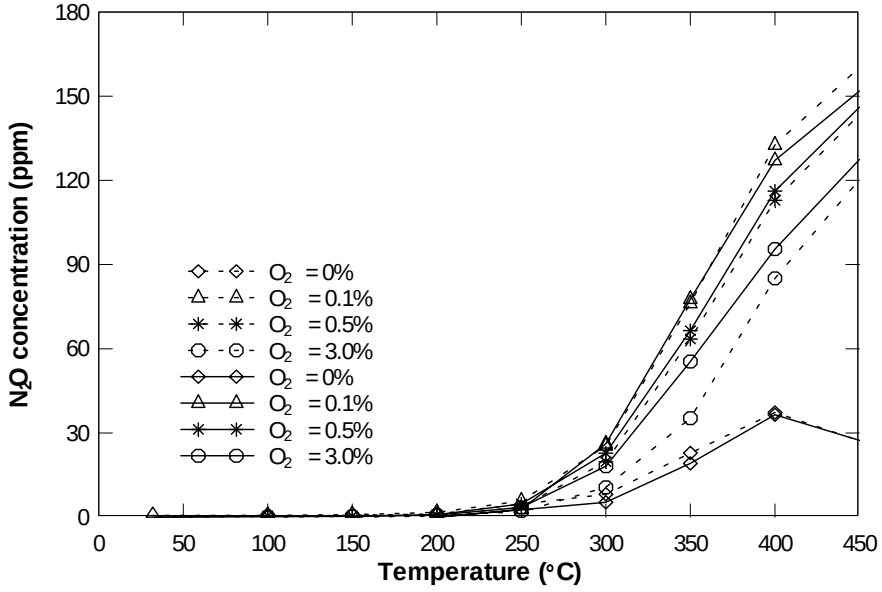

Figure 86. N_2O concentration as a function of the temperature for arrangements of the catalyst. Reaction conditions: [NO] = [NH_3] = 330 ppm, preheating case, 0 - 3.0% O_2, a standard case (broken line), and a third arrangement case (solid line).

Table 16. Maximum NO reduction at the reaction temperature.

Oxygen concentration (%)	Maximum NO reduction (%) / Temperature (°C)		
	Standard case	Second arrangement	Third arrangement
0	89.5 / 450	87.9 / 450	94.6 / 450
0.1	92.9 / 300	99.5 / 300	100 / 300
0.5	96.2 / 300	98.3 / 300	96.1 / 300
3.0	97.2 / 250	91.9 / 250	96.5 / 250

Table 17. The average NO reduction at the temperatures between 200 and 350°C.

Oxygen concentration (%)	Average NO reduction (%)		
	Standard case	Second arrangement	Third arrangement
0	24.5	27.7	25.5
0.1	89.8	96.2	98.4
0.5	93.8	95.9	93.8
3.0	95	90.1	95

Table 16 lists maximum NO reductions and their reaction temperatures for three physical arrangement of a V_2O_5-WO_3/TiO_2 catalyst sample. The highest maximum NO reduction is obtained for the 3.0% O_2 case for single monolith honeycomb sample (standard case). In contrast, for other arrangement case, the highest maximum NO reduction is found at 0.1% O_2. The reaction temperatures obtained maximum NO reductions are identical for all cases at each oxygen concentration and decrease with an increase in oxygen concentration.

Table 18. The lowest reaction temperatures for 100% NH_3 conversion.

Oxygen concentration (%)	Lowest temperature of 100% NH_3 conversion (°C)		
	Standard case	Second arrangement	Third arrangement
0	-	-	-
0.1	400	350	300
0.5	350	350	350
3.0	350	350	350

As mentioned (in section: 6.1.5. Effect of Different Heating Areas), NO reduction over 83% is determined at reaction temperatures between 200 and 350°C in the presence of oxygen for the preheating case (zone 2 + 3) at a space velocity of 10500 h^{-1}. Table 17 lists the average NO reduction at reaction temperatures between 200 and 350°C for three physical arrangements of a V_2O_5-WO_3/TiO_2 catalyst. The average NO reductions for the standard case increase with an increase in oxygen concentration. Unlike the results for the standard case, results for the second arrangement case decrease with an increase in oxygen concentration in the presence of oxygen. For the third arrangement case, the results do not show a certain order. Comparing to the results for the standard case, the average NO reductions for two arrangement cases at the oxygen concentration of 0.1% show great improvement.

Table 18 lists the lowest reaction temperatures of 100% NH_3 conversion for three physical changes of a V_2O_5-WO_3/TiO_2 catalyst. The reaction temperature changes at oxygen concentration of 0.1%, otherwise, 100% NH_3 conversion is determined at the temperature of 350°C for 0.5 and 3.0% O_2.

6.2 Comparison of Results between V_2O_5-WO_3/TiO_2 and V_2O_5/TiO_2 Catalysts from Previous Study

The selective catalytic reduction (SCR) of nitric oxide (NO) with ammonia over V_2O_5/TiO_2 monolithic honeycomb catalysts has been studied in a previous investigation [37]. The comparisons of the results between V_2O_5-WO_3/TiO_2 and V_2O_5/TiO_2 catalysts is presented and discussed case by case for the different reaction conditions.

Table 19 lists the experimental cases for V_2O_5/TiO_2 monolithic honeycomb catalysts. Three NH_3-to-NO ratios of 0.8, 1.0 and 2.0 were tested. The space velocity varied from 7000 to 64000 h^{-1}. Table 20 lists the space velocity calculation for V_2O_5/TiO_2 catalysts. The oxygen concentration increased mainly from 0.1 to 3.0%, and 0% O_2 was tested for the case of the space velocity of 42000 h^{-1}. Zone 2 and 3 were heated as the heating area for all cases.

Table 19. Experimental cases on V_2O_5/TiO_2 monolithic honeycomb catalysts [37].

NH_3-to-NO ratio	Space velocity (h^{-1})	Oxygen concentration (%)
0.8 ([NO] = 330 ppm [NH_3] = 264 ppm)	42000	0.1 0.5 3.0
1.0 ([NO] = 330 ppm [NH_3] = 330 ppm)	7000	0.1 0.5 3.0
	42000	0 0.1 0.5 3.0
	64000	0.1 0.5 3.0
2.0 ([NO] = 330 ppm [NH_3] = 660 ppm)	42000	0.1 0.5 3.0

Table 20. Space velocity calculation for V_2O_5/TiO_2 catalysts [37].

Quartz-tube radius [r] (cm)	Catalyst length [l] (cm)	Catalyst volume [V (= $\pi r^2 l$)] (cm^3)	Space velocity [SV] (h^{-1})
1	3	9.425	7000
0.5	2	1.571	42000
0.5	1.3	1.021	64000

The results from the previous work for V_2O_5/TiO_2 monolithic honeycomb catalysts in the presence of oxygen are reviewed as follows [37]:

(1) An increase in oxygen concentration from 0.1 to 3.0% reduced the reaction temperature of the maximum NO reduction and slightly improved the maximum NO reduction. The N_2O production declined, and NO_2 concentration increased with an increase in oxygen concentration simultaneously.

(2) The increase of the NH_3-to-NO ratio from 0.8 to 2.0 increased the maximum NO reduction from 60 to 75% at a SV = 42000 h^{-1}. However, an accompanied increase in the residual ammonia at 500°C and in N_2O production was also observed, irrespective of the oxygen concentration.

(3) An increase in space velocity from 7000 to 64000 h^{-1} decreased the maximum NO reduction from 95% to as low as 60%, irrespective of the oxygen concentration. It also increased the amount of residual ammonia at 500°C, but an accompanied decrease of the N_2O production from 140 to 90 ppm and the complete elimination of NO_2 concentration were observed.

6.2.1 Effect of Oxygen Concentration

Figures 87 and 88 show the effect of different vanadia-based catalysts on NO reduction and NH_3 conversion, respectively, for the conditions of [NO] = 330 ppm, [NH_3] = 330 ppm, heating area of zone 2 + 3 (preheating case), 0.1 - 3.0% O_2, SV = 7000 h^{-1} over V_2O_5/TiO_2 (solid lines), and SV = 10500 h^{-1} over V_2O_5-WO_3/TiO_2 (broken lines). All data for the V_2O_5/TiO_2 catalyst sample were collected from the previous study [37].

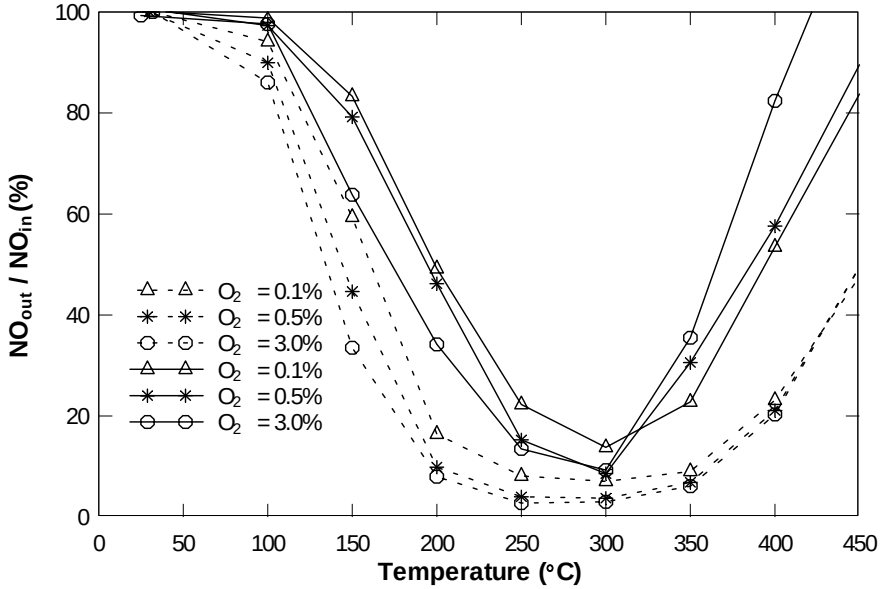

Figure 87. NO reduction as a function of the temperature over different catalysts. Reaction conditions: [NO] = [NH_3] = 330 ppm, 0.1 - 3.0% O_2, preheating case, SV = 7000 h^{-1} over V_2O_5/TiO_2 (solid lines), and SV = 10500 h^{-1} over V_2O_5-WO_3/TiO_2 (broken lines).

In figure 87, for the reference (V_2O_5/TiO_2) catalyst (solid lines), NO reduction increases with an increase in oxygen concentration at reaction temperatures below 300°C, but the reverse occurs at temperatures above 300°C. Over 90% NO reductions are achieved only at the temperature of 300°C for the oxygen concentration of 0.5 and 3.0%. The maximum NO reduction for the 0.1% O_2 case is 86.2% for the reaction temperature of 300°C. The temperature window for NO reduction over 90% is narrower than 50°C shown the temperature range between 250 and 350°C. On the other hand, for the V_2O_5-WO_3/TiO_2 catalyst sample (broken lines), NO reduction increases with the increase of the oxygen concentration for the entire temperature range. The maximum NO reduction is found to be 97% at 250°C at 3.0% O_2. The temperature window over 90% is approximately 150°C shown the temperature range between 200 and 350°C.

In figure 88, NH_3 conversions for both catalysts increase with an increase in oxygen concentration for the entire temperature range.

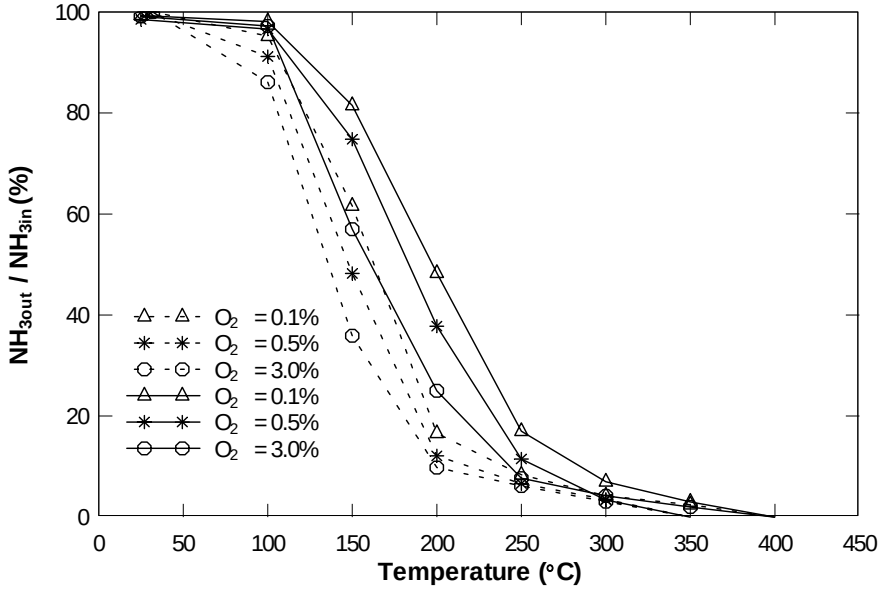

Figure 88. NH_3 conversion as a function of the temperature over different catalysts. Reaction conditions: [NO] = [NH_3] = 330 ppm, 0.1 - 3.0% O_2, preheating case, SV = 7000 h^{-1} over V_2O_5/TiO_2 (solid lines), and SV = 10500 h^{-1} over V_2O_5-WO_3/TiO_2 (broken lines).

6.2.2 Effect of Tungsten Species (WO_3) Addition

It is well known [24, 31] that the promoter, WO_3, significantly improves the catalytic activity of the selective catalytic reduction (SCR) process at lower temperatures and broadens the reaction temperature window of the maximum NO conversion. The results of V_2O_5/TiO_2 and V_2O_5-WO_3/TiO_2 in figures 87 and 88 were not obtained under exactly the same conditions: the space velocity is different (as mentioned before).

In general, higher NO reduction and NH_3 conversion are found at lower space velocities. Though the V_2O_5/TiO_2 sample was tested at a lower space velocity, the results obtained were lower than those for the V_2O_5-WO_3/TiO_2 catalyst for the entire temperature range under the same conditions. This was because of the effect of the addition of tungsten species (WO_3). In figure 87, with the addition of tungsten species, the maximum NO reduction increases from approximately 91% to 97% at 3.0% O_2 and broadens the active reaction temperature window. Figure 88 shows the improvement on NH_3 conversion, as well, with the addition of tungsten species.

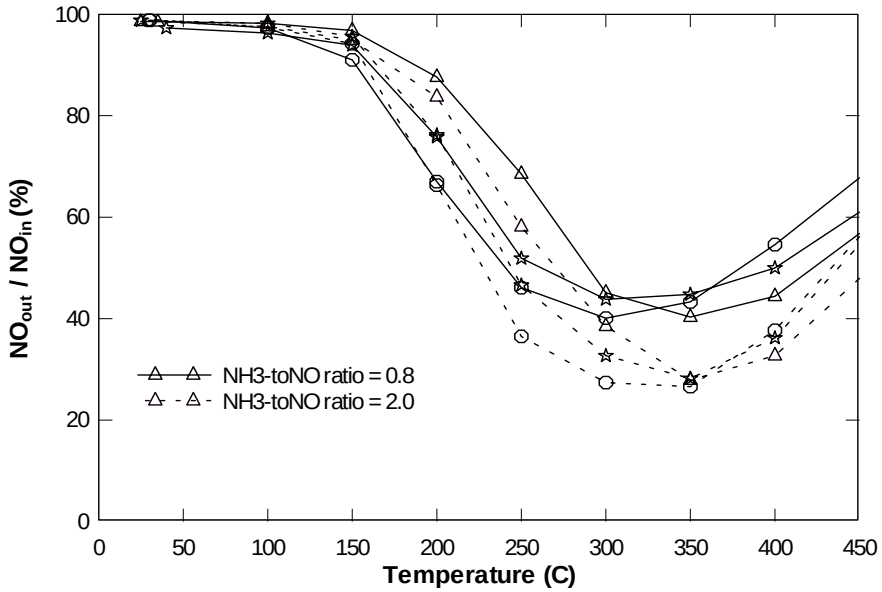

Figure 89. NO reduction as a function of the reaction temperature at various NH_3-to-NO ratios over V_2O_5/TiO_2. Reaction conditions: [NO] = [NH_3] = 330 ppm, 0.1 - 3.0% O_2, preheating case, SV = 42000 h^{-1}, and NH_3-to-NO ratio = 0.8 (solid lines with open symbols) and 2.0 (broken lines with open symbols) [37].

6.2.3 Effect of NH_3-to-NO Ratio

Figures 89 and 90 describe the effect of the variation of NH_3-to-NO ratio on NO reduction and NH_3 conversion, respectively, as a function of the reaction temperature at space velocity of 42000 h^{-1} over V_2O_5/TiO_2 catalyst. All data of the reference sample were provided from the previous investigation [37]. The NH_3-to-NO ratios of 0.8 (solid lines with open symbols) and 2.0 (broken lines with open symbols) are presented in these figures. The symbols indicate the oxygen concentrations of 0.1% (△), 0.5% (☆), and 3.0% (O).

An increase in NH_3-to-NO ratio favors higher NO reduction. The increase of the NH_3-to-NO ratio from 0.8 to 2.0 increased the maximum NO reduction from 60 to 75% as shown in figure 89. On the other hand, NH_3 conversion is decreased with an increase in NH_3-to-NO ratio at the same oxygen concentration. More than 10% of the residual NH_3 conversions are found at 450°C for all oxygen concentration at NH_3-to-NO ratio of 2.0.

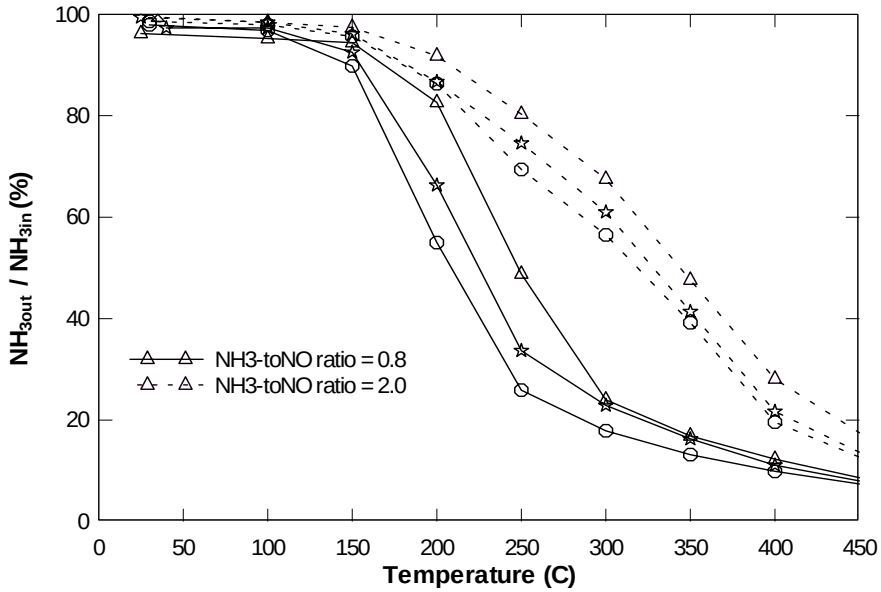

Figure 90. NH_3 conversion as a function of the reaction temperature at various NH_3-to-NO ratios over V_2O_5/TiO_2. Reaction conditions: [NO] = [NH_3] = 330 ppm, 0.1 - 3.0% O_2, preheating case, SV = 42000 h^{-1}, and NH_3-to-NO ratio = 0.8 (solid lines with open symbols) and 2.0 (dashed lines with open symbols) [37].

Figures 51 and 52 show the effect of the variation of NH_3-to-NO ratio on NO reduction and NH_3 conversion, respectively, over V_2O_5-WO_3/TiO_2 at a space velocity of 10500 h^{-1}. A significant increase of NO reduction is observed with an increase in NH_3-to-NO ratio at the same oxygen concentration for the entire reaction temperature range as shown in figure 51. On the contrary, NH_3 conversion was decreased with an increase in NH_3-to-NO ratio at the same oxygen concentration in the presence of oxygen as shown in figure 52. The complete NH_3 conversions were obtained at the reaction temperatures of 250, 350 and 400°C for NH_3-to-NO ratios of 0.8, 1.0 and 2.0, respectively. Therefore, the temperature of 100% NH_3 conversion increased with an increase in NH_3-to-NO ratio.

The results of the variation of NH_3-to-NO ratio on NO reduction and NH_3 conversion for both V_2O_5/TiO_2 and V_2O_5-WO_3/TiO_2 catalysts trend the same, except complete NH_3 conversion is found for V_2O_5-WO_3/TiO_2 catalyst.

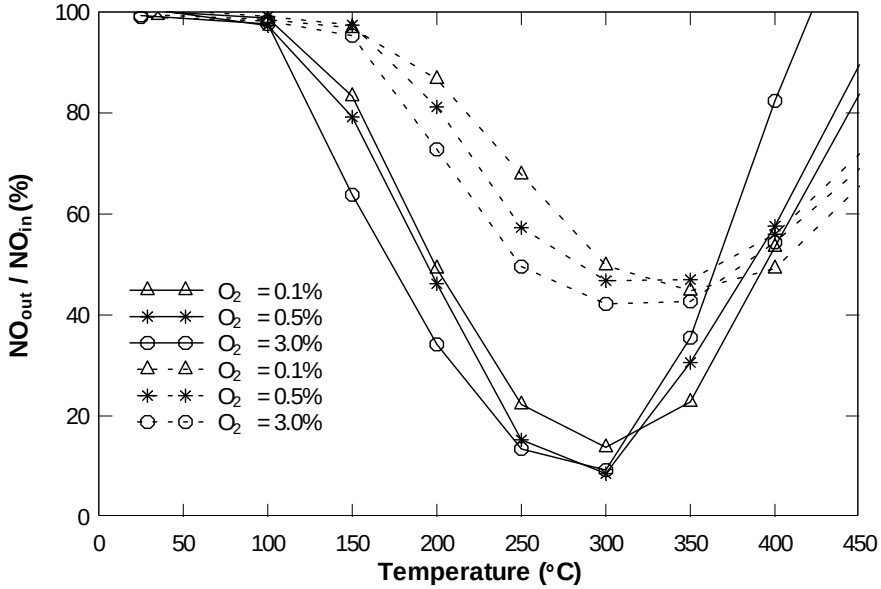

Figure 91. NO reduction as a function of the reaction temperature at various space velocities over V_2O_5/TiO_2. Reaction conditions: [NO] = [NH_3] = 330 ppm, 0.1 - 3.0% O_2, preheating case, SV = 7000 h^{-1} (solid lines) and SV = 64000 h^{-1} (broken lines) [37].

6.2.4 Effect of Space Velocity

NO reduction in figure 91 and NH_3 conversion in figure 92 are described as a function of the reaction temperature at various space velocities over V_2O_5/TiO_2. All data of the reference sample were provided from previous study [37]. In figure 91, the increase of the space velocity from 7000 to 64000 h^{-1} decreases the maximum NO reduction from 95% to as low as 60% at 3.0% O_2. Figure 92 shows that an increase in space velocity reduces the catalytic activity of NH_3 conversion and increases the residual ammonia.

For V_2O_5-WO_3/TiO_2, figures 55 and 56 present the effect of the variation of space velocity on NO reduction and NH_3 conversion, respectively. The results of NO reduction and NH_3 conversion shift toward higher reaction temperature with an increase in space velocity. The lower NO reduction and NH_3 conversion are found at the higher space velocity. The same results are obtained for both V_2O_5/TiO_2 and V_2O_5-WO_3/TiO_2 catalyst samples.

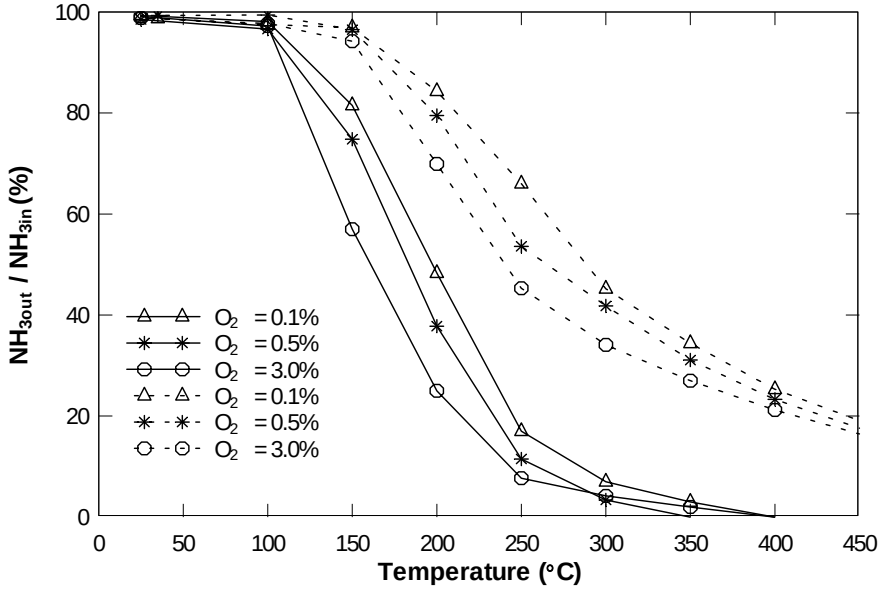

Figure 92. NH_3 conversion as a function of the reaction temperature at various space velocities over V_2O_5/TiO_2. Reaction conditions: [NO] = [NH_3] = 330 ppm, 0.1 - 3.0% O_2, preheating case, SV = 7000 h^{-1} (solid lines) and SV = 64000 h^{-1} (broken lines) [37].

6.2.5 N_2O and NO_2 Production

For both catalysts, high oxygen concentrations decrease the production of N_2O concentration as shown in figure 93. In figure 94, for both catalysts, the changes of NO_2 concentration are not related to changes of the oxygen concentration.

For the V_2O_5/TiO_2 catalyst, an increase in space velocity from 7000 h^{-1} to 64000 h^{-1} reduces N_2O production. No significant difference appears in space velocity from 10500 h^{-1} to 21000 h^{-1} for V_2O_5-WO_3/TiO_2 catalyst as shown in figure 76. The complete elimination of NO_2 is found for both catalysts at high space velocity. (The figure with these results is not presented in this paper)

Like the result for V_2O_5-WO_3/TiO_2 catalyst in figure 74, an increase in NH_3-to-NO ratio increases the production of N_2O from approximately 85 to 180 ppm for the V_2O_5/TiO_2 catalyst. (The figure with these results is not presented in this paper)

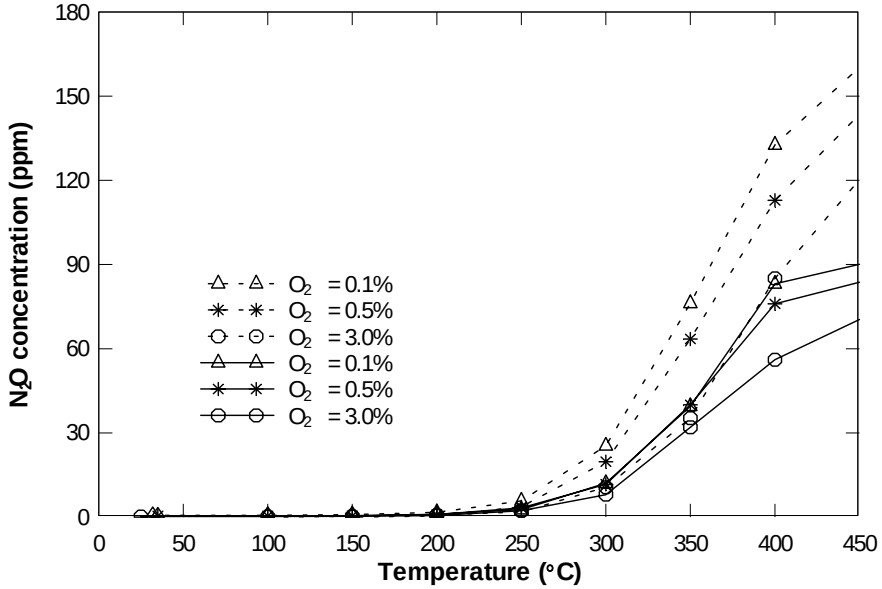

Figure 93. The effect of different catalysts on N_2O concentration. Reaction conditions: [NO] = [NH_3] = 330 ppm, 0.1 - 3.0% O_2, preheating case, SV = 64000 h^{-1} over V_2O_5/TiO_2 (solid lines), and SV = 10500 h^{-1} over V_2O_5-WO_3/TiO_2 (broken lines).

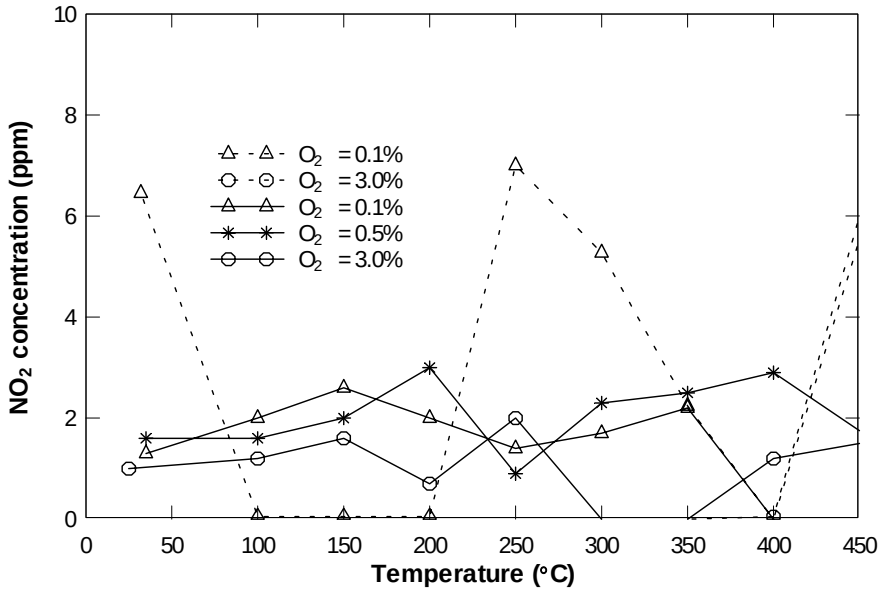

Figure 94. The effect of different catalysts on NO_2 concentration. Reaction conditions: [NO] = [NH_3] = 330 ppm, 0.1 - 3.0% O_2, preheating case, SV = 64000 h^{-1} over V_2O_5/TiO_2 (solid lines), and SV = 10500 h^{-1} over V_2O_5-WO_3/TiO_2 (broken lines).

6.3. Transition of NO and NH_3 Concentrations over Time over a Vanadia-Based (V_2O_5-WO_3/TiO_2) Catalyst

To obtain the final concentration values at the reaction temperature, not only the NO concentration should be stabilized, but also the concentration of ammonia species should reach the steady state. According to a result of this study, the NH_3 species takes a longer time to reach steady state than the NO species at the same reaction temperature.

For the selective non-catalytic reduction (SNCR) of NO with NH_3, 20 - 30 minutes were required to obtain the final value at a single reaction temperature [17]. That is to say, the concentrations of both NO and NH_3 reached steady state within 30 minutes.

On the other hand, more time was required to perform the selective catalytic reduction (SCR) of NO with NH_3. The average times to obtain the final values for each reaction temperature are listed in table 10. The average time decreases with an increase in the reaction temperature. During a single experiment, to stabilize the concentration of both NO and NH_3, the average times ranged from 26 to 134 minutes for the V_2O_5/Ti-PILC catalyst, depending on the reaction temperature. The presence of a catalyst explains this phenomenon. Initially when the gas species started to flow, the catalyst sample apparently absorbed mostly NH_3. Thus, the concentration of NH_3 in the output gases very gradually increased up to 330 ppm (initial NH_3 concentration) at the ambient temperature. It is the reason that the time for the stabilization of NH_3 at ambient takes the longest. It was observed that a sudden burst of the NH_3 concentration was detected by the FTIR spectrometer when the reaction temperature increases from the previous lower temperature. The sudden burst was significant at lower reaction temperatures. This also lengthens the time for stabilization of NH_3 at the reaction temperature.

Unlike the NH_3 species, a sudden decrease of NO concentration was observed when the reaction temperature increases from the previous lower temperature. A sudden burst of the NH_3 species occurred followed by a sudden decrease of NO concentration. The sudden decrease of NO species was significant at lower reaction temperatures.

In this section, the transition of the concentrations of NO and NH_3 over time over V_2O_5-WO_3/TiO_2 is described from their initial values until they become stabilized.

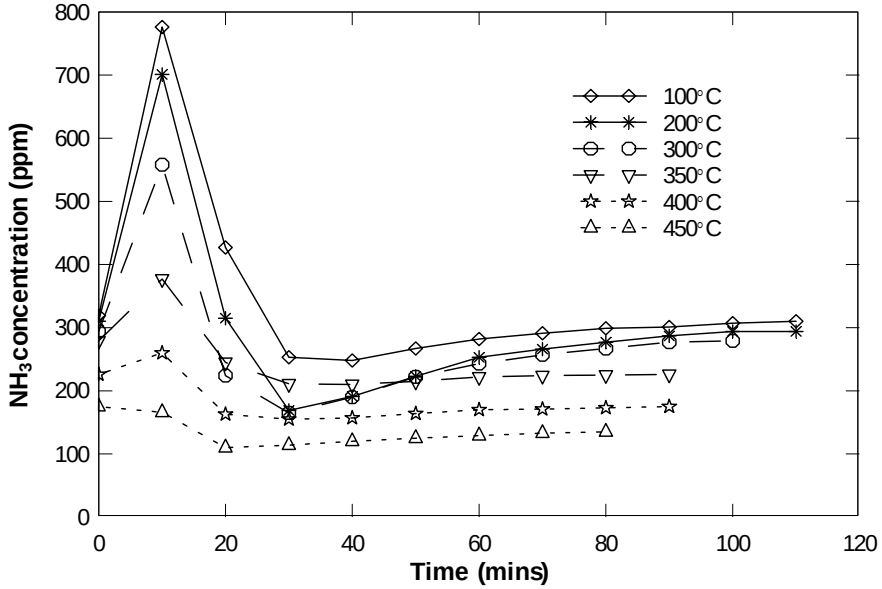

Figure 95. NH_3 concentration as a function of time at different reaction temperatures over V_2O_5-WO_3/TiO_2. Reaction conditions: [NO] = 330 ppm, [NH_3] = 330 ppm, 0% O_2, heating area of zones 2 + 3 (preheating case), and SV = 10500 h^{-1}.

6.3.1 Transition of NH_3 Concentration

Temperatures increase and stabilize within 10 minutes for the following figures in this section, and this result is from figure 38. For example, after the final value (approximately 330 ppm) at ambient (25°C) was obtained, the temperature is increased to the next higher temperature (i.e., 100°C). The "zero" time for these figures is when the temperature increases from the ambient to 100°C. Approximately 5 minutes are required to reach the temperature of 100°C. Every time the reaction temperature increases from a lower temperature to the next higher temperature, 5 minutes or less are required.

Figure 95 shows the transition of NH_3 concentrations over time over V_2O_5-WO_3/ TiO_2 for the reaction conditions of 0% O_2, heating area of zones 2 + 3 (preheating case), and SV = 10500 h^{-1}. The initial NH_3 concentration is 330 ppm at ambient. A sudden burst of NH_3 is observed during the first 10 minutes. Then, the NH_3 concentration reaches the maximum value (up to 800 ppm), and this increase declines at higher temperatures. The sudden burst is significant for temperatures below 300°C.

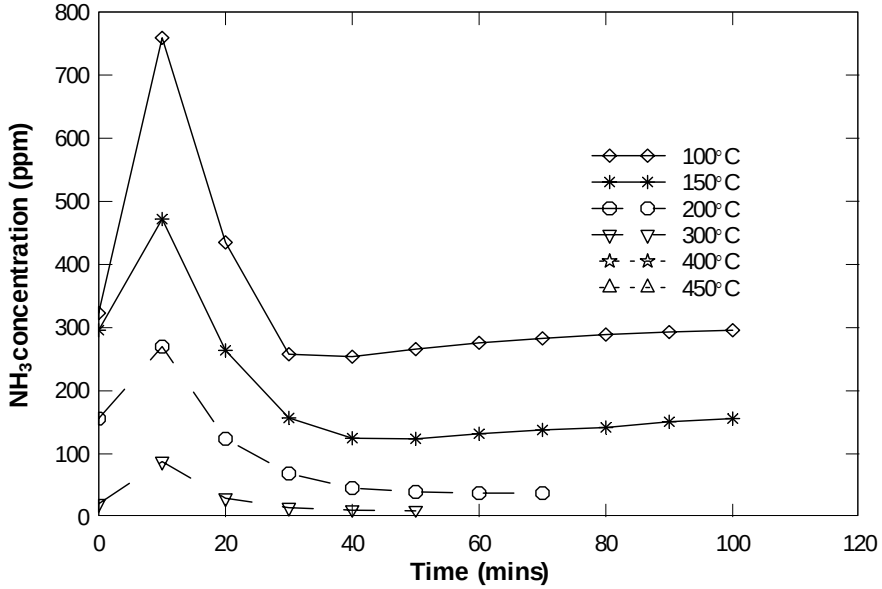

Figure 96. NH_3 concentration as a function of time at different reaction temperatures over V_2O_5-WO_3/TiO_2. Reaction conditions: [NO] = 330 ppm, [NH_3] = 330 ppm, 0.5% O_2, heating area of zones 2 + 3 (preheating case), and SV = 10500 h^{-1}.

Then, after the maximum level, the ammonia concentrations decline slightly lower than the final value. Then, the ammonia concentrations increase very slowly to reach the steady state.

Figure 96 shows the transition of NH_3 concentrations for the 0.5% O_2 case. The initial NH_3 concentration is 330 ppm at the ambient temperature. A similar result is observed. A sudden burst of NH_3 species is observed during the first 10 minutes. Then, the NH_3 concentration reaches the maximum value (~ approximately 800 ppm), and this increase declines at higher temperatures. The sudden burst is significant for the reaction temperatures below 150°C. For the reaction temperatures of 400 and 450°C, 0 ppm of ammonia (or 100% NH_3 conversion) is obtained. After the maximum level, the concentrations decline slightly lower than the final value. Then, the concentrations increase very slowly to reach the steady state. This is the major reason for the long time to stabilize ammonia. The higher maximum concentration is obtained, and then a longer time is required to reach the final value.

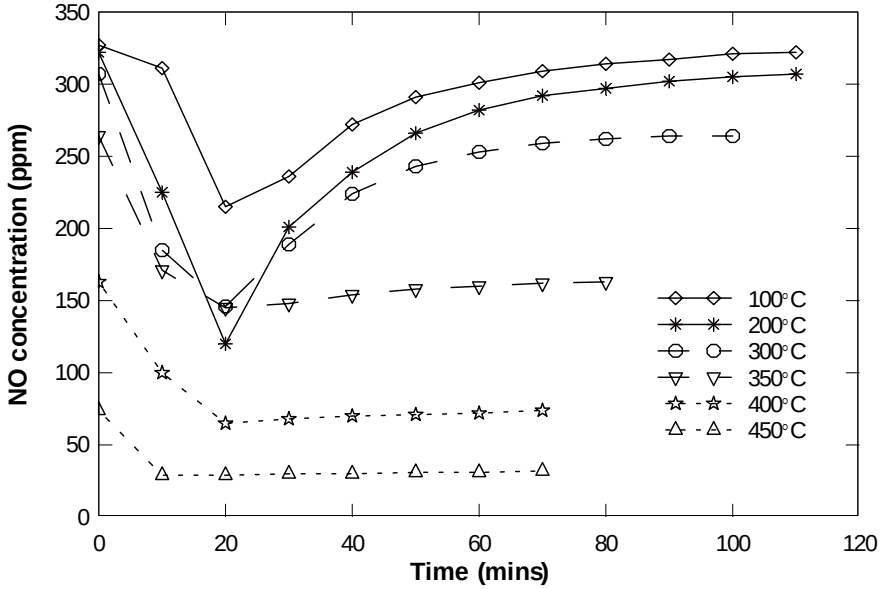

Figure 97. NO concentration as a function of time at different reaction temperatures over V_2O_5-WO_3/TiO_2. Reaction conditions: [NO] = 330 ppm, [NH_3] = 330 ppm, 0% O_2, heating area of zones 2 + 3 (preheating case), and SV = 10500 h^{-1}.

6.3.2 Transition of NO Concentration

Figure 97 shows the transition of NO concentrations over time over V_2O_5-WO_3/ TiO_2 for the reaction conditions of heating area of zones 2 + 3 (preheating case), 0% O_2, and SV = 10500 h^{-1}. The initial NO concentration is 330 ppm at ambient (25°C). During the first 10 minutes, the temperature increases from the previous lower temperature and stabilizes as shown in figure 38. Unlike the ammonia species, the concentration of NO decreases until about 20 minutes later the reaction temperature increased (at 0 minute). The NO concentration decreases more than half of its initial concentration at 200°C. For reaction temperatures below 300°C, the NO concentration after the minimum level increases until it stabilizes, and the large increasing is obtained. Therefore, a great decrease and increase sequentially is observed between 0 and about 40 minutes.

For reaction temperatures above 350°C, the NO concentration trends are different. Though the sudden decrease of NO concentration is observed, the concentration does not increase. After it reaches the minimum concentration, it gradually stabilizes.

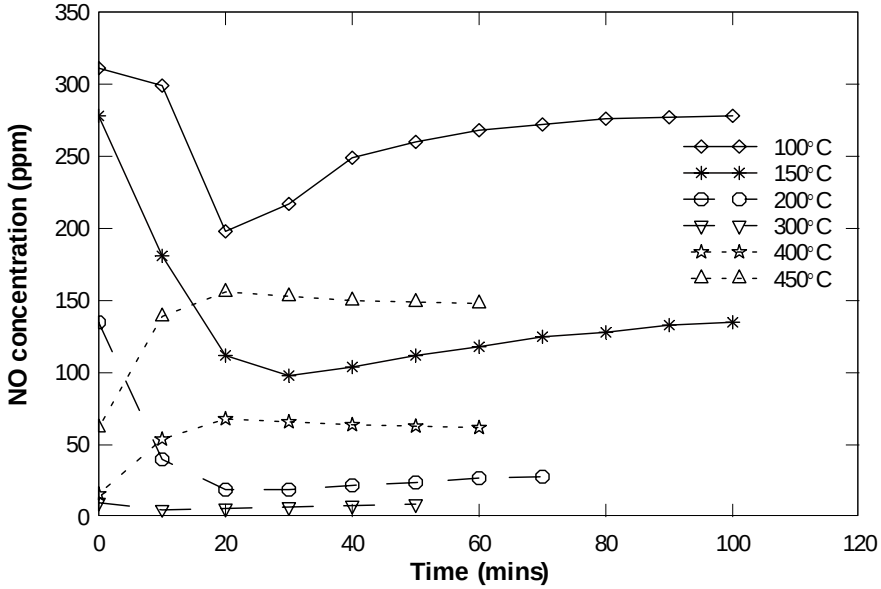

Figure 98. NO concentration as a function of time at different reaction temperatures over V_2O_5-WO_3/TiO_2. Reaction conditions: [NO] = 330 ppm, [NH_3] = 330 ppm, 0.5% O_2, heating area of zones 2 + 3 (preheating case), and SV = 10500 h^{-1}.

The time for stabilizing causes a time delay to determine the final concentration of NO species. The concentration of NO species takes less time to reach steady state than the concentration of NH_3 species at the same reaction temperature. The lower temperatures require more time to stabilize NO and NH_3 species. These phenomena are observed for every single experiment.

Figure 98 shows the different case of the transition of NO concentrations over V_2O_5-WO_3/ TiO_2 for the reaction conditions of [NO] = 330 ppm, heating area of zones 2 + 3 (preheating case), 0.5% O_2, and SV = 10500 h^{-1}. Recall that the result for high reaction temperatures (above 350°C) was shown in figure 97 (0% O_2). For the reaction temperature of 100°C, a similar trend which is a great decrease and increase sequentially is observed. For reaction temperatures of 150 and 200°C, NO concentrations stabilize after a sudden decrease is observed.

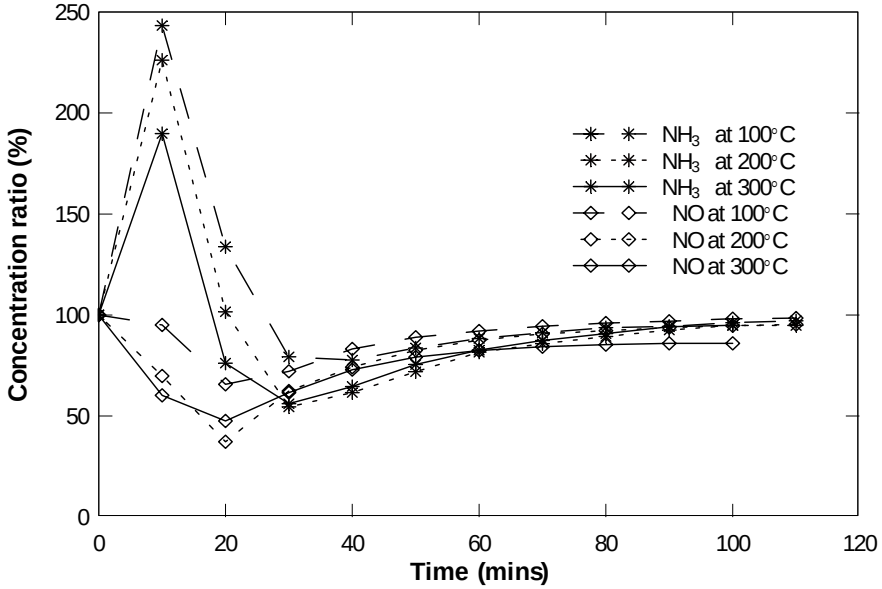

Figure 99. NO and NH_3 concentration ratios for reaction temperatures of 100, 200 and 300°C over V_2O_5-WO_3/TiO_2. Reaction conditions: [NO] = 330 ppm, [NH_3] = 330 ppm, 0% O_2, heating area of zones 2 + 3 (preheating case), and SV = 10500 h^{-1}.

For reaction temperatures of 400 and 450°C, a sudden increase of NO concentration is found in 20 minutes. The sudden increase of NO concentration was not observed in figure 97. Therefore, the sudden increase appears for the case in the presence of oxygen concentration.

Figures 99 and 100 show the concentration ratios for NH_3 (figure 95) and NO (figure 97) species for the different reaction temperature range. The concentration ratio is defined as the ratio of the output (or final) concentration to the initial concentration at each reaction temperature.

Figure 99 describes concentration ratios for NH_3 (figure 95) and NO (figure 97) species as a function of time for reaction temperatures of 100, 200 and 300°C for 0% O_2. For NH_3 species, each result of 100, 200 and 300°C shows similar trend. Also, all results of NO species show nearly the same shape. For the same reaction temperature, an intersection point of NO and NH_3 species is observed between 30 and 40 minutes for all cases.

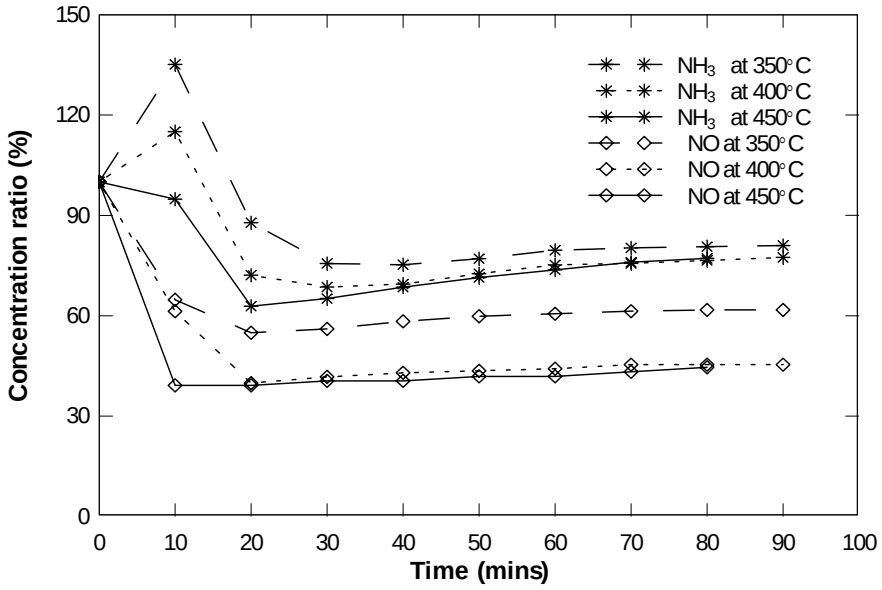

Figure 100. NO and NH_3 concentration ratios for reaction temperatures of 350, 400 and 450°C over V_2O_5-WO_3/TiO_2. Reaction conditions: [NO] = 330 ppm, [NH_3] = 330 ppm, 0% O_2, heating area of zones 2 + 3 (preheating case), and SV = 10500 h^{-1}.

Figures 100 describes concentration ratios for NH_3 (figure 95) and NO (figure 97) species as a function of time for reaction temperatures of 350, 400 and 450°C for 0% O_2. For NH_3 species, each result for reaction temperatures of 350, 400 and 450°C shows a similar trend. Also, each result of NO species for the temperatures of 350, 400 and 450°C shows nearly the same shape. For the same temperature, an intersection point of NO and NH_3 species is not observed for all cases. Therefore, from the results in figures 99 and 100, the intersection point is observed for reaction temperatures below 300°C, but is not observed for reaction temperatures above 350°C.

Figures 101, 102 and 103 present concentration ratios for both NH_3 (figure 96) and NO (figure 98) species for the different reaction temperature ranges.

Figure 100 shows concentration ratios for NH_3 (figure 96) and NO (figure 98) species at the reaction temperature of 100°C for 0.5% O_2. The results for both NO and NH_3 species are similar to the result shape as shown in figure 99 (0% O_2), and an intersection point of NO and NH_3 species is observed around 40 minutes.

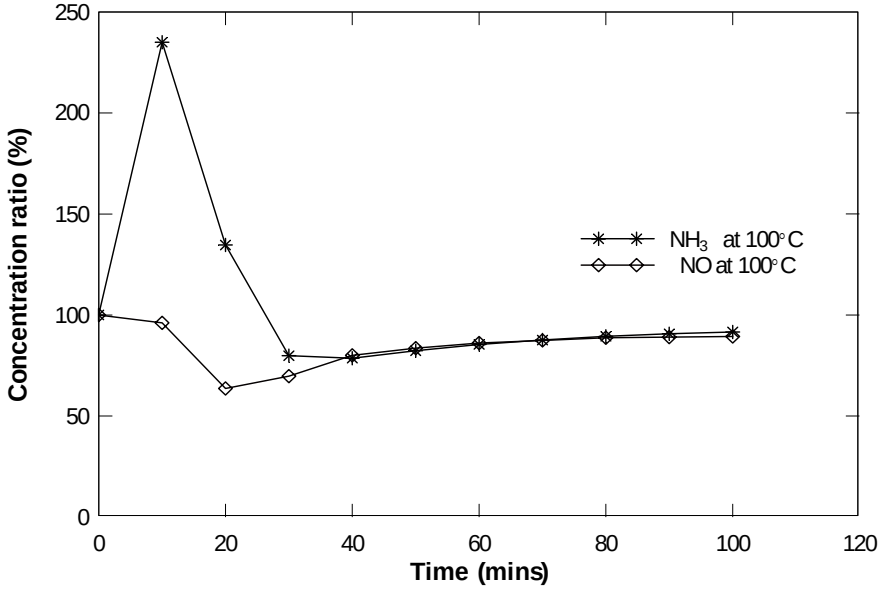

Figure 101. NO and NH_3 concentration ratios as a function of time at 100°C over V_2O_5-WO_3/TiO_2. Reaction conditions: [NO] = 330 ppm, [NH_3] = 330 ppm, 0.5% O_2, heating area of zones 2 + 3 (preheating case), and SV = 10500 h^{-1}.

Figure 102 describes concentration ratios for NH_3 (figure 96) and NO (figure 98) for reaction temperatures of 150 and 200°C for 0.5% O_2. The results for both NO and NH_3 species are similar to the result shape as shown in figure 100 (0% O_2), and an intersection point of concentration ratios of NO and NH_3 is not observed for the same reaction temperature.

In figure 103, an intersection point is not observed. For NH_3 species, 100% concentration ratios are obtained for reaction temperatures of both 400 and 450°C. 100% concentration ratio of NH_3 species indicates no difference between the output (or final) concentration and the initial concentration due to 100% NH_3 conversion was already obtained.

Therefore, from the results in figures 101, 102 and 103, the intersection point is observed for reaction temperatures below 300°C, but is not observed for reaction temperatures above 350°C.

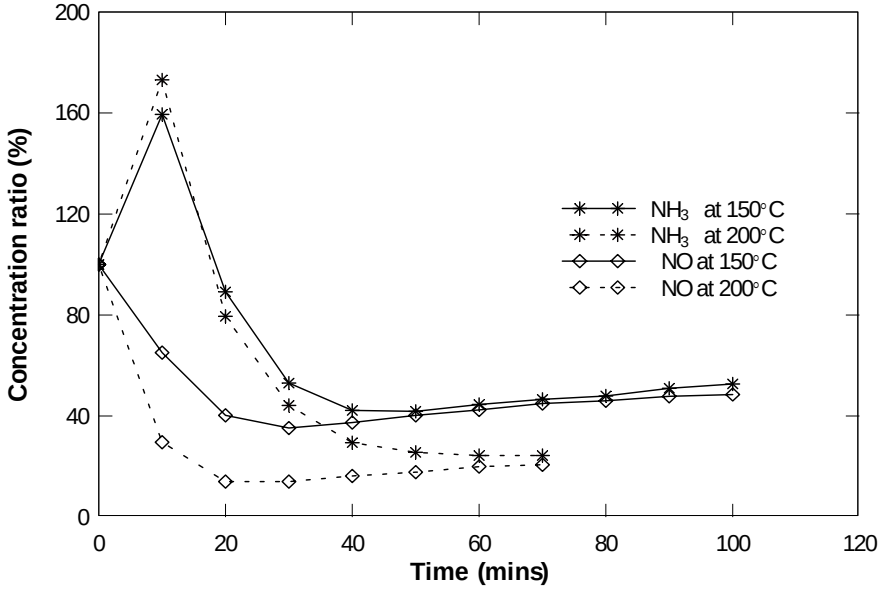

Figure 102. NO and NH_3 concentration ratios for reaction temperatures of 150 and 200°C over V_2O_5-WO_3/TiO_2. Reaction conditions: [NO] = 330 ppm, [NH_3] = 330 ppm, 0.5% O_2, heating area of zones 2 + 3 (preheating case), and SV = 10500 h^{-1}.

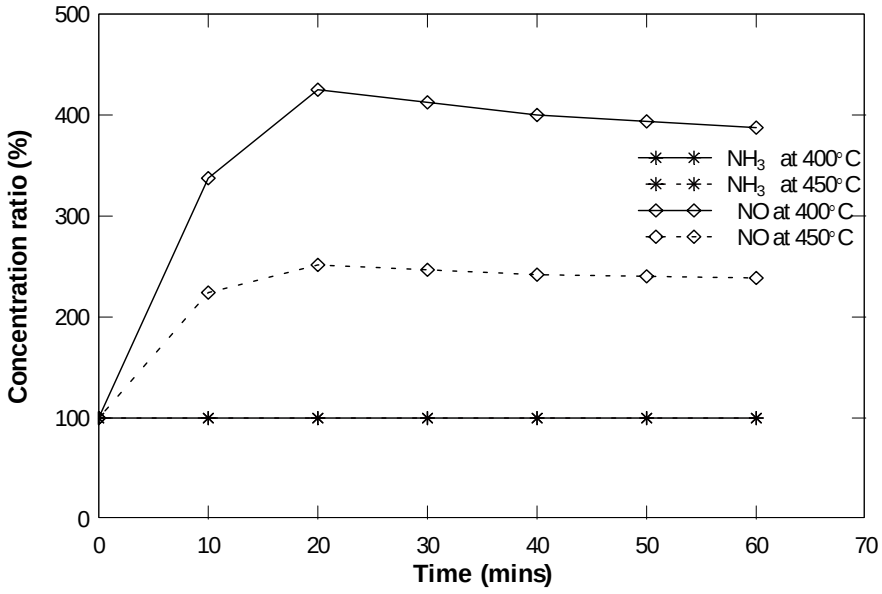

Figure 103. NO and NH_3 concentration ratios as a function of time at 400°C over V_2O_5-WO_3/TiO_2. Reaction conditions: [NO] = 330 ppm, [NH_3] = 330 ppm, 0.5% O_2, heating area of zones 2 + 3 (preheating case), and SV = 10500 h^{-1}.

Table 21. Phenomena observed between 0 and 40 minutes for 0% O_2.

Temperature (°C)	Figure 97	Figure 99	Figure 100
100	Sequential decrease and increase	Intersection point	-
200	Sequential decrease and increase	Intersection point	-
300	Sequential decrease and increase	Intersection point	-
350	Decrease and stabilization	-	No intersection point
400	Decrease and stabilization	-	No intersection point
450	Decrease and stabilization	-	No intersection point

Table 21 lists the phenomena observed under the same conditions for 0% O_2 between 0 and 40 minutes. In figure 97, for the temperatures of 100, 200 and 300°C, a great sequential decrease and increase is observed before each NO concentration stabilizes. For the temperatures of 350, 400 and 450°C, a great decrease is observed. As a consequence, for the entire reaction temperature range, an intersection point (figure 99) is observed when a great sequential decrease and increase (figure 97) is observed. The intersection point (figure 100) is not observed when a great sequential decrease and increase (figure 97) is not observed.

Table 22 lists the phenomena observed under the same conditions for 0.5% O_2 between 0 and 40 minutes. In figure 98, for the reaction temperature of 100°C, a great sequential decrease and increase is observed before each NO concentration stabilizes. For reaction temperatures of 150 and 200°C, a great decrease is observed. For reaction temperatures of 400 and 450°C, a great increase is observed.

Table 22. Phenomena observed between 0 and 40 minutes for 0.5% O_2.

Temperature (°C)	Figure 98	Figure 101	Figure 102	Figure 103
100	Sequential decrease and increase	Intersection point	-	-
150	Decrease and stabilization	-	No intersection point	-
200	Decrease and stabilization	-	No intersection point	-
400	Increase and stabilization	-	-	No intersection point
450	Increase and stabilization	-	-	No intersection point

As a consequence, for the entire reaction temperature range, an intersection point (figure 101) is observed when a great sequential decrease and increase (figure 98) is observed. The intersection point (figures 102 and 103) is not observed when a great sequential decrease and increase (figure 98) is not observed.

6.4 Pillared Interlayer Clay-Based (V_2O_5/Ti-PILC) Catalysts

The selective catalytic reduction (SCR) of nitric oxide (NO) with ammonia over V_2O_5/Ti-PILC monolithic honeycomb catalysts is investigated in this section. The results are presented and discussed case by case for the different reaction conditions as listed in table 23.

Table 23 summarizes the experimental cases performed on V_2O_5/Ti-PILC catalysts in the current study. Two catalyst samples of vanadium loadings were prepared. One was an original catalyst (vanadium contents: 1.78 wt%) from provider. The other was a coated catalyst (vanadium contents: 2.35 wt%) made by the process of the vanadium coating, which the extra vanadium was coated to the original catalyst. The space velocity of 10500 h^{-1} for a catalyst sample of 2 cm in length was used for all cases. The heating area of zones 2 and 3 (preheating case) in the electric heating reactor were activated. NH_3-to-NO ratio was 0.8, 1.0 and 2.0 ([NO] = 330 ppm, [NH_3] = 264 ppm, 330 ppm, and 660 ppm, respectively). Three different oxygen concentrations of 0, 0.1 and 3.0% were performed for all cases over V_2O_5/Ti-PILC catalysts.

Table 23. The experimental cases performed on V_2O_5/Ti-PILC catalysts.

Vanadium (wt%)	Space velocity (h^{-1})	Heating area	NH_3-to-NO ratio	Oxygen concentration (%)
1.78 (original)	10500	Preheating (zone 2 + 3)	1.0	0 0.1 3.0
2.35 (coated)	10500	Preheating (zone 2 + 3)	0.8 ([NO] = 330 ppm [NH_3] = 264 ppm)	0 0.1 3.0
			1.0 ([NO] = 330 ppm [NH_3] = 330 ppm)	0 0.1 3.0
			2.0 ([NO] = 330 ppm [NH_3] = 660 ppm)	0 0.1 3.0

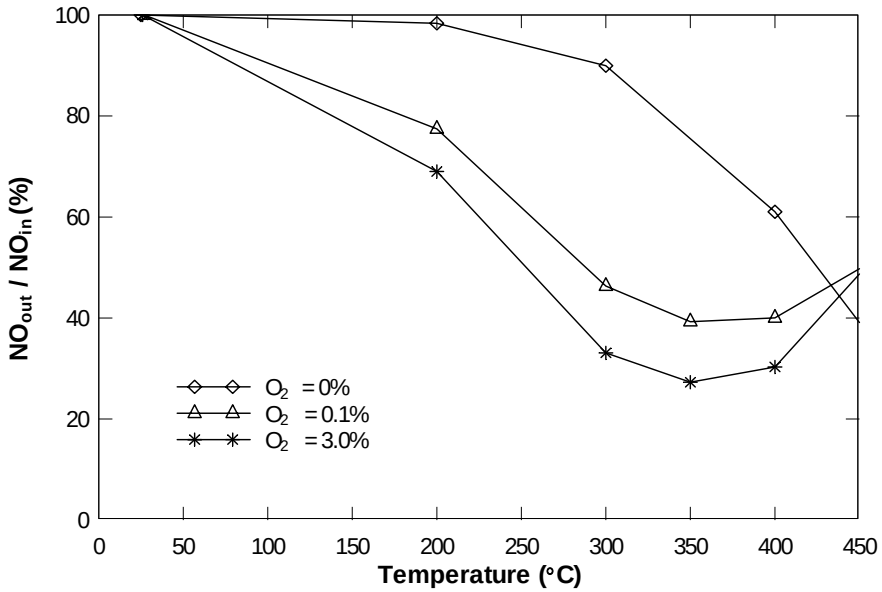

Figure 104. NO reduction as a function of the reaction temperature at various oxygen concentrations over V_2O_5/Ti-PILC. Reaction conditions: [NO] = [NH_3] = 330 ppm, 0 - 3.0% O_2, without vanadium (V_2O_5) coating, heating area of zones 2 + 3 (preheating case), and SV = 10500 h^{-1}.

6.4.1 Effect of Reaction Temperature

Figures 104 and 105 describe NO reductions and NH_3 conversions, respectively, as a function of the reaction temperature at various oxygen concentrations over V_2O_5/Ti-PILC for the conditions of [NO] = [NH_3] = 330 ppm, 0 - 3.0% O_2, without vanadium (V_2O_5) coating, heating area of zones 2 + 3 (preheating case), and SV = 10500 h^{-1}.

In figure 104, NO reductions increase with an increase in reaction temperature, and the maximum NO reductions are obtained at the reaction temperature of 350°C in the presence of oxygen. The maximum NO reductions are 60.7% for 0.1% O_2, and 72.7% for 3.0% O_2. The catalytic activity for NO reduction is very low over V_2O_5/Ti-PILC in the entire temperature range. After NO reduction reaches the maximum value, the reduction of NO decreases for higher reaction temperatures.

In figure 105, ammonia conversions increase with an increase in reaction temperature. The conversions of ammonia more than 15% (or 49.5 ppm) are still left even at the reaction temperature of 450°C.

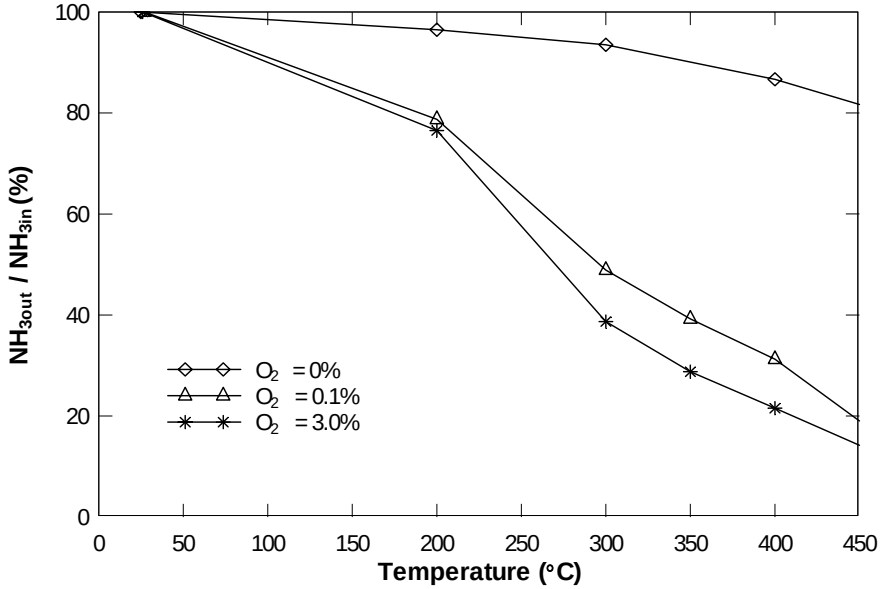

Figure 105. NH_3 conversion as a function of the reaction temperature at various oxygen concentrations over V_2O_5/Ti-PILC. Reaction conditions: [NO] = [NH_3] = 330 ppm, 0 - 3.0% O_2, without vanadium (V_2O_5) coating, heating area of zones 2 + 3 (preheating case), and SV = 10500 h^{-1}.

Figures 106 and 107 show NO reductions and NH_3 conversions, respectively, as a function of the reaction temperature at various oxygen concentrations over V_2O_5/Ti-PILC for the conditions of [NO] = [NH_3] = 330 ppm, 0 - 3.0% O_2, with vanadium (V_2O_5) coating, heating area of zones 2 + 3 (preheating case), and SV = 10500 h^{-1}.

In figure 106, NO reductions increase with an increase in reaction temperature, and the maximum NO reductions are obtained at the reaction temperature of 350°C in the presence of oxygen. The maximum NO reductions are 74.5% for 0.1% O_2, and 79.4% for 3.0% O_2. After NO reduction reaches the maximum value, the reduction of NO decreases for higher reaction temperatures.

In figure 107, ammonia conversions increase with an increase in reaction temperature. The conversions of ammonia less than 10% (or 33 ppm) are still left even at the reaction temperature of 450°C for the cases with oxygen greater than 0%.

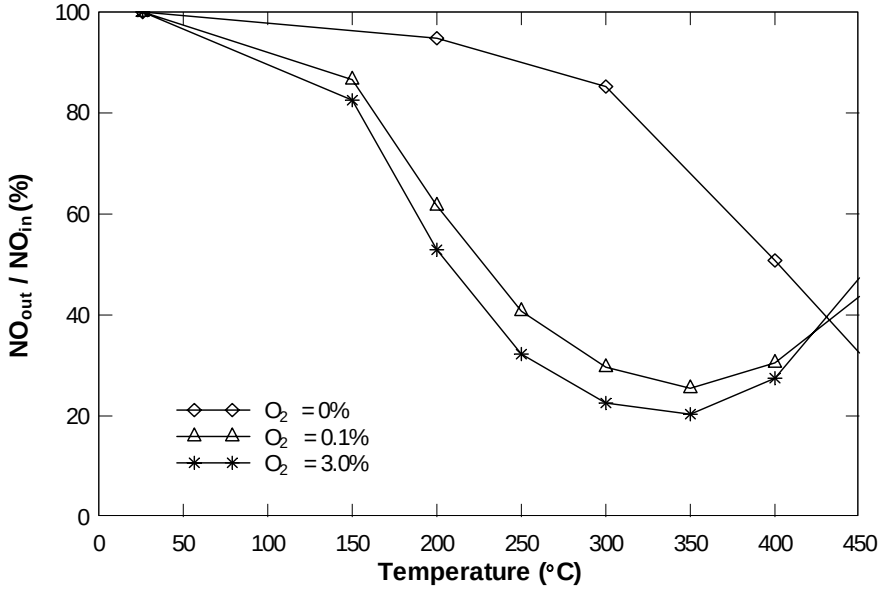

Figure 106. NO reduction as a function of the temperature at various oxygen concentrations over V_2O_5/Ti-PILC. Reaction conditions: [NO] = [NH_3] = 330 ppm, 0 - 3.0% O_2, with vanadium (V_2O_5) coating, preheating case, and SV = 10500 h^{-1}.

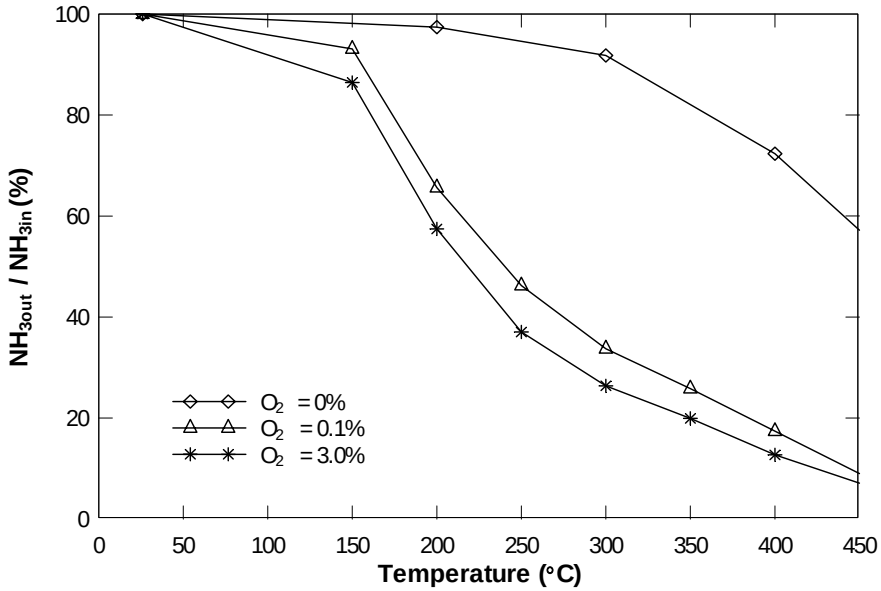

Figure 107. NH_3 conversion as a function of the temperature at various oxygen concentrations over V_2O_5/Ti-PILC. Reaction conditions: [NO] = [NH_3] = 330 ppm, 0 - 3.0% O_2, with vanadium (V_2O_5) coating, preheating case, and SV = 10500 h^{-1}.

6.4.2 Effect of Oxygen Concentration

Figures 104 and 106 describe NO reductions as a function of the reaction temperature at various inlet oxygen concentrations. For both figures, the catalytic activities of NO reduction increase with an increase in oxygen concentration. The increase of oxygen concentration from 0.1 to 3.0% increases the NO reduction up to approximately 13% more at the reaction temperature of 300°C for the result without vanadium coating and up to 9% at the reaction temperature of 200°C for the result of vanadium coating.

Figures 105 and 107 show NH_3 conversions as a function of the reaction temperature at various inlet oxygen concentrations. For both figures, it is observed that the catalytic activities of NH_3 conversions increase with an increase in oxygen concentration from 0 to 3.0%. The presence of small amounts of oxygen concentration facilitates the oxidation of ammonia. The increase of oxygen concentration from 0.1 to 3.0% decreases the conversion of ammonia up to approximately 10% at the reaction temperature of 350°C for the result of no vanadium coating and up to 9% at the reaction temperature of 250°C for the result of vanadium coating.

6.4.3 Effect of Vanadium Coating (or Loading)

Figure 108 shows the effect of the vanadium coating on NO reduction over V_2O_5/Ti-PILC. The solid lines indicate the results using an original catalyst (without the extra vanadium coating), and the broken lines indicate the results using a coated catalyst (with the extra vanadium coating). NO reduction increases with an increase in vanadium contents (from 1.78 to 2.35 wt%) in the presence and absence of oxygen. For the 0% O_2 case, NO reduction of the maximum increase is approximately 10.2% (33.7 ppm) at 400°C. For the 0.1% O_2 case, the maximum increase is 16.7% (55.1 ppm) at 300°C. For the 3.0% O_2 case, the maximum increase is 16.1% (53.1 ppm) at 200°C.

Figure 109 shows the effect of the vanadium coating on NH_3 conversion over V_2O_5/Ti-PILC. NH_3 conversion increases with an increase in vanadium contents in the presence and absence of oxygen, and the maximum increase of NH_3 conversion are approximately 24.5% (80.9 ppm) at the reaction temperature of 450°C for the 0% O_2 case.

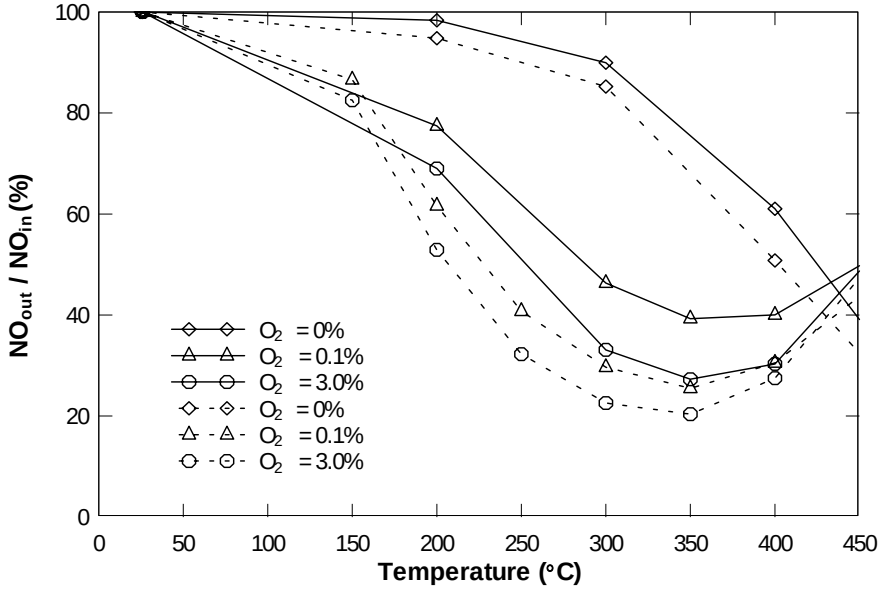

Figure 108. The effect of the vanadium coating on NO reduction over V_2O_5/Ti-PILC. Reaction conditions: [NO] = [NH_3] = 330 ppm, 0 - 3.0% O_2, preheating case, SV = 10500 h^{-1}, without vanadium coating (solid lines), and with vanadium coating (broken lines).

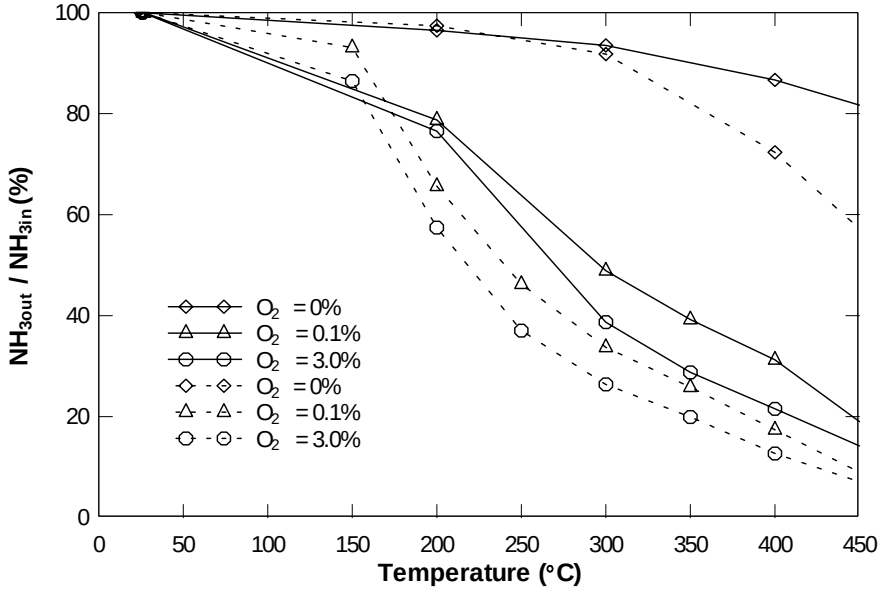

Figure 109. The effect of the vanadium coating on NH_3 conversion over V_2O_5/Ti-PILC. Reaction conditions: [NO] = [NH_3] = 330 ppm, 0 - 3.0% O_2, preheating case, SV = 10500 h^{-1}, without vanadium coating (solid lines), and with vanadium coating (broken lines).

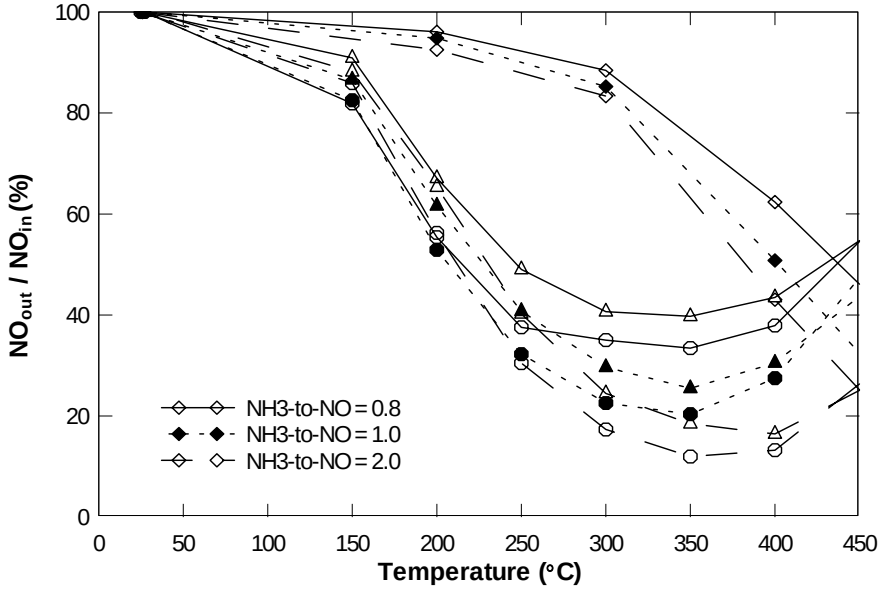

Figure 110. NO reduction as a function of the reaction temperature at various NH_3-to-NO ratios over V_2O_5/Ti-PILC. Reaction conditions: 0 - 3.0% O_2, preheating case, SV = 10500 h^{-1}, and NH_3-to-NO ratio = 0.8 (solid lines with open symbols), 1.0 (dashed lines with closed symbols), and 2.0 (broken lines with open symbols).

For the 0.1% O_2 case, the maximum increase of NH_3 conversion is 15.1% (49.8 ppm) at the temperature of 300°C. For the 3.0% O_2 case, the maximum increase is 19.1% (63 ppm) at the reaction temperature of 200°C.

6.4.4 Effect of NH_3-to-NO Ratio

Figures 110 and 111 describe the effect of NH_3-to-NO ratio (or inlet ammonia concentration) on NO reductions and NH_3 conversions, respectively, over V_2O_5/Ti-PILC for the conditions of [NO] = 330 ppm, [NH_3] = 264, 330 and 660 ppm, 0 - 3.0% O_2, vanadium coating, heating area of zones 2 + 3 (preheating case), and SV = 10500 h^{-1}. These results are from NH_3-to-NO ratio of 0.8 (solid lines with open symbols), NH_3-to-NO ratio of 1.0 (dashed lines with closed symbols), NH_3-to-NO ratio of 2.0 (broken lines with open symbols). The symbols indicate oxygen concentrations of 0% (◇), 0.1% (△) and 3.0% (O). The inlet ammonia concentrations are 264, 330 and 660 ppm for NH_3-to-NO ratio of 0.8, 1.0 and 2.0, respectively.

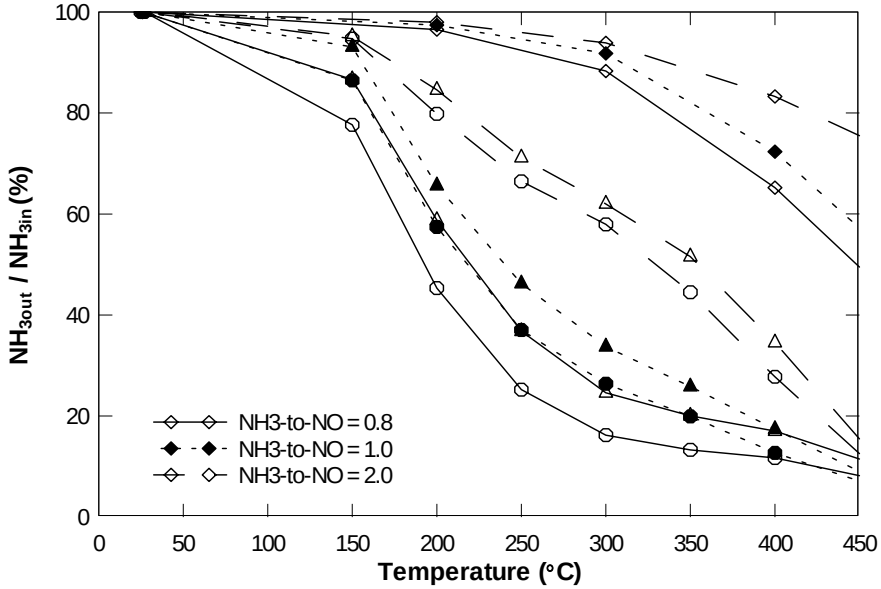

Figure 111. NH_3 conversion as a function of the reaction temperature at various NH_3-to-NO ratios over V_2O_5/Ti-PILC. Reaction conditions: 0 - 3.0% O_2, preheating case, SV = 10500 h^{-1}, and NH_3-to-NO ratio = 0.8 (solid lines with open symbols), 1.0 (dashed lines with closed symbols), and 2.0 (broken lines with open symbols).

Figure 110 describes the effect of the variation of NH_3-to-NO ratio (or inlet ammonia concentration) on NO reduction. NO reduction increases with an increase in inlet ammonia concentration. The highest NO reductions are found at the reaction temperatures of 350°C for almost all cases, except for 0.1% O_2 of NH_3-to-NO ratio = 2.0 (broken line with open triangle). The average increase of NO reduction at the temperatures between 300 and 450°C is approximately 24% with an increase in NH_3-to-NO ratio from 0.8 to 2.0.

Figure 111 shows the effect of the variation of NH_3-to-NO ratio on NH_3 conversion. NH_3 conversion declines with an increase in NH_3-to-NO ratio. NH_3 conversions of NH_3-to-NO ratio of 0.8 are the highest result. The average decrease of NH_3 conversion at the temperatures between 200 and 350°C is approximately 37% with an increase in NH_3-to-NO ratio from 0.8 to 2.0. Though the result of NH_3-to-NO ratio of 0.8 shows the best, concentrations less than 10% are still left even at the temperature of 450°C.

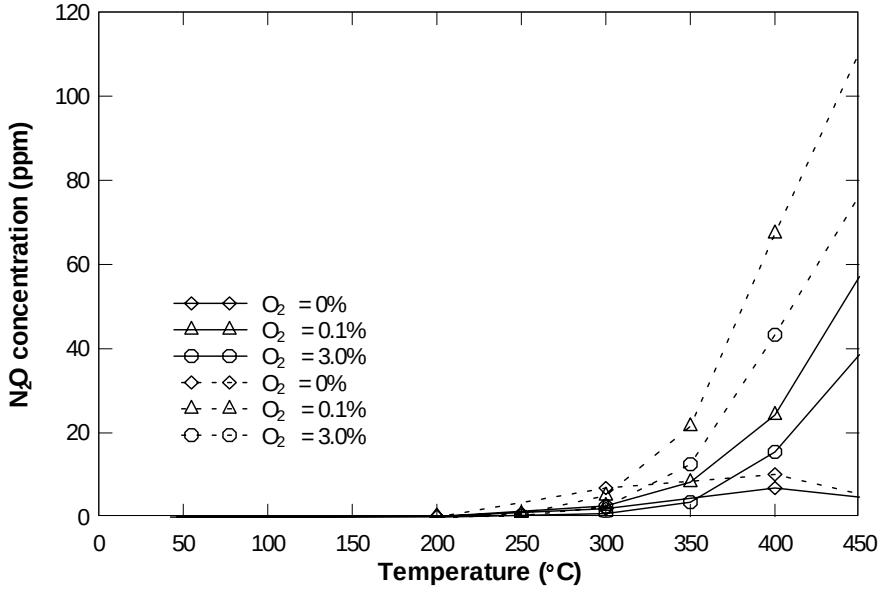

Figure 112. The effect of the vanadium coating on N_2O concentration at various oxygen concentrations over V_2O_5/Ti-PILC. Reaction conditions: [NO] = [NH_3] = 330 ppm, 0 - 3.0% O_2, preheating case, and SV = 10500 h^{-1}, without vanadium coating (solid lines), with vanadium coating (broken lines).

6.4.5 N_2O and NO_2 Production

The productions of nitrous oxide (N_2O) and nitrogen dioxide (NO_2) for the selective catalytic reduction of NO with ammonia over V_2O_5/Ti-PILC catalysts are presented in this section. The results of NO_2 and N_2O productions are discussed for the different reaction conditions as listed in table 23. The catalytic reactions occur for the conditions based on [NO] = [NH_3] = 330 ppm, oxygen concentrations of 0 - 3.0%, heating area of zones 2 + 3 (preheating case), and SV = 10500 h^{-1}.

Figure 112 presents the effect of the vanadium coating on nitrogen dioxide (N_2O) concentration at various oxygen concentrations. For both conditions with coating and without coating, the productions of N_2O decrease with an increase in oxygen concentrations from 0.1 to 3.0%, while the productions are obtained very low in the absence of oxygen. The concentration drop from 0.1 to 3.0% O_2 is larger for the coating case than for the no coating case at the same reaction temperature.

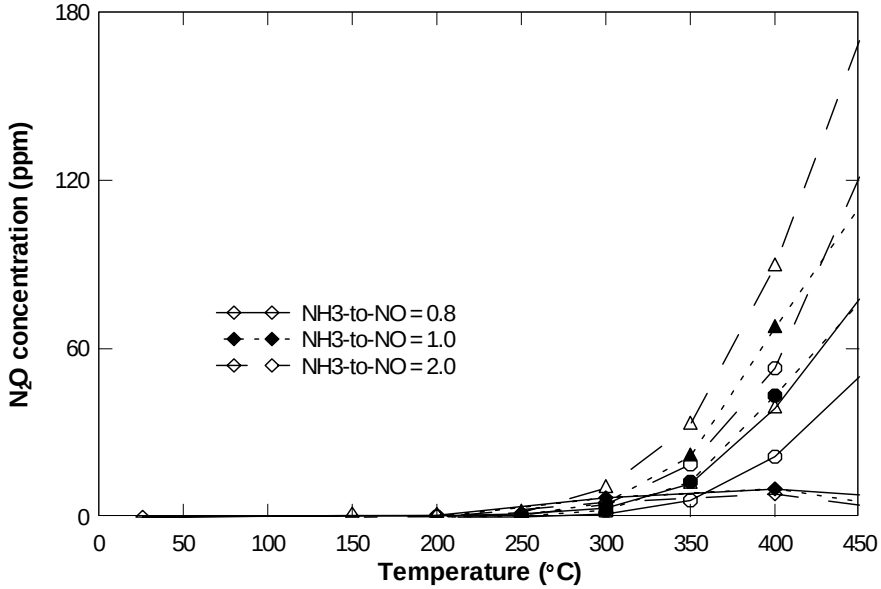

Figure 113. The effect of the various NH_3-to-NO ratios on N_2O concentration over V_2O_5/ Ti-PILC. Reaction conditions: 0 - 3.0% O_2, preheating case, SV = 10500 h^{-1}, and NH_3-to-NO ratio = 0.8 (solid lines with open symbols), 1.0 (dashed lines with closed symbols), and 2.0 (broken lines with open symbols).

The increase of small amounts of vanadium contents increases the production of N_2O, up to approximately four times for low temperatures and approximately three times for high temperatures. For both 0.1 and 3.0% O_2, the maximum concentration at the highest temperature increases twice with an increase in vanadium contents.

Figure 113 shows the effect of NH_3-to-NO ratio (or inlet ammonia concentration) on nitrogen dioxide (N_2O) concentration at various oxygen concentrations. N_2O productions are obtained very low in the absence of oxygen, whereas the concentrations are pretty high in the presence of oxygen. An increase in the inlet ammonia concentration increases the production of N_2O. At the highest reaction temperature, the concentration drop from 0.1 to 3.0% O_2 is 28 ppm for NH_3-to-NO ratio = 0.8, 34 ppm for NH_3-to-NO ratio = 1.0 and 49 ppm for NH_3-to-NO ratio = 2.0.

The concentrations of NO_2 were not produced from all experimental cases over V_2O_5/Ti-PILC catalysts both in the presence and absence of oxygen in entire ranges of the reaction temperature.

6.5 Comparison of Result among Cu-ZSM-5, V_2O_5-WO_3/TiO_2, and V_2O_5/Ti-PILC

The results between V_2O_5-WO_3/TiO_2 and V_2O_5/TiO_2 catalysts were already discussed in the section, 6.2 Result Comparison between V_2O_5-WO_3/TiO_2 and V_2O_5/TiO_2 Catalysts from Previous Study. The addition of tungsten species (WO_3) increased NO reduction and NO_3 conversion and broadened the active temperature window for all cases at various oxygen concentrations under the similar conditions.

The results among three catalysts which are V_2O_5-WO_3/TiO_2 (current study), V_2O_5/Ti-PILC (current study) and Cu-ZSM-5 (previous investigation) [37] are briefly compared, and the effects of three different parameters which are the inlet oxygen concentration, space velocity and NH_3-to-NO ratio are discussed in this section.

The effects of four different parameters were investigated for the Cu-ZSM-5 monolithic honeycomb catalyst [37]. The results [37] can be briefly reviewed as below:

(1) The inlet oxygen concentration was varied from 0 to 3%. The increase of oxygen concentration from 0.1 to 3% reduced the reaction temperatures of the maximum NO reduction and 100% NH_3 conversion. For oxygen from 0.1 to 3%, the temperature window of NO reduction was about the same. However, an accompanied increase in the concentrations of both N_2O and NO_2 species was observed as oxygen increased.

(2) Three space velocities of 7000, 42000 and 64000 h^{-1} were tested. An increase in space velocity decreased the maximum NO reduction and N_2O production. It increased the reaction temperature of 100% NH_3 conversion, but no effect on NO_2 concentration was observed.

(3) NH_3-to-NO ratio was varied from 0.8 (NH_3 = 264 ppm) to 2.0 (NH_3 = 660 ppm). The increase of the inlet ammonia concentration (or NH_3-to-NO ratio) increased the maximum NO reduction, the reaction temperature of 100% NH_3 conversion and the production of N_2O specie.

(4) The effect of catalyst pretreatment was investigated. A catalyst was exposed in the gas stream (total flow rate of 1100 sccm) to hydrogen (H_2) for an hour at a reaction temperature of 300°C as a pretreatment process. No significant effect on the NO reduction and NH_3 conversion was observed.

All of the following comparisons are for conditions of [NO] = 330 ppm, [NH_3] = 330 ppm, oxygen concentrations of 0 - 3.0%, and heating area of zones 2 + 3 (preheating case).

For the inlet oxygen concentration, high NO reductions and NH_3 conversions are obtained in the presence of a small amount of oxygen for all three catalysts. An increase in oxygen concentration increases the removals of both NO and NH_3 species, however, the increase of oxygen concentration from 0.1 to 3.0% has no significant influence for all three catalysts. In the presence of oxygen, the reaction temperatures of the maximum NO reduction are 300°C for V_2O_5-WO_3/TiO_2 and 350°C for V_2O_5/Ti-PILC, while they reduce for the Cu-ZSM-5 catalyst. An increase in oxygen concentration decreases the production of N_2O in the presence of oxygen for both V_2O_5-WO_3/TiO_2 and V_2O_5/Ti-PILC catalysts.

For the space velocity, the results of both NO reductions and NH_3 conversions shift toward lower reaction temperature with the decrease of space velocity for V_2O_5-WO_3/TiO_2 catalysts (same as the Cu-ZSM-5 catalyst). For V_2O_5-WO_3/TiO_2 catalysts, the active temperature window (NO > 88% and NH_3 > 87% based on convenience) was broadened 50°C with a decrease in space velocity. No significant effect on the production of N_2O is observed, but a decrease in space velocity increases the production of NO_2. The effect of space velocity for V_2O_5/Ti-PILC catalysts was not investigated in the current work.

For NH_3-to-NO ratio (or inlet ammonia concentration), the results for all three catalysts show similar trend. An increase in NH_3-to-NO ratio increases NO reduction, the reaction temperature of 100% NH_3 conversion and N_2O production. For lower reaction temperatures, no significant difference for the removal of NO and NH_3 is observed. For higher reaction temperatures, however, significant increase of NO reduction and decrease of NH_3 conversions are observed for both V_2O_5-WO_3/TiO_2 and V_2O_5/Ti-PILC catalysts.

7. SUMMARY AND CONCLUSIONS

Two catalyst samples, vanadia-based (V_2O_5-WO_3/TiO_2) and pillared interlayer clay-based (V_2O_5/Ti-PILC) monolithic honeycomb catalysts, were investigated for the selective catalytic reduction (SCR) of nitric oxide (NO) with ammonia as the reducing agent from simulated exhaust streams in a laboratory laminar-flow reactor. The experiments used a number of gas compositions (N_2, O_2, NO, and NH_3) to simulate different combustion gases.

The effects of six parameters were investigated for V_2O_5-WO_3/TiO_2 catalysts. The results can be summarized as below:

(1) The simulated gases were heated from ambient to 450°C. In the presence of oxygen, NO reduction and NH_3 conversion increased very quickly (average value of 15% to 85%) for temperatures between 100 and 250°C for the heating area of zone 2 and between 100 and 200°C for zones 2 + 3 (preheating case). The maximum NO reductions were obtained at 350°C for the zone 2 case and at 300°C for zones 2 + 3 (preheating case). In the current work, the active temperature window (based on NO > 88% and NH_3 > 83%) for each catalyst depended on the space velocity and the heating area.

(2) The effect of the inlet oxygen concentration variations from 0 to 3% was observed. An increase in oxygen concentration increased the removal of both NO and NH_3 species. High NO reductions and NH_3 conversions were obtained in the presence of a small amount of oxygen, however, the increase of oxygen concentration from 0.1 to 3.0% had no significant influence on the removal of either NO or NH_3 species. An increase in oxygen concentration decreased the production of N_2O in the presence of oxygen, but had no significant effect on the production of NO_2.

(3) NH_3-to-NO ratio (or inlet ammonia concentration) was investigated from 0.8 (NH_3 = 264 ppm) to 2.0 (NH_3 = 660 ppm). An increase in NH_3-to-NO ratio increased NO reduction, the reaction temperature of 100% NH_3 conversion and N_2O production.

For lower temperatures, no significant difference for the removal of NO and NH_3 was observed, while a great increase of NO reduction and decrease of NH_3 conversions were observed for higher temperatures. No great effect on NO_2 production was observed.

(4) The space velocity was tested from 10500 to 21000 h^{-1}. A decrease in space velocity caused the NO reduction and NH_3 conversion to shift toward lower reaction temperatures and increased the catalytic activities of NO reductions and NH_3 conversions. The active temperature window (based on NO > 88% and NH_3 > 87%) was broadened about 50°C with a decrease in space velocity for the same heating area. No great effect was observed for either N_2O or NO_2 productions at the same heating area.

(5) The effect of two different heating areas which were (a) zone 2 and (b) zones 2 + 3 (preheating case) was observed. An increase in the heating area decreased the reaction temperature of the maximum NO reduction from 350 to 300°C. At the space velocity of 10500 h^{-1}, the active temperature window (based on NO > 83% and NH_3 > 87%) was observed at the temperatures between 250 and 400°C for heating area of only zone 2, and between 200 and 350°C for the preheating case. An increase of the heating area caused the NO reductions and NH_3 conversions to shift toward lower reaction temperatures. The same trend was obtained at space velocity of 21000 h^{-1}. It indicates that the temperature of the simulated gas in the preheating case is higher than in the case of zone 2 only. An increase in heating area increased the production of N_2O at the same space velocity, but no significant effect was observed for NO_2 production.

(6) Three different catalyst conditions were tested: standard, second arrangement and third arrangement. The results of the second and third arrangements on NO reductions and NH_3 conversions were shown to be a little bit higher than those of the standard case for all temperatures, but these differences were small. No great effect on N_2O production was observed. NO_2 production for the standard case was less than for the second arrangement, but more than for the third arrangement.

The effects of four parameters were investigated for V_2O_5/Ti-PILC catalysts. The results can be summarized as below:

(1) The simulated gases were heated from the ambient temperature (25°C) to 450°C. NO reductions and NH_3 concentrations increased with an increase in reaction temperature, and the maximum NO reductions were obtained at the reaction temperature of 350°C in the presence of oxygen. After NO reduction reached the maximum value, NO reduction decreased at higher reaction temperatures. NH_3 concentrations less than 10% were still left even at the highest reaction temperature for all cases.

(2) The inlet oxygen concentration was investigated from 0 to 3%. An increase in oxygen concentration increased both NO reduction and NH_3 conversion. High NO reductions and NH_3 conversions were obtained in the presence of a small amount of oxygen, however, the increase of oxygen concentration from 0.1 to 3.0% had no significant influence on the removal of both NO and NH_3 species. An increase in oxygen concentration decreased the production of N_2O in the presence of oxygen.

(3) The effect of vanadium coating on the catalyst surface was observed. The catalyst with vanadium coating showed higher NO reductions and NH_3 conversions than the catalyst without vanadium coating. Higher production of N_2O was obtained in the experimental case with vanadium coating.

(4) NH_3-to-NO ratio (or inlet ammonia concentration) was tested from 0.8 (NH_3 = 264 ppm) to 2.0 (NH_3 = 660 ppm). For lower reaction temperatures, no significant difference for the removal of NO and NH_3 was observed. For higher reaction temperatures, however, significant increase of NO reduction and decrease of NH_3 conversions were observed. An increase in NH_3-to-NO ratio increased the production of N_2O.

0 ppm of NO_2 production was obtained for all cases over V_2O_5/Ti-PILC catalysts.

The results on NO reduction and NH_3 conversion for the V_2O_5-WO_3/TiO_2 catalyst are higher and more effective than for the V_2O_5/Ti-PILC catalyst. For the identical reaction conditions of [NO] = 330 ppm, [NH_3] = 264, 330 or 660 ppm, 0 - 3.0% O_2, heating area of zones 2 + 3 (preheating case), and space velocity of 10500 h^{-1}, higher removal of both NO and NH_3 species and the wider active reaction temperature window were observed. On the other hand, the production of nitrous oxide (N_2O) and nitrogen dioxide (NO_2) for the V_2O_5-WO_3/TiO_2 catalyst were higher than for the V_2O_5/Ti-PILC catalyst.

The results of the comparison between V_2O_5/TiO_2 and V_2O_5-WO_3/TiO_2 are briefly summarized as followed:

With the addition of tungsten species (WO_3) to V_2O_5/TiO_2 catalysts, the maximum NO reduction increased and broadened the active temperature window very large (approximately 50 to 150°C), and the great improvement on NH_3 conversion was found. The results of the productions of N_2O and NO_2 were not compared due to the different operating conditions.

The results of the comparison among Cu-ZSM-5, V_2O_5-WO_3/TiO_2, and V_2O_5/Ti-PILC are briefly summarized as followed:

An increase in oxygen concentration increased the removal of both NO and NH_3 species, however, there was no significant influence from 0.1 to 3.0% O_2 for all three catalysts. For V_2O_5-WO_3/TiO_2 catalysts, a decrease in space velocity shifted the removal of both NO and NH_3 species toward lower reaction temperature and broadened the active temperature window approximately 50°C. An increase in NH_3-to-NO ratio (or inlet ammonia concentration) increases NO reduction, increases the reaction temperature of 100% NH_3 conversion, and increases N_2O production for Cu-ZSM-5, V_2O_5-WO_3/TiO_2 catalysts. For higher reaction temperatures, significant increase of NO reduction and decrease of NH_3 conversions were observed for both V_2O_5-WO_3/TiO_2 and V_2O_5/Ti-PILC catalysts.

8. RECOMMENDATIONS

Recommendations for future work are listed as below:

(1) The coated amounts of vanadium for the V_2O_5/Ti-PILC catalyst were small in the current work, and only one case was investigated. Thus, the effect of various vanadium loadings needs to be investigated.

(2) The effect of space velocity needs to be investigated for a V_2O_5/Ti-PILC catalyst.

(3) The effect of heating area needs to be investigated for a V_2O_5/Ti-PILC catalyst.

(4) The effect of various arrangements was investigated for a V_2O_5-WO_3/TiO_2 catalyst. Therefore, the effect of various arrangements of a catalyst needs to be investigated for a V_2O_5/Ti-PILC catalyst.

(5) The effect of the presence of water (H_2O) and sulfur dioxide (SO_2) needs to be investigated for a V_2O_5/Ti-PILC catalyst.

REFERENCES

1. Colls, J., *Air Pollution*, Second Edition, London; Spon Press, 2002.

2. Freudenrich, C., "How Ozone Pollution Works - What is Ozone," http://science.howstuffworks.com/ozone-pollution1.htm, Oct. 2003.

3. Clarke, A. G., Radojevic, M., and Harrison, R. M., *Atmospheric Acidity: Sources, Consequences and Abatement*, London, Elsevier, 1992.

4. Cheung, T., Bhargava, S. K., Hobday, M., and Foger, K., "Adsorption of NO on Cu Exchanged Zeolites, an FTIR Study: Effects of Cu Levels, NO Pressure and Catalyst Pre-treatment," *Journal of Catalysis*, 158: 301-310, 1996.

5. Alasfour, F. N., "NO_x Emission from a Spark Ignition Engine using 30% Iso-Butanol-Gasoline Blend: Part 1 - Preheating Inlet Air," *Applied Thermal Engineering*, 18(5): 245-256, 1998.

6. Cooper, C. and Alley, F., *Air Pollution Control: A Design Approach*, PWS Inc., Boston, 1986.

7. Robert Mondt, J., *Cleaner Cars: The History and Technology of Emission Control since the 1960s*, Warrendale, Pa: Society of Automotive Engineers, 2000.

8. Puri, I., *Environmental Implications of Combustion Processes*, Boca Raton, Fla.: CRC Press Inc., 1993.

9. Davison, A., "The Costs of Enrichment - Air Quality", http://www.ncl.ac.uk/gane/page8.htm, Oct. 2003.

10. National Aeronautics and Space Administration (NASA) Facts, *Ozone: What Is It, and Why Do We Care About It*, Cape Girardeau, MO, NF-198, 1993.

11. Ferguson, C. R. and Kirkpatrick, A. T., *Internal Combustion Engines: Applied Thermodynamics*, Second Edition, New York, John Wiley & Sons, Inc., 2001.

12. John B. Heywood, *Internal Combustion Engine Fundamentals*, New York, McGraw-Hill, 1988.

13. Glarborg, P., Miller, J. A., and Kee, R. J., "Kinetic Modeling and Sensitivity Analysis of Nitrogen Oxide Formation in Well-Stirred Reactors," *Combust. Flame*, 65: 177-202, 1986.

14. Paul Degobert, "Automobiles and Pollution," Warrendale, PA.: Society of Automotive Engineers, Inc., 1995.

15. Lyon, R. K. and Hardy, J. E., "Discovery and Development of the Thermal DeNO_x Process," *Ind. Eng. Chem. Fundam*., 25: 19-24, 1986.

16. Miller, J. A. and Bowman, C. T., "Mechanisms and Modeling of Nitrogen Chemistry in Combustion," *Prog. Energy Combust. Sci*., 15: 287-338, 1989.

17. Park, Y. H., "An Investigation of Urea Decomposition and Selective Non-Catalytic Removal of Nitric Oxides with Urea," Thesis, Texas A&M University, May 2003.

18. Dűrr Environmental. Inc., "NO_x Emission control: Emission Origins and Available Control Solutions," http://www.durrenvironmental.com/NOXCS.asp, Nov. 2003.

19. Ham, S. W. and Nam, I. S., *The Royal Society of Chemistry, ,* "*Catalysis*," Volume 16, London: Chemical Society, 2002.

20. Heck, R. M. and Farrauto, R. J., with Gulati, S. T., *Catalytic Air Pollution Control: Commercial Technology*, New York: Wiley-Interscience, 2002.

21. Heck, R. M., "Catalytic Abatement of Nitrogen Oxides-Stationary Applications," *Catalysis Today*, 53: 519-523, 1999.

22. Radojevic, M., "Reduction of Nitrogen Oxides in Flue Gases," *Environmental Pollution*, 102, S1: 685-689, 1998.

23. Choo, S.T., Lee, Y.G., Nam, I. S., Ham, S. W., and Lee, J. B., "Characteristics of V_2O_5 Supported on Sulfated TiO_2 for Selective Catalytic Reduction of NO by NH_3," *Applied Catalysis A: General*, 200: 177-188, 2000.

24. Long, R. Q. and Yang, R. T., "Selective Catalytic Reduction of NO with Ammonia over V_2O_5 Doped TiO_2 Pillared Clay Catalyst," *Applied Catalysis B: Environmental*, 24: 13-21, 2000.

25. Chae, H. J., Nam, I. S., Yang, H. S, Song, S. L., and Hur, I. D., "Use of V_2O_5/Ti-PILC Catalyst for the Reduction of NO by NH_3," *Journal of Chemical Engineering of Japan*, 34(2): 148-153, 2001.

26. Busca, G., Lietti, L., Ramis, G., and Berti, F., "Chemical and Mechanistic Aspects of the Selective Catalytic Reduction of NO_x by Ammonia over Oxide Catalysts: A Review," *Applied Catalysis B: Environmental*, 18: 1-36, 1998.

27. Bosch, F., and Janssen, F., "Formation and Control of Nitrogen Oxides," *Catalysis Today*, 2: 369-532, 1998.

28. Parvlescu, V. I., Grange, P., and Delmon, B., "Catalytic Removal of NO," *Catalysis Today*, 46: 233–316, 1998.

29. Madia, G., Elsener, M., Koebel, M., Raimondi, F., and Wokaun, A., "Thermal Stability of Vanadia-Tungsta-Titania Catalysts in the SCR Process," *Applied Catalysis B: Environmental*, 39: 181-190, 2002.

30. Choi, J. H., Kim, S. K., and Bak, Y. C., "The Reactivity of V_2O_5-WO_3-TiO_2 Catalyst Supported on a Ceramic Filter Candle for Selective Reduction of NO," *Korean J. Chem. Eng.*, 18(5): 719-724, 2001.

31. Chen, J. P. and Yang, R. T., "Role of WO_3 in Mixed V_2O_5-WO_3-TiO_2 Catalyst for Selective Catalytic Reduction of Nitric Oxide with Ammonia," *Applied Catalysis A: General*, 80: 135-148, 1992.

32. Lee, I. Y., Kim, D. W., Lee, J. B., and Yoo, K. O., "A Practical Scale Evaluation of Sulfated V_2O_5/TiO_2 Catalyst from Metatitanic Acid for Selective Catalytic Reduction of NO by NH_3," *Chemical Engineering Journal*, 90: 267-272, 2002.

33. Liuqing, T., Daiqi, Y. and Hong, L., "Catalytic Performance of a Novel Ceramic-Supported Vanadium Oxide Catalyst for NO Reduction with NH_3," *Catalysis Today*, 78: 159-170, 2003.

34. Koebel, M., Madia, G., Raimondi, F., and Wokaun, A., "Enhanced Reoxidation of Vanadia by NO_2 in the Fast SCR Reaction," *Journal of Catalysis*, 209: 159-165, 2002.

35. Koh, J. Y., Yim S. D. and Nam, I. S., "Modeling of Honeycomb Reactor Extruded for Selective Catalytic Reduction of NO_x by NH_3," *Proceedings of the 9th APCChE Congress and CHENECA 2002*, University of Canterbury, Christchurch, NZ, 29 September - 3 October 2002.

36. Gutberlet, H. and Schallert, B., "Selective Catalytic Reduction of NO_x from Coal Fired Power Plants," *Catalysis Today*, 16: 207-235, 1993.

37. Gupta, S., "Selective Catalytic Reduction (SCR) of Nitric Oxide with Ammonia Using Cu-ZSM-5 and Va-Based Honeycomb Monolith Catalysts: Effect of H_2 Pretreatment, NH_3-to-NO Ratio, O_2, and Space Velocity," Thesis, Texas A&M University, August 2003.

38. Chae, H. J., Nam, I. S., Ham, S. W., and Hong, S. B., "Physicochemical Characteristics of Pillared Interlayered Clays," *Catalysis Today*, 68: 31-40, 2001.

39. Valverde, J. L., de Lucas, A., Sanchez, P., Dorado, F., and Romero, A., "Cation Exchanged and Impregnated Ti-Pillared Clays for Selective Catalytic Reduction on NO_x by Propylene," *Applied Catalysis B: Environmental*, 43: 43-56, 2003.

40. Yang, R. T., Chen, J. P., Kikkinides, E. S., Cheng, L. S., and Cichanowicz, J. E., "Pillared Clays as Superior Catalysts for Selective Catalytic Reduction of NO with NH_3," *Ind. Eng. Chem. Res*., 31: 1440-1445, 1992.

41. Chmielarz, L., Kustrowski, P., Zbroja, M., Rafalska-Lasocha, A., Dudek, B., and Dziembaj, R., "SCR of NO by NH_3 on Alumina or Titania-Pillared Montmorillonite Various Modified with Cu or Co: Part I. General Characterization and Catalysts Screening," *Applied Catalysis B: Environmental*, 45: 103-116, 2003.

42. Long, R. Q. and Yang, R. T., "The Promoting Role of Rare Earth Oxides on Fe-Exchanged TiO_2-Pillared Clay for Selective Catalytic Reduction of Nitric Oxide by Ammonia," *Applied Catalysis B: Environmental*, 27: 87-95, 2000.

43. Long, R. Q. and Yang, R. T., "Catalytic Performance and Characterization of VO^{2+}-Exchanged Titania-Pillared Clays for Selective Catalytic Reduction of Nitric Oxide with Ammonia," *Journal of Catalysis*, 196: 73-85, 2000.

44. Busca, G., Lietti, L., Ramis, G., and Berti, F., "Chemical and Mechanistic Aspects of the Selective Catalytic Reduction of NO_x by Ammonia over Oxide Catalysts: A Review," *Applied Catalysis B: Environmental*, 18, 1: 1-36, 1998.

45. Khalfallah Boudali, L., Ghorbel A. and Grange, P., "Selective Catalytic Reduction of NO by NH_3 on Sulfated Titanium-Pillared Clay," *Catalysis Letters*, 86(4): 251-256, March 2003.

46. Cheng, L. S., Yang R. T. and Chen, N., "Iron Oxide and Chromia Supported on Titania-Pillared Clay for Selective Catalytic Reduction of Nitric Oxide with Ammonia," *Journal of Catalysis*, 164: 70-81, 1996.

47. Vicente, M. A., Belver, C., Trujillano, R., Bañares-Muñoz, M. A., Rives, V., Korili, S. A., Gil, A., Gandía, L. M., and Lambert, J. -F., "Preparation and Characterisation of Vanadium Catalysts Supported over Alumina-Pillared Clays," *Catalysis Today*, 78: 181-190, 2003.

48. Long, R. Q. and Yang, R. T., "Selective Catalytic Reduction of Nitrogen Oxides by Ammonia over Fe^{3+}-Exchanged TiO_2-Pillared Clay Catalysts," *Journal of Catalysis*, 186: 254-268, 1999.

49. Long, R. Q. and Yang, R. T., "FTIR and Kinetic Studies of the Mechanism of Fe^{3+}-Exchanged TiO_2-Pillared Clay Catalysts for Selective Catalytic Reduction of NO with Ammonia," *Journal of Catalysis*, 190: 22-31, 2000.

50. Long, R. Q., Chang, M. T. and Yang, R. T., "Enhancement of Activities by Sulfation on Fe-Exchanged TiO_2-Pillared Clay for Selective Catalytic Reduction of NO by Ammonia," *Applied Catalysis B: Environmental*, 33: 97-107, 2001.

51. Gentemann, A. "Flow Reactor Experiments on the Selective Non-Catalytic Removal of Nitrogen Oxides," Thesis, Texas A&M University, May 2001.

52. Mangan, J., "The Calibration and Use of Mass Flow Controllers for Use in NOx Reduction Experiments," Department of Mechanical Engineering 485 Report, Texas A&M University, 2000.

53. Baek, K. H., "Selective Non-Catalytic Reduction NO_x by Ammonia: Experiments and Model Calculations," Dissertation, Texas A&M University, May 2003.

54. Postech Environmental Catalysis Laboratory (PECL), Department of Chemical Engineering Pohang University of Science and Technology, Korea, http://cedb.postech.ac.kr/~envcat/, Oct. 2003.

55. Swagelok Company, "FW, F and TF Series Filters - Complete Catalog," http://www.swagelok.com, Nov. 2003.

56. KWH Catalysts, Inc., http://www.k-w-h.com/start-e.html, Nov. 2003.

APPENDIX 1

MASS FLOW CONTROLLERS CALIBRATION PROCEDURE

The mass flow controllers controlled the flow rate of each species. The MFCs were calibrated with a pure gas by means of the water displacement method prior to the main experiment as described in figure 27. To calibrate them, a flask and a basin to contain water, a thermometer to measure water and ambient temperature, a ruler to measure the height of water level, and a stop-watch to measure time were used.

First of all, to stabilize the MFC, it should be turned on an hour or more before the calibration started. The MFC was checked at zero set point to confirm no gas flowing. The five or six values that planned to measure were selected. The flask filled with water completely was very carefully upside down into the basin. Then, the gas was flowed out surroundings until reaching the steady state, and the gas tube was inserted into the bottom of the flask in the basin. The stop-watch was started with inserting timing simultaneously.

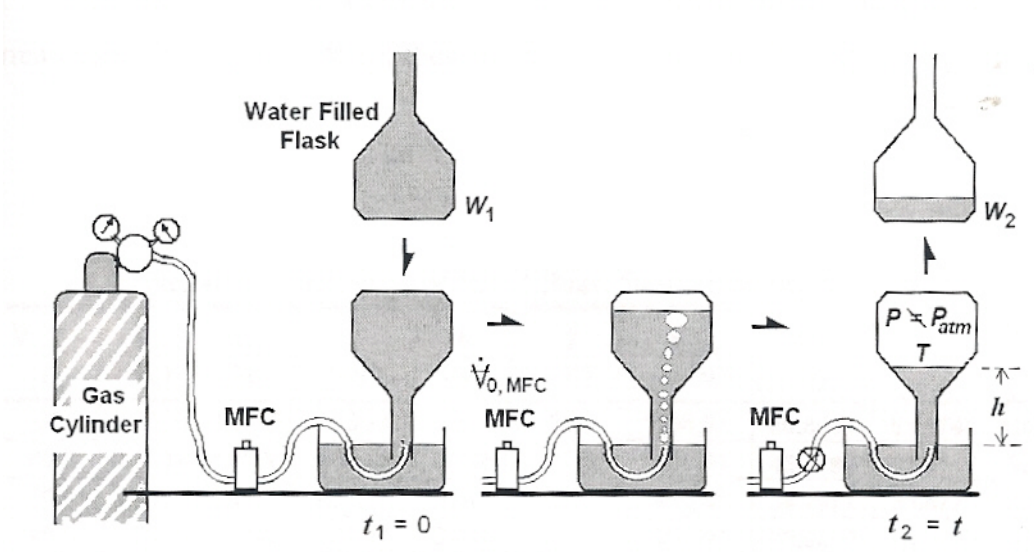

Figure A-1. MFC calibration system by water displacement method [53].

The gas flowing through the MFC with a desired set volume flow rate was bubbled into the flask. Once a reasonable amount of gas was stored in the flask, the tube was taken out from the flask, and the timer was stopped simultaneously. The set and read points of MFC, the final height of water, the density of water, time period, water and surrounding temperatures, initial and final mass of water. The volume of the water displaced by the gas was measured over time period.

$$\dot{\forall} = \frac{\Delta \forall}{\Delta t} \equiv \frac{M_1 - M_2}{\rho_{H2O} \cdot t} \tag{A.1}$$

where $\dot{\forall}$ is the volume flow rate, M1 and M_2 are weights of water at the beginning and the end and ρ_{H2O} is the density of water.

From the ideal gas behaviors of the pure gas ($P\forall = mRT$), the volume flow rate ($\dot{\forall}$) can be corrected to the initial volume flow rate ($\dot{\forall}_0$) at T_0 and P_0.

$$\dot{\forall} = \dot{\forall}_o \left(\frac{P_0}{P} \right) \left(\frac{T}{T_0} \right) \tag{A.2}$$

$$\dot{\forall}_0 = \left(\frac{P}{P_0} \right) \left(\frac{T_0}{T} \right) \left(\frac{M_1 - M_2}{\rho_{H2O} \cdot t} \right) \tag{A.3}$$

where T_0 is the ambient temperatures, P_0 is P_{atm}, T is also the ambient temperature because the calibration process is performed under fixed conditions

The pressure of the gas can be calculated by using the water height (in cm) at the end and the specific gravity (in m^2/sec) as followed

$$P = P_0 - \rho_{H2O} \cdot gh \tag{A.4}$$

$$\dot{\forall}_0 = \left(\frac{P_0 - \rho_{H2O} \cdot gh}{P_0} \right) \left(\frac{M_1 - M_2}{\rho_{H2O} \cdot t} \right) \tag{A.5}$$

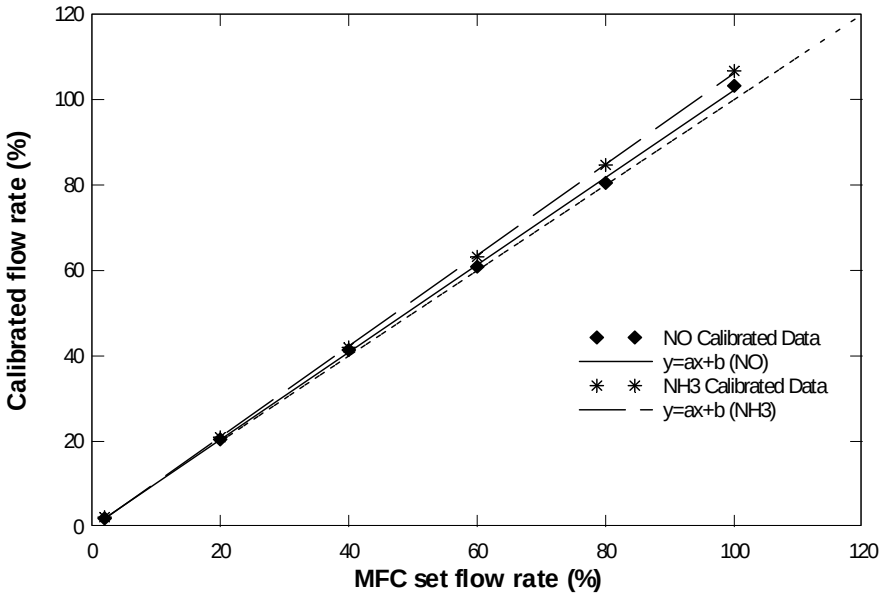

Figure A-2. MFC calibration plots for NO and NH_3 species.

Table A-1. Two coefficients of the curve-fit functions for NO and NH_3 species.

MFC number	Used gas	y = ax + b	
		a	b
#1-3	NO/N_2	1.0225	-0.0362
#2-1	NH_3/N_2	1.064	-0.2505

With all data from above procedures between the MFC set flow rates and its calibrated flow rates ($\dot{\forall}_0$ in %), the linear fits and their functions in the form of y = ax + b of MFC #1-3 and #2-1 are illustrated in figure A-2. The linear fits have been found to be the root-mean-square accuracies better than 0.999. Table A-1 lists two coefficients of the curve-fit functions for NO and NH_3 species.

APPENDIX 2

TEMPERATURE DISTRIBUTION IN THE FURNACE

The temperature distribution of the simulated gas was measured by setting the reactor temperature at 250 and 450°C, and the flow rate of 1100 sccm of pure nitrogen was used. The reaction temperatures were taken in axial direction. The K-type thermocouple was inserted inside of the furnace from the outlet to the inlet side, so inserting direction is opposite to the gas flowing direction as shown in figure A-3. The K-type thermocouple theory is explained in more detail by Baek [53]. The thermocouple was not located at the center but at the bottom of a quartz-tube because of the weight of the thermocouple probe. The reaction temperature at each point required to reach steady state. Two heating areas were tested: (a) zone 2 activated and (b) zones 2 and 3 (preheating case) activated. For the heating area of zone 2, two reaction temperatures of 250 and 450°C were selected. For the preheating case, three reaction temperatures of 800, 1100 and 1300 K were selected [17].

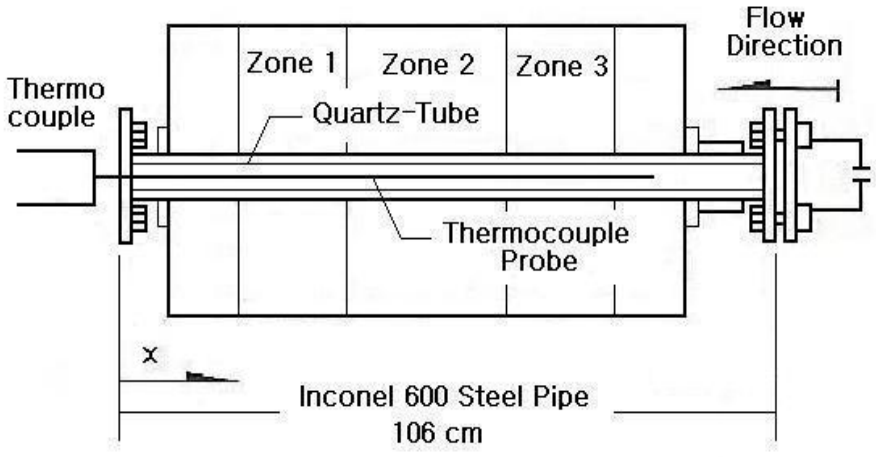

Figure A-3. Measurement of the reactor temperature by K-type thermocouple.

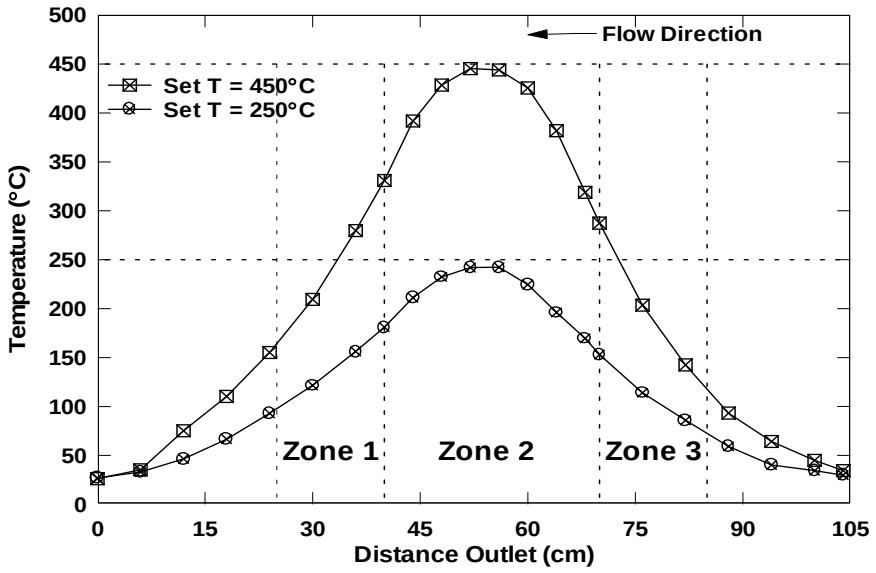

Figure A-4. Axial temperature distribution with zone 2 activated over a 2 cm long catalyst at reaction temperatures of 250 and 450°C.

1. Temperature Distribution of Activated Zone 2 of the furnace

Figure A-4 shows the temperature distribution resulting from zone 2 being activated over a 2 cm long catalyst. Two different reaction temperatures of 250 and 450°C were set, and the reaction temperatures were taken at 4 or 6 cm increase in axial direction. The measured temperatures compared to the set temperature for the heating zone were a little lower (~ 10°C). The reaction temperatures at both ends of the zone 2 drop up to 150°C for the temperature of 450°C. The heat loss could be attributed by imperfect sealing of the reactor which could be affected by the ambient temperature. The catalyst samples were put between 53 and 57 cm in the quartz-tube for the cases of heating area of zone 2. For both reaction temperatures, the maximum temperatures were obtained between 52 and 56 cm.

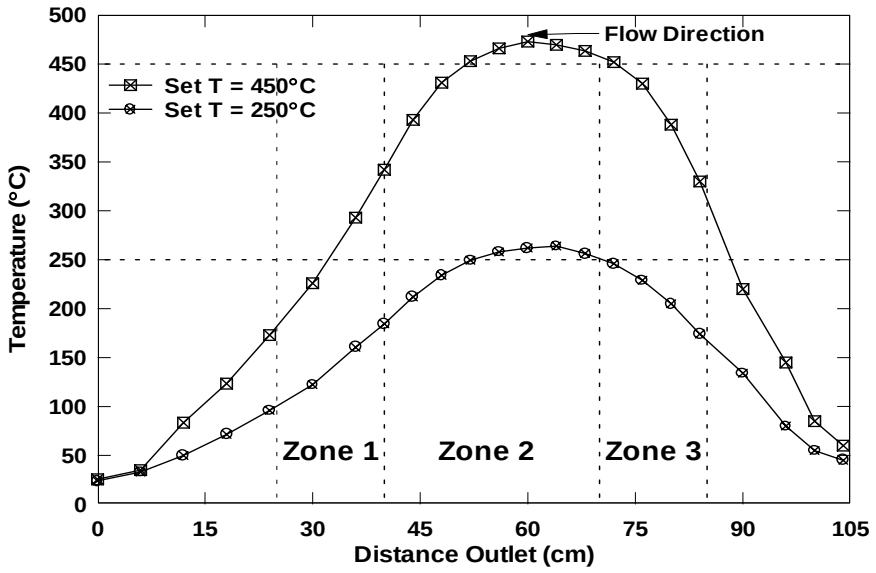

Figure A-5. Axial temperature distribution with zones 2 and 3 activated at reaction temperatures of 250 and 450°C.

2. Temperature Distribution of Activated Zones 2 and 3 of the furnace

Figure A-5 shows the temperature distribution resulting from zones 2 and 3 (preheating case) being activated. Two different reaction temperatures of 250 and 450°C were set, and the reaction temperatures were taken at 4 or 6 cm increase in axial direction. Unlike the zone 2 case, the measured temperatures reached the set temperature earlier and even little higher. The catalyst samples were put between 53 and 57 cm in the quartz-tube for the preheating cases. For both reaction temperatures, the maximum temperatures were obtained between 56 and 58 cm. Therefore, as the reaction occurs, the reaction temperature of the simulated gas is little higher in the preheating case than in the heating area of zone 2. The reaction temperatures at both ends of the zones 2 + 3 drop up to 150°C for the temperature of 450°C. The heat loss could be attributed by imperfect sealing of the reactor that could be affected by the ambient temperature.

APPENDIX 3

THE DETAILS OF THE CATALYST SAMPLES

1. V_2O_5-WO_3/TiO_2 honeycomb monolithic catalyst

V_2O_5-WO_3/TiO_2 honeycomb monolithic catalyst sample was provided by KWH Catalysts, Inc. [56] in USA. Table A-2 lists more specifications of the sample.

Table A-2. More specifications about V_2O_5-WO_3/TiO_2 honeycomb monolithic catalyst.

Material	Tetragonal-shaped square-channel titania-vanadia-tungsten based honeycomb monolithic catalyst
Appearance	Dark-green/gray color
Specific gravity	1.8
pH (potential of hydrogen)	5
Specific surface area	1,015 m^2/m^3
Height × Width × Length	6 inches × 6 inches × 11 inches
Cell size	(1/3) cm × (1/3) cm
Operating temperature (advised)	< 430 ˚C
Other properties	Toxic and odorless

2. V_2O_5/Ti-PILC honeycomb monolithic catalyst

V_2O_5/Ti-PILC honeycomb catalyst sample was provided by Postech Environmental Catalysis Laboratory (PECL) [54] in Department of Chemical Engineering Pohang University of Science and Technology in Korea. Table A-3 lists more specifications of the sample. Vanadium content in each catalyst was analyzed by Neutron Activation Analysis (NAA).

Table A-3. More specifications about V_2O_5/Ti-PILC honeycomb monolithic catalyst.

Material	Vanadia- titania-pillared interlayer clay (PILC) honeycomb monolithic catalyst
Ti content	35 wt.%
BET surface area	110 m^2/g
Height × Width × Length	11 cm × 11 cm × 13 cm
Cell size	3.8 mm × 3.8 mm
Inorganic binder	10 wt.%

Table A-4. Vanadium content in the V_2O_5/Ti-PILC catalyst sample by NAA.

Catalyst	Vanadium contents (wt.%)
Original	1.78
After coating	2.35
Coated content	0.57

APPENDIX 4
VANADIUM(V_2O_5) COATING PROCEDURE

The V_2O_5/Ti-PILC honeycomb monolithic catalyst sample needed to be coated with vanadium to increase their catalytic activity for the selective catalytic reduction of NO with ammonia. The coating procedure was provided by Postech Environmental Catalysis Laboratory (PECL) in Pohang University of Science and Technology in Korea. Ammonium metavanadate (NH_4VO_3) and oxalic acid ($(COOH)_2$) were provided by Sigma-Aldrich Co.

The preparation supplies were NH_4VO_3, $(COOH)_2$, distilled water, a pH (potential of hydrogen) measurement instrument to measure the pH of V precursory solution , a thermometer, a heater to heat the solution, and a micro-scale to weigh the catalyst before and after coating.

First of all, ammonium metavanadate (NH_4VO_3) was completely dissolved in distilled water at temperatures between 60°C and 70°C. Small amounts of oxalic acid ($(COOH)_2$) were added into the solution to make the pH of the aqueous solution between 2.5 - 3.0. V precursory solution was prepared.

Then, V_2O_5/Ti-PILC samples were dipped into the solution and dried at the temperature of 100°C several times to coat vanadium on their surface. After enough dipping and drying, the samples were calcined at the temperature of 500°C in flowing oxygen (O_2) for 20 hours to decompose the ammonium salts into oxides [24, 31].

VITA

Hyuk Jin Oh was born in Jeon-Ju, Republic of Korea (ROK) on October 20, 1975. He enrolled in precision mechanical engineering at Chonbuk National University in the spring of 1994. He served in the military between 1995 and 1998. After graduating in August 2001 with a Bachelor of Science degree, he enrolled at Texas A&M University in the fall of 2001 to pursue a Master of Science degree in mechanical engineering.

Hyuk Jin Oh can be reached at e-mail: hyukjinoh@hotmail.com and will maintain his permanent address at his home:
B/101, Yoojin Chungha APT, Hyoja 3 Dong, Wansan-Gu, Jeon-Ju, Jeon-Buk, Republic of Korea 560-856